NASA TECHNICAL MEMORANDUM


NASA TM X-2113

NASA TM X-2113



# LONGITUDINAL AERODYNAMIC CHARACTERISTICS OF THREE REPRESENTATIVE HYPERSONIC CRUISE CONFIGURATIONS AT MACH NUMBERS FROM 0.65 TO 10.70

*by Walter P. Nelms, Jr., and John A. Axelson*

*Ames Research Center*
*Moffett Field, Calif. 94035*

NATIONAL AERONAUTICS AND SPACE ADMINISTRATION • WASHINGTON, D. C. • OCTOBER 1970

| 1. Report No. | 2. Government Accession No. | 3. Recipient's Catalog No. |
|---|---|---|
| NASA TM X-2113 | | |

| 4. Title and Subtitle | 5. Report Date |
|---|---|
| **LONGITUDINAL AERODYNAMIC CHARACTERISTICS OF THREE REPRESENTATIVE HYPERSONIC CRUISE CONFIGURATIONS AT MACH NUMBERS FROM 0.65 TO 10.70** | October 1970 |
| | 6. Performing Organization Code: A-3597 |
| 7. Author(s): Walter P. Nelms, Jr., and John A. Axelson | 8. Performing Organization Report No. |
| 9. Performing Organization Name and Address: NASA Ames Research Center, Moffett Field, Calif. 94035 | 10. Work Unit No.: 126-13-03-01-00-21 |
| | 11. Contract or Grant No. |
| 12. Sponsoring Agency Name and Address: National Aeronautics and Space Administration, Washington, D. C. 20546 | 13. Type of Report and Period Covered: Technical Memorandum |
| | 14. Sponsoring Agency Code |

15. Supplementary Notes

16. Abstract

An experimental investigation of the aerodynamic characteristics of three representative hypersonic cruise configurations was conducted at Mach numbers from 0.65 to 10.70. The models were designed to the same general specifications for air-breathing, liquid-hydrogen-fueled, hypersonic cruise configurations; two were discrete wing-body concepts and the third resembled a blended wing-body design. This report examines the detailed effects of variations in angle of attack, Mach number, and configuration buildup on the longitudinal aerodynamic characteristics of the three models.

| 17. Key Words (Suggested by Author(s)) | 18. Distribution Statement |
|---|---|
| Hypersonic Aircraft<br>Aircraft Stability<br>Longitudinal Stability<br>Lift-Drag Ratio | Unclassified – Unlimited |

| 19. Security Classif. (of this report) | 20. Security Classif. (of this page) | 21. No. of Pages | 22. Price* |
|---|---|---|---|
| Unclassified | Unclassified | 84 | $3.00 |

*For sale by the Clearinghouse for Federal Scientific and Technical Information
Springfield, Virginia 22151

## NOTATION

The longitudinal force and moment coefficients are referred to the stability system of axes. Moment reference centers are located at the 25–, 35–, and 5–percent points of the mean aerodynamic chords for the reference, flat bottom, and blended models, respectively. All force and moment coefficients are based on the wing reference area for the respective models.

| | |
|---|---|
| a.c. | aerodynamic center defined at $\left(\frac{L}{D}\right)_{max}$, percent $\bar{c}$ |
| $\bar{c}$ | mean aerodynamic chord of wing |
| $C_D$ | drag coefficient, $\frac{drag}{qS}$ |
| $C_{D_{b_n}}$ | nacelle base-drag coefficient |
| $C_{D_i}$ | nacelle stream-tube drag coefficient |
| $C_{D_o}$ | drag coefficient at zero lift |
| $C_L$ | lift coefficient, $\frac{lift}{qS}$ |
| $C_{L_o}$ | lift coefficient at zero angle of attack |
| $C_{L_\alpha}$ | lift-curve slope at zero lift |
| $C_m$ | pitching-moment coefficient, $\frac{pitching\ moment}{qS\bar{c}}$ |
| $C_{m_o}$ | pitching-moment coefficient at zero lift |
| d | model body diameter |
| $d_{max}$ | maximum body diameter |
| K | boundary-layer trip (grit) size, in. |
| $\frac{L}{D}$ | lift-drag ratio |
| $\left(\frac{L}{D}\right)_{max}$ | maximum lift-drag ratio |

| | |
|---|---|
| $l$ | overall body length |
| M | free-stream Mach number |
| p | free-stream static pressure |
| q | free-stream dynamic pressure |
| Re | unit Reynolds number, per foot |
| S | wing planform area (reference area) |
| $\frac{t}{c}$ | airfoil thickness-to-chord ratio |
| TP | tangency point |
| x | longitudinal coordinate, measured rearward from model nose |
| $\alpha$ | angle of attack (referred to fuselage center line) |
| $\gamma$ | ratio of specific heats, 1.4 for air |

The following code has been devised to designate the various components of the models:

| | |
|---|---|
| B | body with symmetrical profile nose |
| $B_1$ | body with nose drooped in profile (flat-bottom model only) |
| F | flaps |
| N | nacelle stabilizer |
| $N_1$ | wing-mounted nacelles (reference model only) |
| $N_2$ | armpit-mounted nacelles (reference model only) |
| R | wing-mounted fins |
| V | center line vertical tail |
| W | wing with $\frac{t}{c} = 0.04$ |
| $W_1$ | wing with $\frac{t}{c} = 0.03$ |

# LONGITUDINAL AERODYNAMIC CHARACTERISTICS OF THREE REPRESENTATIVE HYPERSONIC CRUISE CONFIGURATIONS AT MACH NUMBERS FROM 0.65 TO 10.70

Walter P. Nelms, Jr., and John A. Axelson

Ames Research Center

## SUMMARY

An experimental investigation of the longitudinal aerodynamic characteristics of three representative hypersonic cruise configurations was conducted at Mach numbers from 0.65 to 10.70. The models were designed to represent air-breathing, liquid-hydrogen-fueled, hypersonic cruise configurations; two were discrete wing-body concepts and the third resembled a blended wing-body design. Detailed effects of varying angle of attack, Mach number, and configuration buildup were considered.

The basic wing-body configurations with vertical tails on the center line and without nacelles had similar lift and drag characteristics despite the marked differences in geometry. Adding the nacelles reduced the maximum lift-drag ratios but increased the static longitudinal stability. At the hypersonic speeds, variations in Mach number had little effect on the aerodynamic characteristics. The pitching moments at zero lift were negative at transonic speeds and approached zero at the hypersonic Mach numbers. Increasing supersonic Mach numbers resulted in forward travel of the aerodynamic centers amounting to between 13 and 17 percent of the mean aerodynamic chords for the three complete models.

## INTRODUCTION

Studies by both NASA and the industry have indicated that hydrogen-fueled hypersonic aircraft offer attractive performance capabilities for both cruise and boost missions (refs. 1–4). To date, these studies have been based primarily on estimated aerodynamic characteristics due to the lack of experimental data on configurations having large fuselage volumes consistent with the fuel requirements of the hypersonic mission. For this reason, a program has been undertaken to investigate the experimental aerodynamic characteristics of three configurations representative of air-breathing, liquid-hydrogen-fueled, hypersonic cruise aircraft over a Mach number range of 0.65 to 10.70.

The experimental investigation was made in the Ames 6– by 6–Foot Transonic, 1– by 3–Foot Supersonic, and 3.5–Foot Hypersonic Wind Tunnels over a Mach number range from 0.65 to 10.70. The Reynolds number was held constant at $3.5 \times 10^6$ per foot for most of the tests; at Mach numbers 2.0 and 10.7, the Reynolds number was limited to $2.5 \times 10^6$ and $2.0 \times 10^6$ per foot, respectively, because of wind-tunnel limitations. Data were taken over a nominal angle-of-attack range from –4° to +12° at 0° sideslip angle.

## MODELS

Detailed drawings of the three models are shown in figure 1 and pertinent dimensions of the various model components are presented in table 1. Figure 2 presents photographs of three complete model configurations.

All three models were designed as air-breathing, liquid-hydrogen-fueled, turboramjet–powered, hypersonic cruise aircraft having a gross weight of approximately a 0.5 million pounds, a cruise Mach number near 6, a wing area of 6,250 square feet, and a fuselage volume of 72,000 cubic feet. The wings, with an aspect ratio of 1.46, had flat undersurfaces for minimizing local flow acceleration and hypersonic boundary-layer growth ahead of the inlets. The nacelles were placed in the wing compression field and positioned so as to minimize jet impingement on the structure downstream of the nacelle exits. The plane containing the wing lower surface passed through the fuselage center line on the three models.

### Reference Model

The reference model shown in figures 1(a) and 1(b) is representative of a concept derived from the analytical studies of reference 1; the scale was 1 inch = 16 feet. The fuselage was circular in cross section and had a fineness ratio of 12, with a Sears-Haack profile (fig. 1(a)) extending back 11.13 inches from the nose. Aft of this station, the body was opened up into a cone frustum to permit entrance of the sting support. The flat-bottomed delta wing had a 70° sweptback leading edge and a 4-percent-thick wedge-slab-wedge airfoil section with ridge lines on the upper surface at 30 and 70 percent of the local chords. On this model, the wing leading edge intersected the body at its maximum diameter. The vertical tail, mounted on the body center line, had a symmetrical diamond airfoil section with a maximum thickness-to-chord ratio of 4 percent located at midchord and leading-edge and trailing-edge sweepback angles of 60° and 13°, respectively. The exposed area of the vertical tail was approximately one-fourth of the wing reference area.

The two-dimensional engine nacelles mounted on the wings (fig. 1(a)) had external contours that simulated a design containing two turboramjet engines per nacelle with an exit area twice the inlet area. The nacelles had ducts of constant internal area without inlet precompression ramps or provision for boundary-layer bypass. The external expansions and constant area internal passages resulted in sizable nacelle base areas (fig. 1(a) and table 1). Figure 1(b) shows an alternate location for the engine nacelles on the reference model, namely, under the wing in an armpit position at the wing-body intersection. The nacelles in this location had the same inlet area and length as those outboard, but had streamwise exterior sides. There was allowance for an exit-to-inlet area ratio of 2 on the original Sears-Haack body, but on the wind-tunnel model the afterbody was opened up to allow for the sting support, thereby reducing the exit areas of these nacelles.

### Flat-Bottom Model

The flat-bottom configuration (fig. 1(c)) is designated so because of the flat undersurfaces on all model components; the scale was 1 inch = 15 feet. In profile, the fuselage had a circular-arc nose and afterbody and a cylindrical midsection, but was laterally flat along the entire bottom. Two

forebody sections were tested on this model, the symmetrical nose having its apex on the fuselage center line and the drooped nose with the apex 1/4 inch below the center line. With either nose, the body had an area-equivalent fineness ratio of 14.5. The 70° sweptback flat-bottomed delta wing was tested with 4- and 3-percent-thick wedge-slab-wedge airfoil sections with rounded ridge lines at 35 and 70 percent of the local chords on the upper surface.

The vertical tail mounted on the body center line had leading-edge and trailing-edge sweepback angles of 70° and 24°, respectively, with an exposed area approximately equal to one-tenth the wing reference area. The vertical tail had a symmetrical wedge-slab-wedge airfoil section with rounded ridge lines at the 1/4- and 3/4-chord locations and with a maximum thickness-to-chord ratio of 4 percent. This model was also equipped with identical pairs of wing-mounted 70° sweptback fins with approximately half of their area located above and half below the wings. The combined area of the three vertical surfaces totaled to the same one-fourth of the wing reference area as that of the single large vertical tail on the reference model. The nacelle and horizontal-stabilizer combination was designed to bypass the boundary layers from the adjacent wing and body surfaces and to capture air from the compression field under the wing in flight. The model had two-dimensional nacelles with the forward lower surface utilized as precompression ramps and with expanding internal ducts having exit areas twice the inlet areas. (The flat-bottom model also incorporated a pair of wing-mounted flaps conceived to deflect downward in front of the inlets to afford protection from debris ingestion during powered ground operations. On the ground, the inlets would draw air from the upper surface of the wing. This flap mode is not pertinent to the present study.)

### Blended Model

The blended model shown in figure 1(d) had a body of elliptical cross section merged to a 3-percent-thick 80°–65° double delta wing with clipped tips. The elliptical cross section of the body had a 16/9 ratio of major-to-minor axes. The scale of this model was 1 inch = 15 feet. In profile, this model had a circular-arc nose and afterbody with a midsection of constant depth. Considering an average of the major and minor axes, the effective fineness ratio of this body was about 9.8. The flat-bottom wing had a double-wedge airfoil section with inboard and outboard rounded ridge lines at 64-percent chord on the upper surface. The vertical tail on the center line and the outboard fins on this model were similar to those used on the flat-bottom configuration. The nacelles were inverted, but similar to those on the flat-bottom model, with the precompression ramps above the two-dimensional inlet. A gap between the wing and nacelles allowed for boundary-layer bypass. The expanding internal ducts had a ratio of exit-to-inlet areas of 2.0.

## TESTS

Experimental data were obtained in air in three Ames wind tunnels over a Mach number range of 0.65 to 10.70. The 6– by 6–foot transonic tunnel is a closed-circuit, continuous-flow facility with a sliding block nozzle and a slotted wall test section; in this tunnel, the Mach number was varied from 0.65 to 1.99. The 1– by 3–foot supersonic tunnel is a closed-circuit, continuous-flow facility with a flexible wall nozzle; Mach numbers were varied from 1.99 to 4.81 in this tunnel. Mach numbers of 5.31, 7.42, and 10.70 were obtained in the 3.5–foot hypersonic

tunnel, which uses replaceable nozzles; this tunnel is a blowdown facility in which incoming air is preheated by a pebble-bed heater to prevent liquefaction of air in the test section. The stagnation temperature was maintained at 800° F for Mach numbers of 5.31 and 7.42 and at 1400° F for Mach number 10.70. Data were taken at a constant Reynolds number of $3.5\times10^6$ per foot at all Mach numbers except at 1.99 and 10.70 where the Reynolds number was limited to $2.5\times10^6$ and $2.0\times10^6$ per foot, respectively, because of wind-tunnel limitations.

The models were sting-mounted through the rear of the fuselages. Force and moment measurements were made with an internally mounted six-component strain-gage balance over a nominal angle-of-attack range from −4° to +12° at 0° angle of sideslip. The angle of attack was corrected for both wind-tunnel flow misalinement and for balance and sting deflections caused by aerodynamic loads. Fuselage base pressure was measured and the drag data were adjusted to a condition corresponding to free-stream static pressure on the base.

At several test Mach numbers, pressure surveys were made of the flow through the engine nacelles of the reference and flat-bottom models, and the results were used to compute corrections for nacelle stream-tube drag. Also, the pressure was measured on the base of the wing-mounted nacelles of the reference configuration to provide for adjusting the axial force to a condition corresponding to free-stream static pressure on the nacelle base. The basic aerodynamic data presented have not been corrected for nacelle stream-tube and nacelle base drag, but corrections have been applied to some of the results summarized in a later section.

Generally, transition was not fixed on the models, but grit studies were conducted at several of the lower Mach numbers on the reference configuration to provide an all-turbulent boundary layer as a basis for data evaluation. At the hypersonic speeds, no effective method was found for fixing transition near the leading edges of the model components to achieve fully turbulent flow. Studies utilizing sublimation techniques and Reynolds number variation indicated the hypersonic boundary layers to be nearly all laminar with possible small areas of transitional flow. The results of the grit and Reynolds number variation studies are presented in a later section of the report.

Based on repeatability of the data and known precision of the measuring equipment, the test Mach numbers 0.65–4.81 and 5.31–10.70 are considered accurate within ±0.01 and ±0.05, respectively; the corresponding dimensionless aerodynamic coefficients are considered accurate within ±2 and ±3 percent, respectively. The angles of attack are considered to be accurate within ±0.2°.

## RESULTS AND DISCUSSION

Figures 3 through 8 present the basic longitudinal data of the three configurations, and figures 9 through 14 show these results summarized as a function of Mach number. Figures 15 through 18 present information from the boundary layer and nacelle stream tube drag studies. These figures are summarized in the following table which indicates the configurations and briefly notes the purpose of each figure.

| Figure | Model configuration | Purpose of figure |
|---|---|---|
| 3 | B – Reference model<br>B – Flat-bottom model<br>B – Blended model | Comparison of the bodies alone |
| 4 | WBV – Reference model<br>$W_1BV$ – Flat-bottom model<br>$W_1BV$ – Blended model | Comparison of the wing-body–vertical-tail configurations |
| 5 | WB<br>WBV<br>$WBVN_1$<br>$WBVN_2$ | Reference configuration component buildup |
| 6 | $W_1B$<br>$W_1BV$<br>$W_1BVN$<br>$W_1BVRFN$ | Flat-bottom configuration component buildup; wing t/c = 0.03 |
| 7 | $WB_1V$<br>$WB_1VRF$<br>$WB_1VRFN$ | Flat-bottom configuration component buildup; drooped nose, wing t/c = 0.04 |
| 8 | $W_1B$<br>$W_1BV$<br>$W_1BVN$<br>$W_1BVRN$ | Blended configuration component buildup |
| 9 thru 14 | All configurations | Results from figures 3–8 summarized as a function of Mach number |
| 15 | WBV – Reference model | Boundary-layer transition results |
| 16 | WBV – Reference model | Reynolds number variation results |
| 17 and 18 | Complete configurations | Internal drag results |

## Longitudinal Aerodynamic Characteristics

The longitudinal aerodynamic characteristics are presented over a range of lift coefficients for the component buildup of each model in figures 3 through 8; these results are summarized over the test Mach number range in figures 9 through 14. All aerodynamic coefficients are based on the wing reference area and mean aerodynamic chord (table 1). The moment reference centers are at

different percentage locations of the respective mean aerodynamic chords, but they are very close to 61-percent body length in all three cases. The results for configurations with nacelles are not corrected for nacelle stream-tube drag and nacelle base drag. The aerodynamic centers were evaluated near maximum lift-drag ratio. The rise in the drag coefficient with increasing hypersonic Mach number is primarily a consequence of the lower test Reynolds number at Mach number 10.70.

*Body alone*– The longitudinal aerodynamic characteristics of the bodies alone are presented in figure 3 and are summarized as a function of Mach number in figure 9. For all the Mach numbers shown, the blended body had the highest $C_{L_\alpha}$, and at the hypersonic speeds, this same body exhibited the greatest value of lift coefficient for a given angle of attack. Near $(L/D)_{max}$, the lift-curve slopes for the three bodies were generally the same. The flat-bottom body with the symmetrical profile nose produced a positive $C_{L_0}$ at Mach 1.10, but this value approached zero at the higher speeds. The blended body generally had the largest $C_{D_0}$ primarily because of the smaller effective fineness ratio of this body compared to the other two. Except at M = 10.70, the reference body had the lowest $C_{D_0}$. At the hypersonic Mach numbers, the flat-bottom body produced the highest $(L/D)_{max}$; the $(L/D)_{max}$ of the other two bodies was about equal.

Figure 3(a) indicates that for the flat-bottom body at Mach 1.10 zero lift was not obtained. A negative value of $C_{m_0}$ could be inferred by extrapolation of the data. At hypersonic speeds $C_{m_0}$ was nearly zero for all three bodies. It should be noted that the three bodies alone had about the same longitudinal stability when referenced to the body length. The data herein (figs. 3 and 9) are referred to the wing reference dimensions because primary attention is given to the complete model configurations.

*Wing-body–vertical-tail*– In figures 4 and 10, the longitudinal aerodynamic characteristics are presented for the three models including wing, body, and vertical tail on the center line but with nacelles removed. The lift curves were approximately linear to an angle of attack of 10° up to a Mach number of about 5, but became progressively less linear above this speed with increasing lift-curve slope at the higher lift coefficients. As was the case for the bodies alone at the higher Mach numbers, the blended configuration had the highest lift coefficients for a given angle of attack. This is believed attributable to the greater planform area relative to the wing reference area of the blended configuration in comparison to the other two models. As shown in figure 10, the results indicated little difference in the $(L/D)_{max}$ of these three configurations throughout the test Mach number range. The greater value of $C_{D_0}$ obtained for the blended model was due primarily to the lower fineness ratio of the body. The nearly identical values of untrimmed $(L/D)_{max}$ for the three models decreased from about 8 at a Mach number of 0.9 to about 4.3 at a Mach number of 6.

At the hypersonic speeds, all three wing-body–vertical-tail configurations had small positive values of $C_{m_0}$. At the transonic speeds, the cambered wings produced negative values of $C_{m_0}$ (fig. 10). The differences in $C_{m_0}$ for the three models are believed due to the differences in wing-body interference, body geometry, wing leading edges of the blended model, and the aft closure of the reference fuselage.

The pitching-moment curves for the wing-body–vertical-tail configurations (fig. 4) were approximately linear to the highest values of lift coefficient for Mach numbers through 2.0. A more forward location of the aerodynamic center for the blended configuration (fig. 10) reflects the effect of the wider forebody and the forward projection of the wing in relation to the other two models. For all three configurations, the forward movement of the aerodynamic centers with increasing supersonic Mach number is believed to be a result of the increased loadings on the fuselage forebodies. The overall aerodynamic center travel from its most rearward to its most forward location (nacelles off) was 30-percent $\bar{c}$ for the blended model and about 20-percent $\bar{c}$ for the reference and flat-bottom configurations.

A significant point to observe in figure 10 is that changes in test Mach number resulted in more pronounced effects on the aerodynamic characteristics at transonic and supersonic speeds than at hypersonic Mach numbers. In fact, most aerodynamic characteristics were found to be almost invariant with changes in hypersonic Mach number.

*Reference model*– The longitudinal aerodynamic characteristics for the reference model are presented for the wing-body configuration alone and in combination with the vertical tail and with nacelles in either the wing-mounted or armpit location as functions of lift coefficient (fig. 5) and of Mach number (fig. 11). Adding the vertical tail and engine nacelles to the wing-body configuration had no effect on $C_{L_\alpha}$ (fig. 11), but above about $M = 3.0$ the added lifting surface of the nacelles tended to increase lift coefficient for a given angle of attack (fig. 5). As expected, the addition of components to the model increased the $C_{D_0}$ and lowered $(L/D)_{max}$ at all speeds. The lower drag increment for the armpit nacelles is not necessarily considered an advantage because of the incomplete simulation of the armpit nacelles on the model (see Models section) and because of the flow of the body boundary layer into these inlets rather than the higher energy air associated with the wing-mounted nacelles.

The addition of components had only small effects on $C_{m_0}$ as shown in figure 11. The wing-mounted nacelles ($N_1$) reduced the small positive $C_{m_0}$ to near zero at the higher Mach numbers, but had the beneficial effect of increasing static longitudinal stability. The overall travel of the aerodynamic center was reduced from about 20-percent $\bar{c}$ for the wing-body to 17-percent $\bar{c}$ for the complete configuration with wing-mounted nacelles.

*Flat-bottom model*– Figures 6 and 12 present the longitudinal aerodynamic characteristics of the flat-bottom model with a symmetrical profile nose and a 3-percent-thick wing. As was the case with the reference model, adding components to the basic wing-body combination had little effect on $C_{L_\alpha}$ (fig. 12) while the $C_{D_0}$ was increased and $(L/D)_{max}$ decreased. Also, the addition of the nacelles moved the aerodynamic centers aft for the limited Mach numbers shown.

Figures 7 and 13 give the longitudinal aerodynamic characteristics for the flat-bottom model with the drooped nose and a wing thickness of 4 percent. Adding components on this model tended to have a greater effect on $C_{L_\alpha}$ than was the case for the other models. A comparison of the results for the flat-bottom model with the two noses and wing thicknesses ($W_1BV$ and $WB_1V$) indicates little difference in lift and drag characteristics but a noticeable difference in pitching moments. The drooped nose produced a more negative $C_{m_0}$ and a smaller aerodynamic center

travel (figs. 10 and 13). The overall aerodynamic center travel with Mach number for the complete model with the drooped nose (fig. 13) was about 13-percent $\bar{c}$.

*Blended model*– The longitudinal aerodynamic characteristics for the blended model are presented in figure 8 for variations in lift coefficient and are summarized as a function of Mach number in figure 14. The test results for this model were similar to those of the other two configurations. Adding components had practically no effect on $C_{L_\alpha}$ but tended to increase the drag coefficient and reduce the maximum L/D. As with the reference configuration, the engine nacelles, when added to this model, reduced the positive $C_{m_o}$ to near zero at the higher Mach numbers. Adding the nacelles and fins reduced the overall aerodynamic center travel with Mach number, resulting in a movement of about 13-percent $\bar{c}$.

## Boundary-Layer Studies

Studies were conducted to determine the nature of the boundary layer on the wind-tunnel models. Some of the results of these investigations are presented in this section.

*Grit studies*– Studies using grit-type boundary-layer trips were conducted at Mach numbers 0.90, 1.30, and 1.99 to establish the drag level for the reference model with an all-turbulent boundary layer. Six different grit sizes were applied near the wing and vertical-tail leading edges and the fuselage nose of the wing-body–vertical-tail configuration. A drag polar was then obtained for each grit size at the same Mach numbers, and the drag level for an all-turbulent boundary layer was determined by the procedures described in reference 5. These results are presented in figure 15.

For the subsonic Mach number of 0.90, the drag coefficient was plotted versus grit size for various lift coefficients as shown in figure 15(a). The plateau on the curve defines the grit-free drag level (ref. 5) for an all-turbulent boundary layer for the particular value of lift coefficient. The values of drag coefficient defined in this manner were then plotted in the lower part of figure 15(a) in the form of a grit-free drag polar for an all-turbulent boundary layer. Figures 15(b) and (c) present the results obtained for the supersonic Mach numbers of 1.30 and 1.99. Here the drag coefficient is plotted versus grit size squared for various lift coefficients. A linear extrapolation of the data to zero-grit size (ordinate) defines the drag levels for an all-turbulent boundary layer for each lift coefficient (ref. 5). As before, the grit-free drag polars for an all-turbulent boundary layer are shown plotted at the bottom of the two figures. The results obtained from these grit studies are summarized in figure 15(d) in the form of $C_{D_o}$ and $(L/D)_{max}$ as a function of Mach number as indicated by the circular symbols. For comparison, the data for the wing-body–vertical-tail configuration with untripped boundary layer (from fig. 11) are also presented in figure 15(d). As can be seen, extrapolating to all-turbulent boundary-layer conditions on the model resulted in a decrease in $(L/D)_{max}$ of about 24, 13, and 15 percent at Mach numbers 0.90, 1.30, and 1.99, respectively.

*Reynolds number variations*– In contrast to the grit studies at the lower speeds, no effective method was found to fix transition near the leading edge of the model components at the hypersonic Mach numbers. On the basis of sublimation studies at Mach number 5.31 using the reference model, it was concluded that the boundary layer was mostly laminar with possible small areas of transitional flow. To support this conclusion, the unit Reynolds number was varied in tests

of the wing-body–vertical-tail configuration of the reference model. Three unit Reynolds numbers were investigated at each of the hypersonic Mach numbers of 5.31, 7.42, and 10.70; the resulting drag polars are shown plotted at the top of figures 16(a), (b), and (c). Since it was suspected that the boundary layer on the model was laminar, the values of $C_{D_0}$ and drag coefficient at $(L/D)_{max}$ from the polars at different Reynolds numbers were plotted versus a parameter $1/\sqrt{Re}$, which is representative of a drag-coefficient variation associated with a laminar boundary layer. These results are shown at the bottom of figures 16(a), (b), and (c). An extrapolation of the resulting straight lines back to the ordinate (infinite Re), as represented by the dashed lines, indicates the pressure drag of the configuration, which agrees well with the calculated values of pressure drag for the model (indicated by the filled diamond-shaped symbols). These theoretical estimates were based on tangent-cone theory for the body and tangent-wedge theory for the wing and vertical tail using reference 6. A Prandtl-Meyer expansion was employed on the leeward or expansion surfaces.

An attempt was made to apply the foregoing drag data to a variation with Reynolds number representative of turbulent boundary-layer conditions, but there was a clear lack of correlation. Thus, this analysis and the sublimation studies indicate that the boundary layer on the model was mostly laminar at the hypersonic Mach numbers of this investigation.

## Nacelle Stream-Tube Drag Studies

The foregoing data for the configurations with engine nacelles were not corrected for the drag associated with the air flowing through the simulated ducts. Internal drag is generally accounted for in the propulsive thrust rather than being combined with the external aerodynamics of the configuration. For this reason, pressure surveys of the flow through the nacelles of the models were conducted at most Mach numbers of this investigation and the results used to compute values of nacelle stream-tube drag. The flow through the nacelles was found to have negligible effect on the pitching-moment results since the nacelles were located sufficiently close to the model center line.

In order to determine the nacelle stream-tube drag, detailed total and static-pressure surveys were made of the flow at the duct exists. The total pressure was measured using a three-tube rake for the reference model and two five-tube rakes (one in each duct) for the flat-bottom model. Since the nacelles were similar, the results obtained for the flat-bottom model were assumed valid for the blended model. Static-pressure measurements were made with taps provided in the internal walls of the ducts near the exits. These values of pressure were used in the following equation to compute the nacelle stream-tube drag coefficients for the various free-stream Mach numbers and angles of attack for sections of the duct exit area ($A_e$).

$$C_{D_i} = \frac{2A_e}{S}\frac{p_e}{p}\frac{M_e}{M}\sqrt{\frac{1 + [(\gamma - 1)/2]M_e^2}{1 + [(\gamma - 1)/2]M^2}} + \frac{2}{\gamma M^2}\frac{A_e}{S}\left[1 - \frac{p_e}{p}(1 + \gamma M_e^2)\right]\cos\alpha$$

where $p_e$ and $M_e$ are the exit static pressure and exit Mach numbers of each section, respectively. This drag increment is composed primarily of nacelle internal drag but also includes any losses imparted to the stream tube entering the inlet by the forward components of the model. The drag

increments for the various sections of the exit areas were then summed into a total nacelle stream-tube drag correction. These values of nacelle stream-tube drag coefficient based on wing reference area are shown in figure 17 as a function of angle of attack for various free-stream Mach numbers. Figures 17(a) and (b) present the nacelle stream-tube drag data for the reference model, while the results for the flat-bottom and blended configurations are shown in figure 17(c).

On the reference model with wing-mounted nacelles ($N_1$), the expanding external contours and constant internal area ducts resulted in a base area on each nacelle (fig. 1(a) and table 1). The drag associated with this base area was included in the previously shown experimental data. Therefore, static-pressure tubes were installed in the base of the nacelles and base pressure measurements were made at the various test Mach numbers and angles of attack. The results of this survey are shown in figure 17(a) in the form of a base-drag coefficient based on wing reference area. Because of the straight external sides on the armpit-mounted nacelles of the reference model, and because of the internal expansion in the ducts of the flat-bottom and blended models, there were no nacelle base areas; therefore, no corrections were required.

The nacelle stream-tube drag corrections and nacelle base-drag corrections (where applicable) were applied to the aerodynamics of the three complete configurations and the results are presented in figure 18 in terms of $C_{D_0}$ and $(L/D)_{max}$ as functions of Mach number. In figure 18(a), the combined effects of the nacelle stream-tube and nacelle base drag (from fig. 17(a)) are shown by dashed lines for the reference model with wing-mounted nacelles. The dashed lines in figures 18(b), (c), and (d) represent the corrected aerodynamic results for the remaining configurations. For comparison, figure 18 also shows the uncorrected values of $C_{D_0}$ and $(L/D)_{max}$ for the complete configurations (from figs. 11, 13, and 14). The results at Mach number 6 interpolated for the three models show that the nacelle stream-tube corrections lowered the $C_{D_0}$ values about 5 to 9 percent while increasing the maximum L/D about 7 to 13 percent. At this Mach number, the final corrected values of untrimmed $(L/D)_{max}$ for the complete models were about 4.2, 3.6, and 3.7 for the reference, flat-bottom, and blended models, respectively. The complete models had different controls, stabilizers, and nacelles and compare closer aerodynamically when the wing-body configurations with vertical tails on the center line are considered (figs. 4 and 10).

## CONCLUSIONS

An experimental investigation has been conducted for Mach numbers from 0.65 to 10.70 to determine the longitudinal aerodynamic characteristics of three models representative of hypersonic cruise aircraft. The three different models were designed to the same general specifications for an air-breathing, liquid-hydrogen-fueled, hypersonic cruise configuration with a gross weight of about a 0.5-million pounds. Two of the configurations were discrete wing-body concepts and the third resembled a blended wing-body design. The detailed effects of varying angle of attack, Mach number, and configuration buildup were investigated. The results indicate the following conclusions:

1. In spite of the marked differences in geometry, the three basic models comprised of wing, body, and vertical tail on the center line, with nacelles removed, had similar lift and drag characteristics. The models in this configuration developed untrimmed maximum lift-drag ratios near 4.3 at a Mach number of 6.

2. The addition of components to the models increased the zero-lift drag coefficients and reduced the maximum lift-drag ratios, but had some beneficial effects on the static longitudinal stability.

3. Generally, in the transonic and supersonic speed ranges, the models exhibited negative values of pitching moment at zero lift, but values near zero were obtained for the hypersonic Mach numbers.

4. The aerodynamic centers tended to move forward with increasing supersonic Mach number, and for the three complete configurations, the travel from the most rearward to the most forward location was about 13 or 17 percent of the mean aerodynamic chord depending on the model.

5. Changes in test Mach number resulted in more pronounced effects on the aerodynamic characteristics at transonic and supersonic speeds than at hypersonic Mach numbers. In fact, most aerodynamic characteristics were found to be almost invariant with changes in hypersonic Mach number.

Ames Research Center
National Aeroanautics and Space Administration
Moffett Field, Calif. 94035, April 29, 1970

## REFERENCES


1. Gregory, Thomas J.; Petersen, Richard H.; and Wyss, John A.: Performance Tradeoffs and Research Problems for Hypersonic Transports. J. Aircraft, vol. 2, no. 4, 1965, pp. 266–271.

2. Petersen, Richard H.; Gregory, Thomas J.; and Smith, Cynthia L.: Some Comparisons of Turboramjet-Powered Hypersonic Aircraft for Cruise and Boost Missions. J. Aircraft, vol. 3, no. 5, 1966, pp. 398–405.

3. General Dynamics/Convair Division: Performance Potential of Hydrogen Fueled, Airbreathing Cruise Aircraft. Rep. GD/C–DCB–66–004, vols. 1–4 (Contract NAS2–3180), May and Sept. 1966.

4. Lockheed–California Company: Study of Advanced Airbreathing Launch Vehicles With Cruise Capability. Rep. LR 21042, vols. 1–6 (Contract NAS2–4084), Feb. 1968.

5. Braslow, Albert L.; Hicks, Raymond M.; and Harris, Roy V., Jr.: Use of Grit-Type Boundary-Layer-Transition Trips on Wind-Tunnel Models. NASA TN D–3579, 1966.

6. Gentry, Arvel E.: Hypersonic Arbitrary-Body Aerodynamic Computer Program. Douglas Rep. DAC 56080, vols. 1 and 2, 1967.

TABLE 1.- MODEL GEOMETRY

[Dimensions are in inches and areas in square inches]

| Component | Reference model | Flat-bottom model | Blended model |
|---|---|---|---|
| Fuselage | B | B and $B_1$ | B |
| Length, $l$ | 17.81 | 19.33 | 15.33 |
| Maximum dia., $d_{max}$ | 1.48 | 1.33 | 2.00 |
| Profile | Sears-Haack with frustum of cone afterbody | Circular-arc nose and afterbody; cylindrical midsection | Circular-arc nose and afterbody; cylindrical midsection |
| Wing | W | W and $W_1$ | $W_1$ |
| Span | 5.96 | 6.36 | 6.36 |
| Aspect ratio | 1.46 | 1.46 | 1.46 |
| Center line chord | 8.19 | 8.73 | 7.55 |
| Mean aero. chord, $\bar{c}$ | 5.46 | 5.82 | 5.28 |
| Planform area, S | 24.41 | 27.70 | 27.70 |
| Maximum t/c | 0.04 | 0.04 and 0.03 | 0.03 |
| Leading-edge sweep | 70° | 70° | 80°-65° |
| Trailing-edge sweep | 0° | 0° | 0° |
| Vertical tail | V | V | V |
| Exposed span | 2.48 | 1.34 | 1.44 |
| Exposed root chord | 4.33 | 3.20 | 3.69 |
| Tip chord | 0.60 | 0.41 | 0.41 |
| Exposed area | 6.40 | 2.41 | 2.94 |
| Maximum t/c | 0.04 | 0.04 | 0.04 |
| Leading-edge sweep | 60° | 70° | 70° |
| Trailing-edge sweep | 13° | 24° | 24° |
| Wing-mounted fins | --- | R | R |
| Height | --- | 1.00 | 1.00 |
| Center line chord | --- | 2.78 | 2.78 |
| Tip chord | --- | 1.38 | 1.38 |
| Area, pair | --- | 4.16 | 4.16 |
| Leading-edge sweep | --- | 70° | 70° |
| Trailing-edge sweep | --- | 0° | 0° |
| Nacelles | $N_1$ and $N_2$ | N | N |
| Duct length | 2.19 | 2.38 | 2.38 |
| Ramp length | --- | 1.00 | 1.00 |
| Overall length | 2.19 | 3.38 | 3.38 |
| Inlet area, total | 0.28 | 0.32 | 0.32 |
| Exit area, total | 0.28 | 0.64 | 0.64 |
| Base area, total | 0.29 ($N_1$ only) | 0 | 0 |

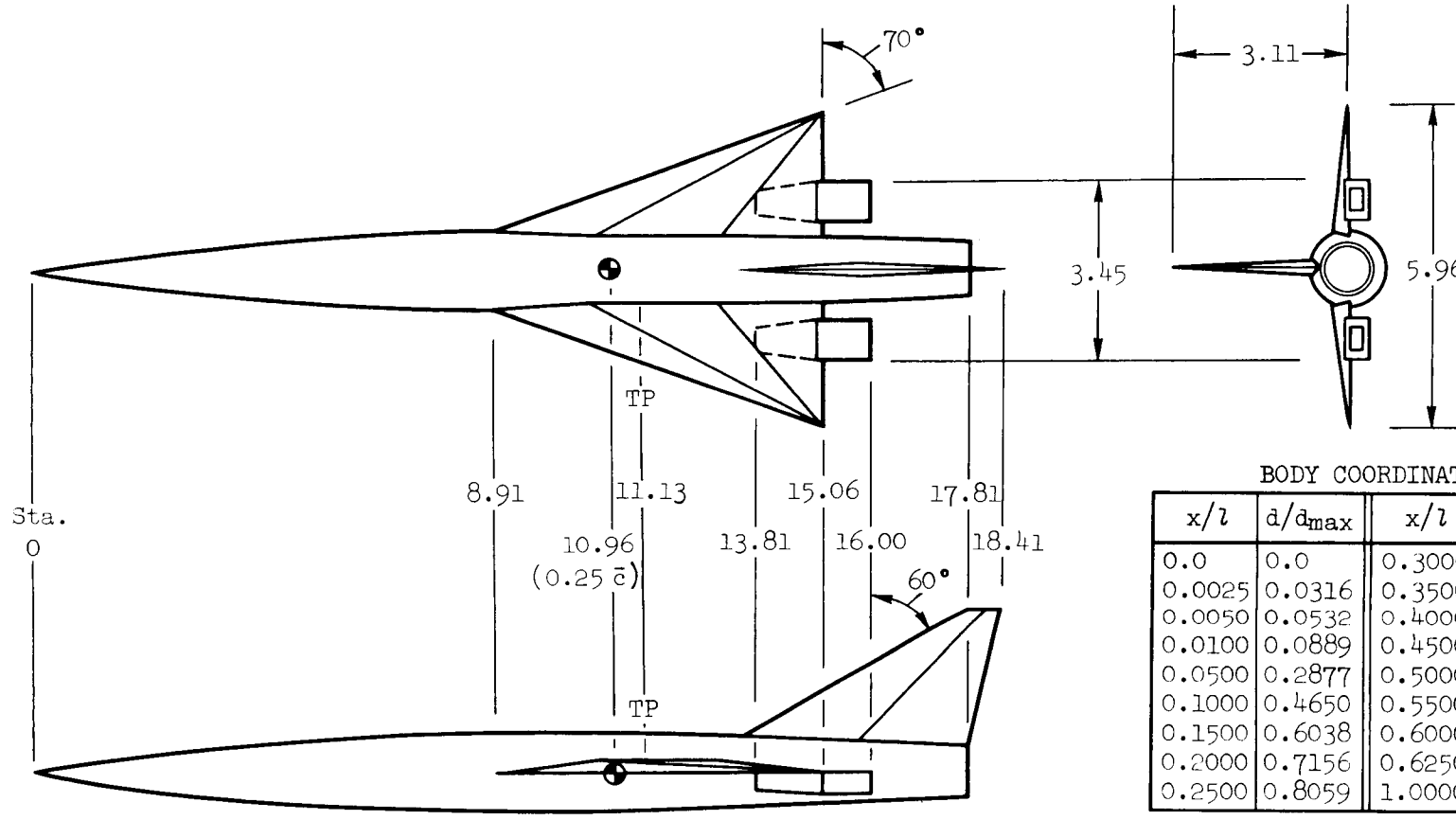


BODY COORDINATES

| x/l | d/d_max | x/l | d/d_max |
|---|---|---|---|
| 0.0 | 0.0 | 0.3000 | 0.8774 |
| 0.0025 | 0.0316 | 0.3500 | 0.9326 |
| 0.0050 | 0.0532 | 0.4000 | 0.9703 |
| 0.0100 | 0.0889 | 0.4500 | 0.9926 |
| 0.0500 | 0.2877 | 0.5000 | 1.0000 |
| 0.1000 | 0.4650 | 0.5500 | 0.9926 |
| 0.1500 | 0.6038 | 0.6000 | 0.9703 |
| 0.2000 | 0.7156 | 0.6250 | 0.9535 |
| 0.2500 | 0.8059 | 1.0000 | 0.6739 |

$$d/d_{max} = \left[1 - \left(1 - \frac{2x}{l}\right)^2\right]^{3/4}$$

$d_{max} = 1.48$, $l = 17.81$

(a) Reference model with wing-mounted nacelles ($N_1$)

Figure 1.- Model drawings; all dimensions are in inches.

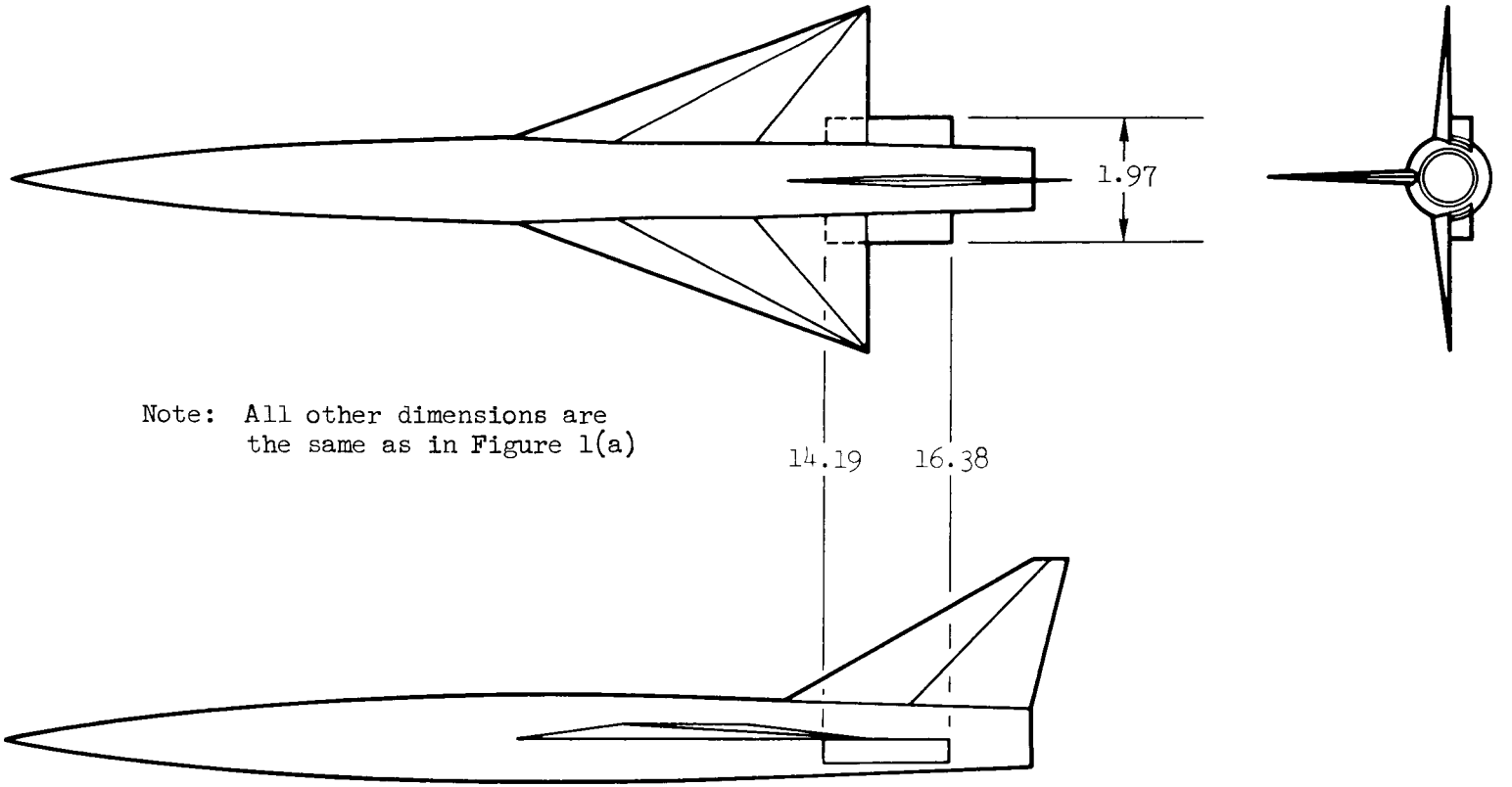


(b) Reference model with armpit-mounted nacelles ($N_2$)

Figure 1.- Continued.

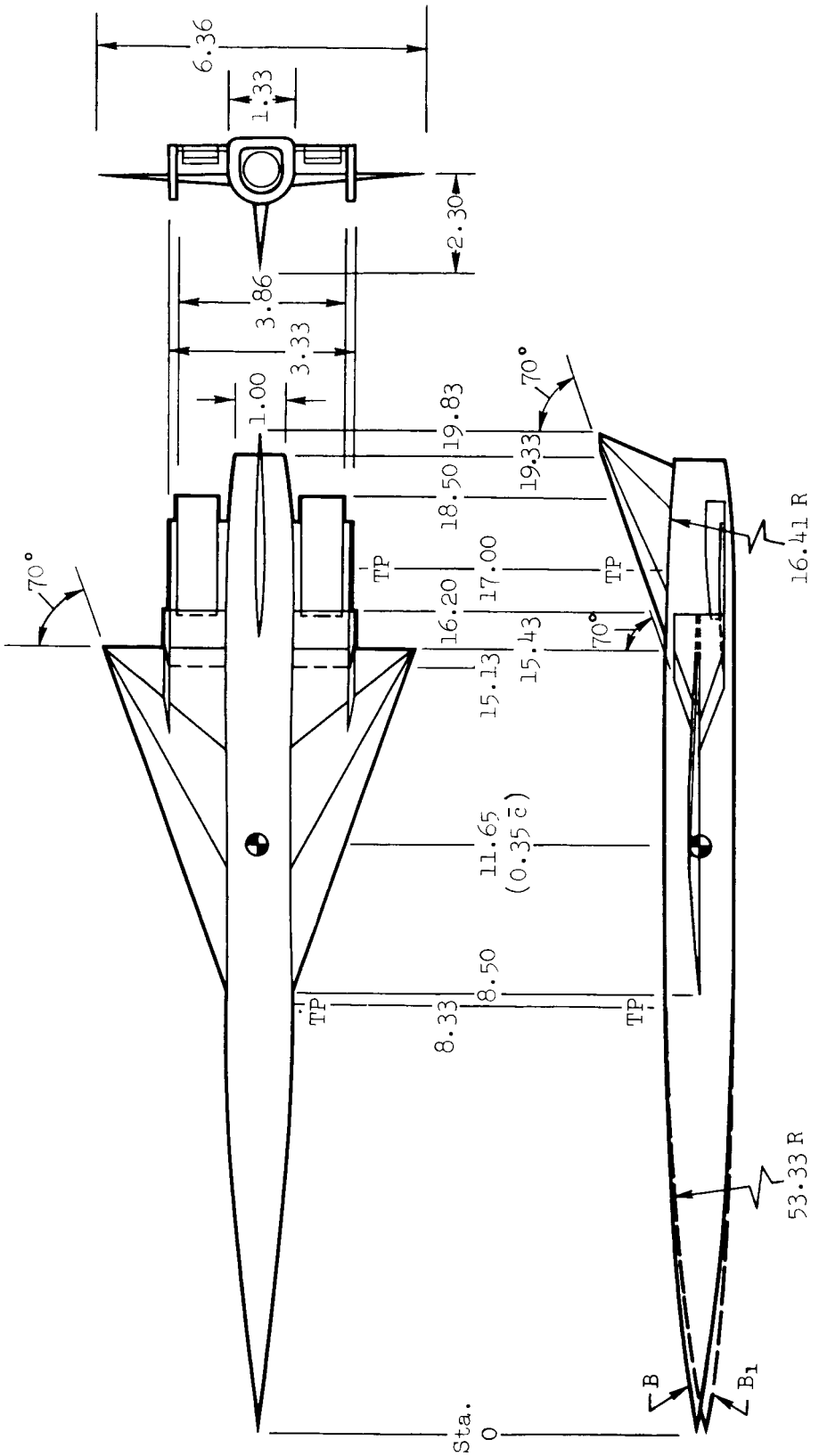


(c) Flat-bottom model

Figure 1.- Continued.

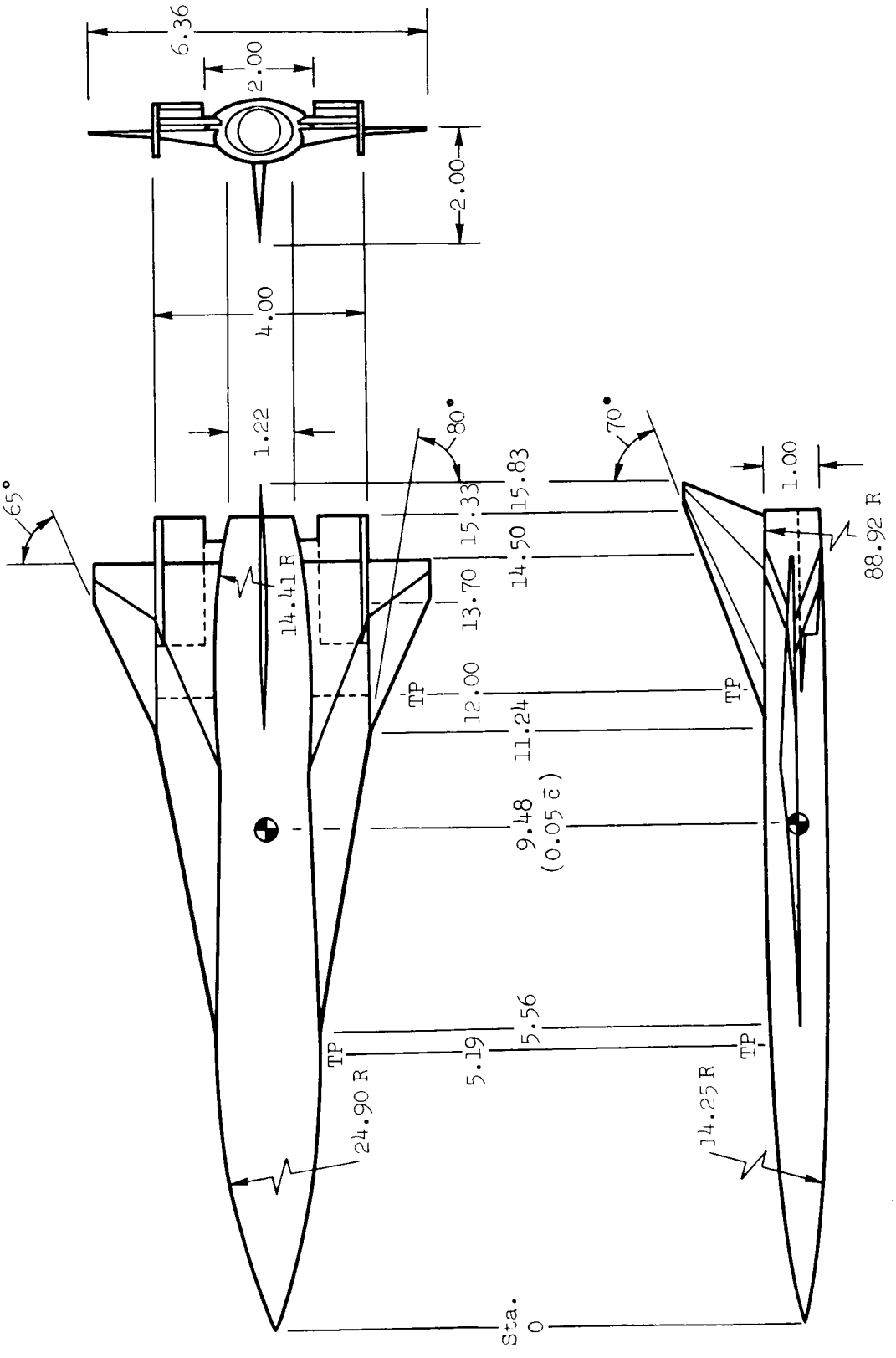


(d) Blended model

Figure 1.- Concluded.

Top View

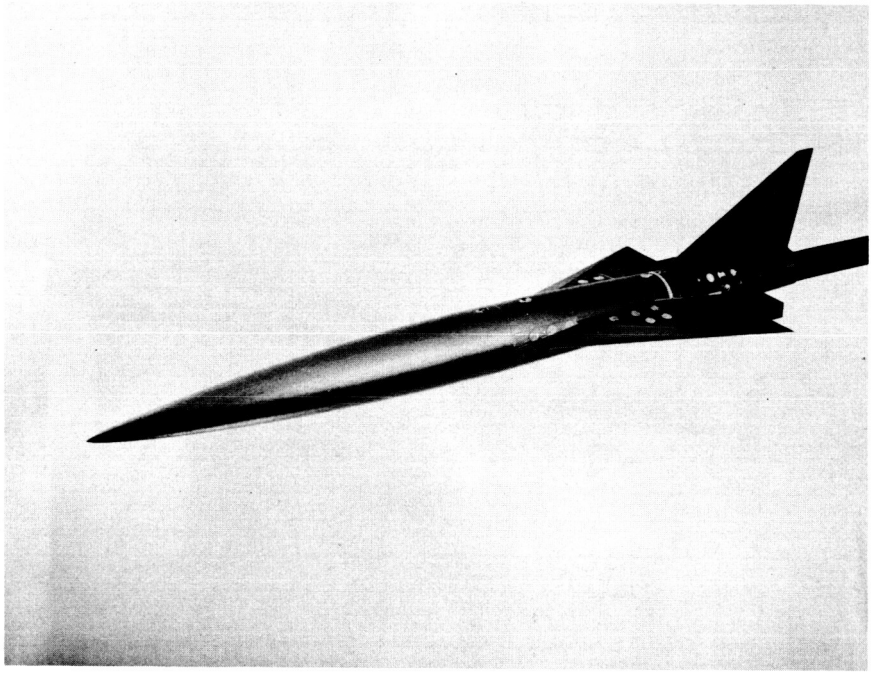

Bottom View

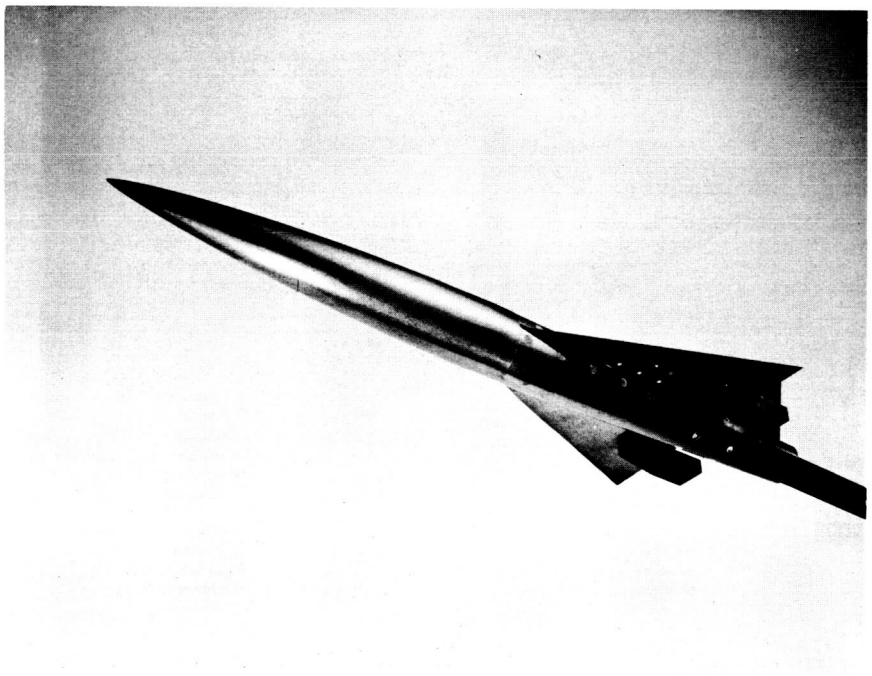

(a) Reference model with wing-mounted nacelles ($WBVN_1$)

Figure 2.- Model photographs.

Top View

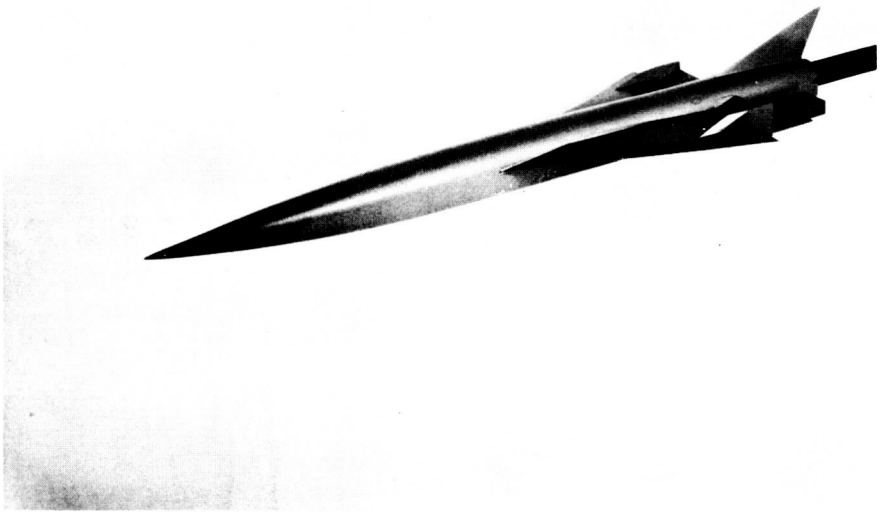

Bottom View

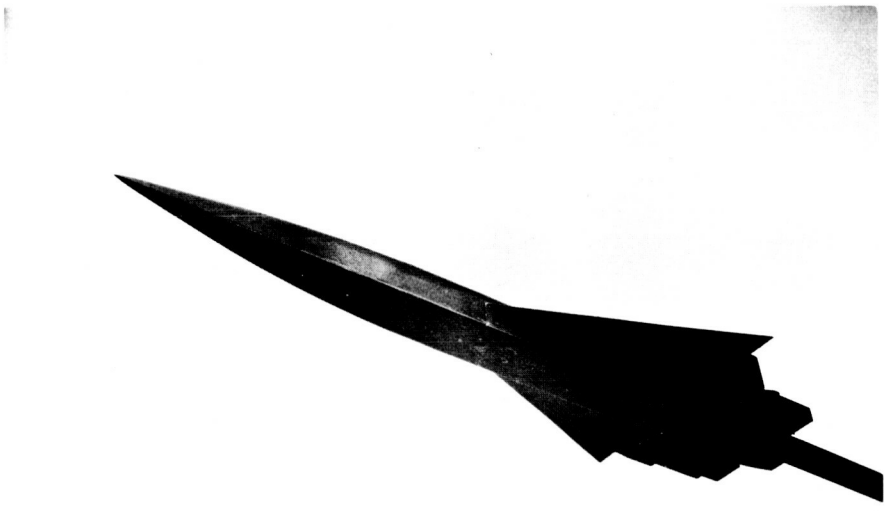

(b) Flat-bottom model ($W_1$BVRFN)

Figure 2.- Continued.

Top View

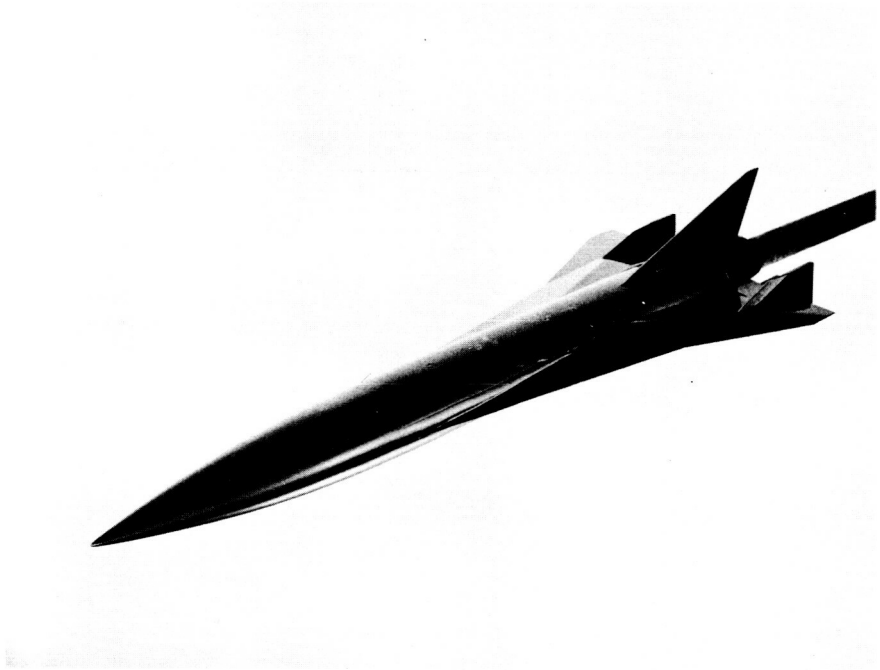

Bottom View

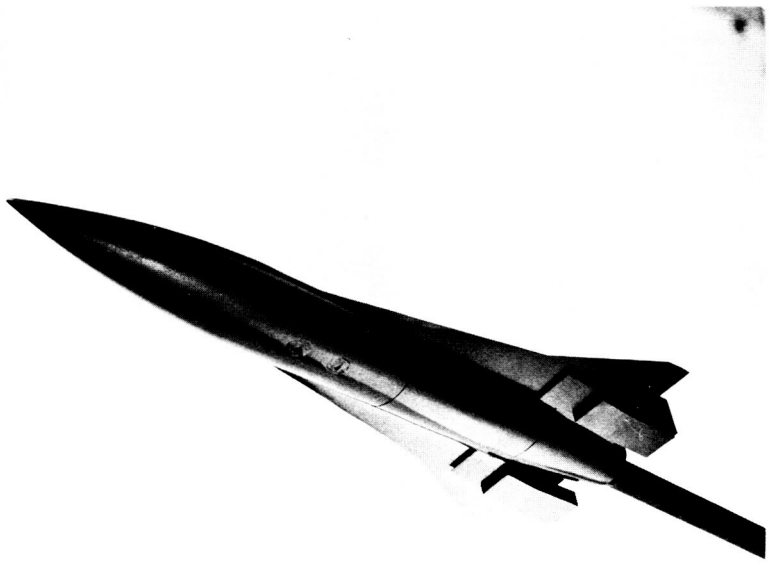

(c) Blended model ($W_1$BVRN)

Figure 2.- Concluded.

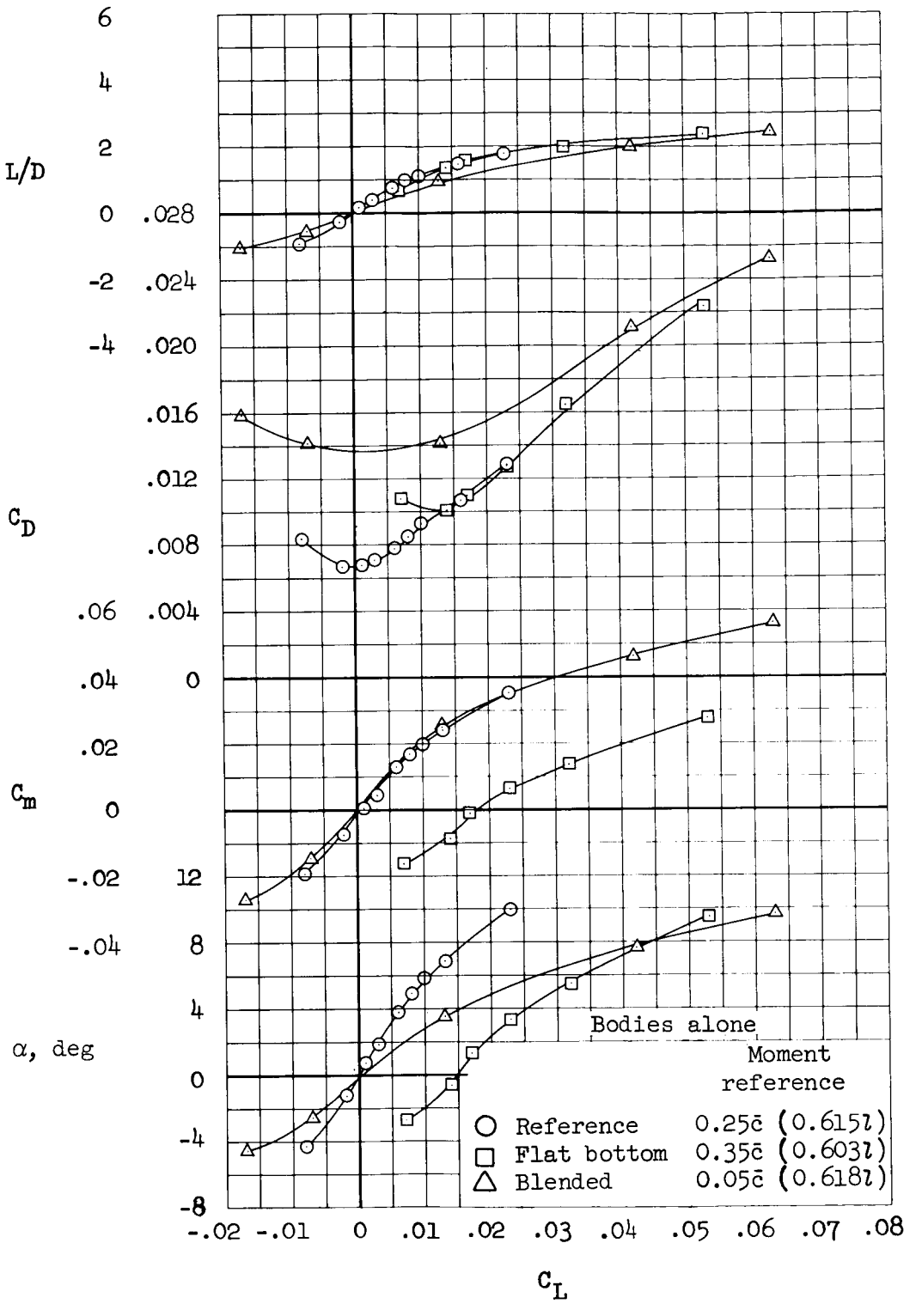


(a) M = 1.10

Figure 3.- Longitudinal aerodynamic characteristics of the bodies alone; based on wing reference area.

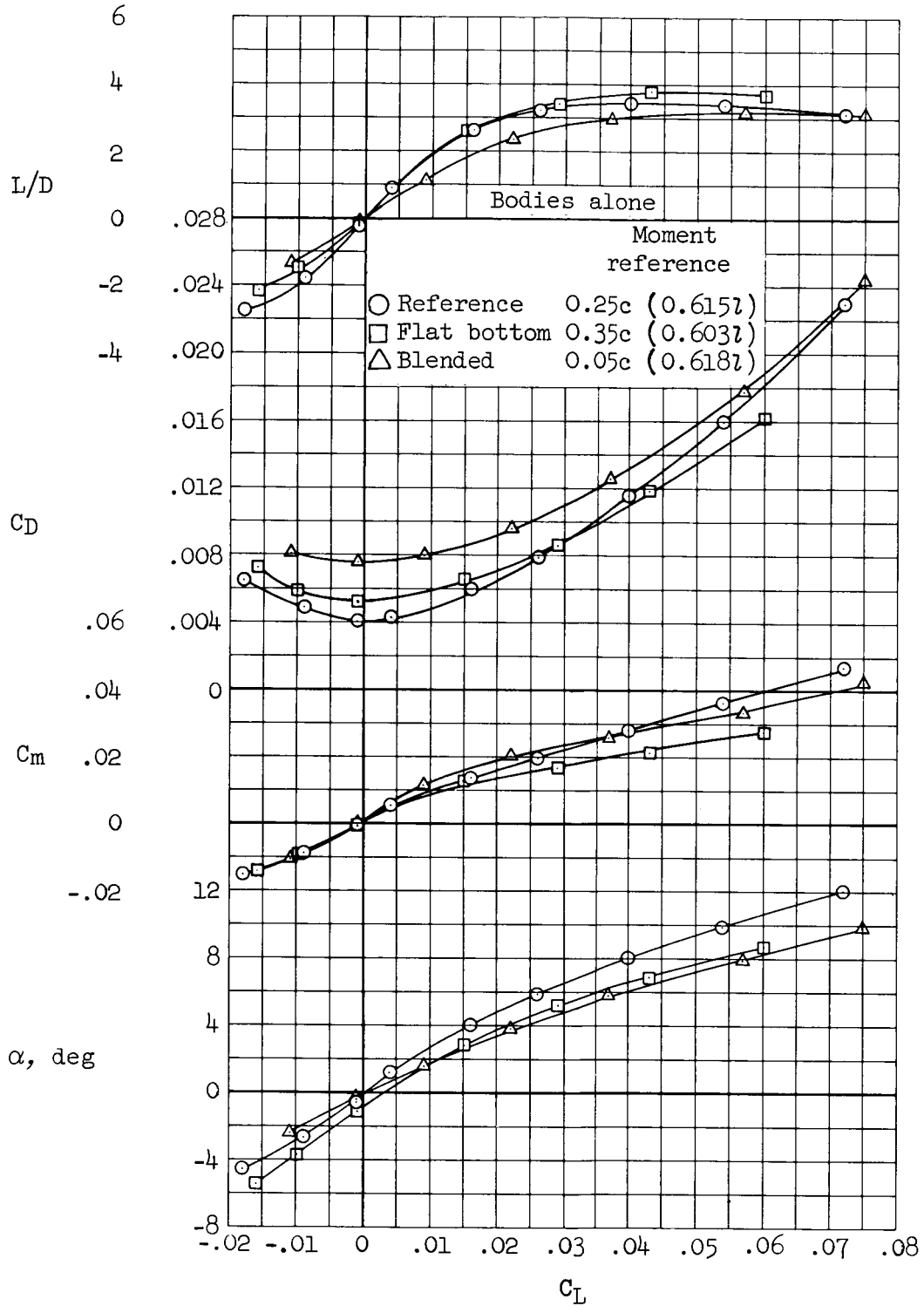


(b) M = 5.31

Figure 3.- Continued.

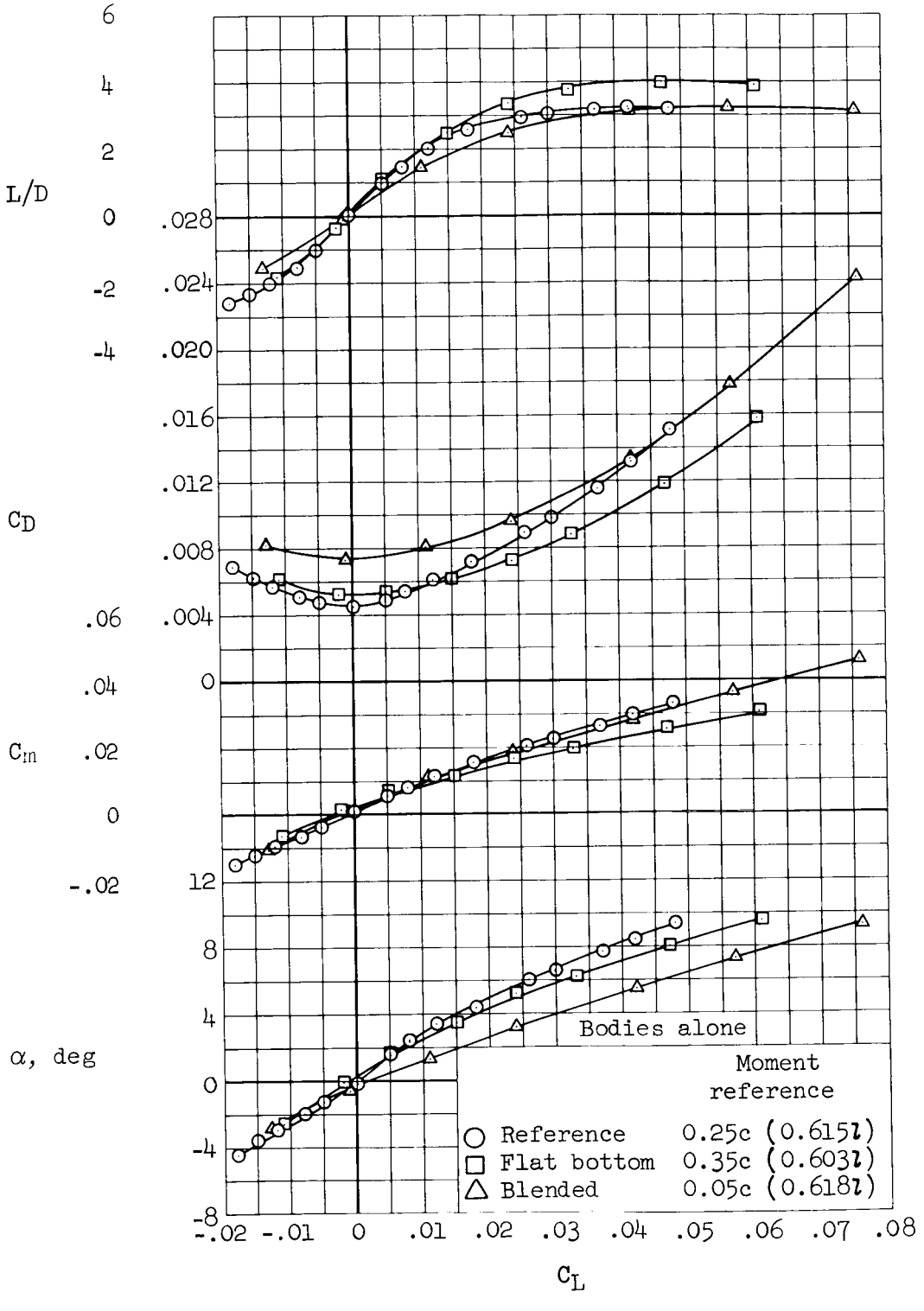


(c) M = 7.42

Figure 3.- Continued.

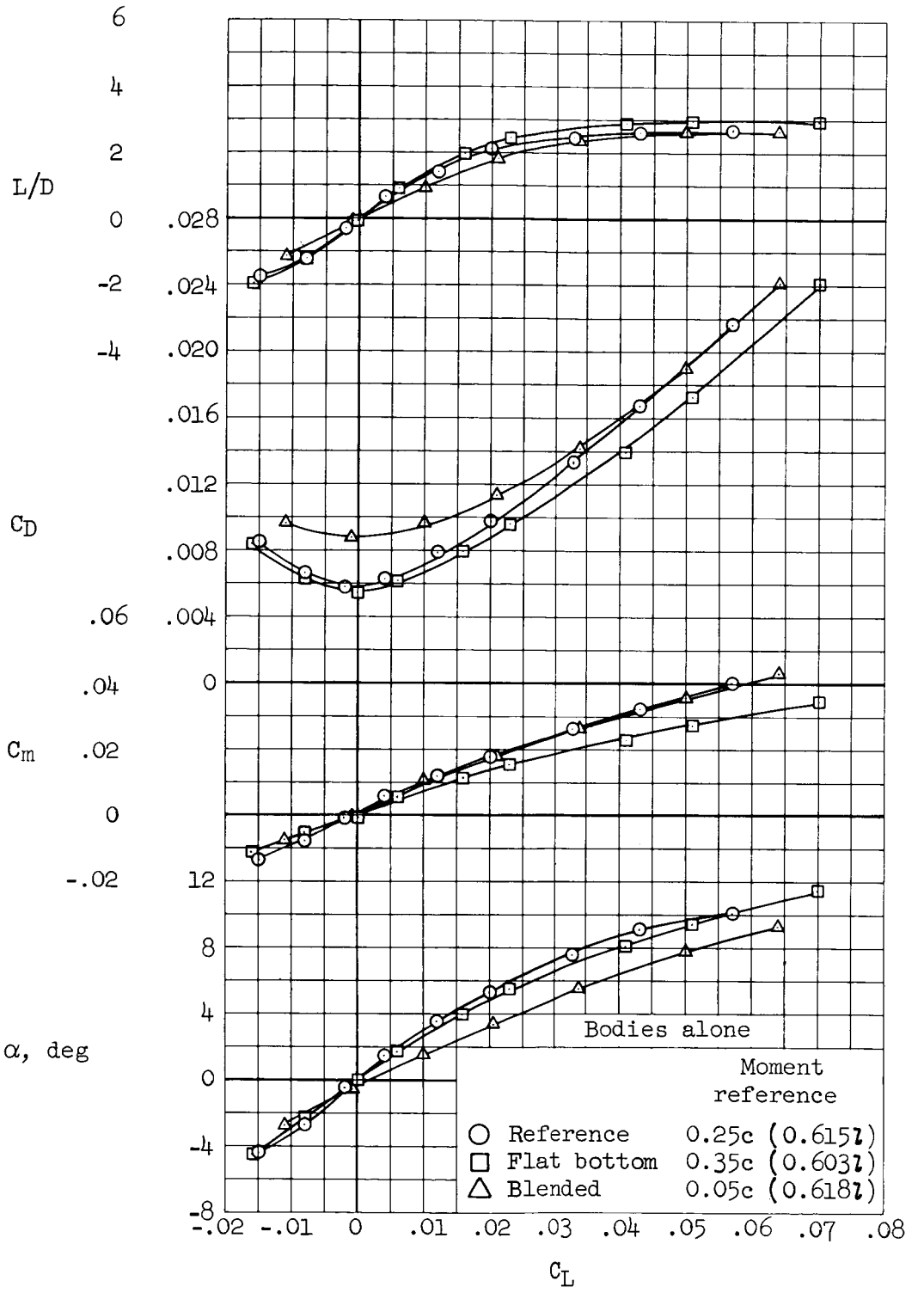


(d) M = 10.70

Figure 3.- Concluded.

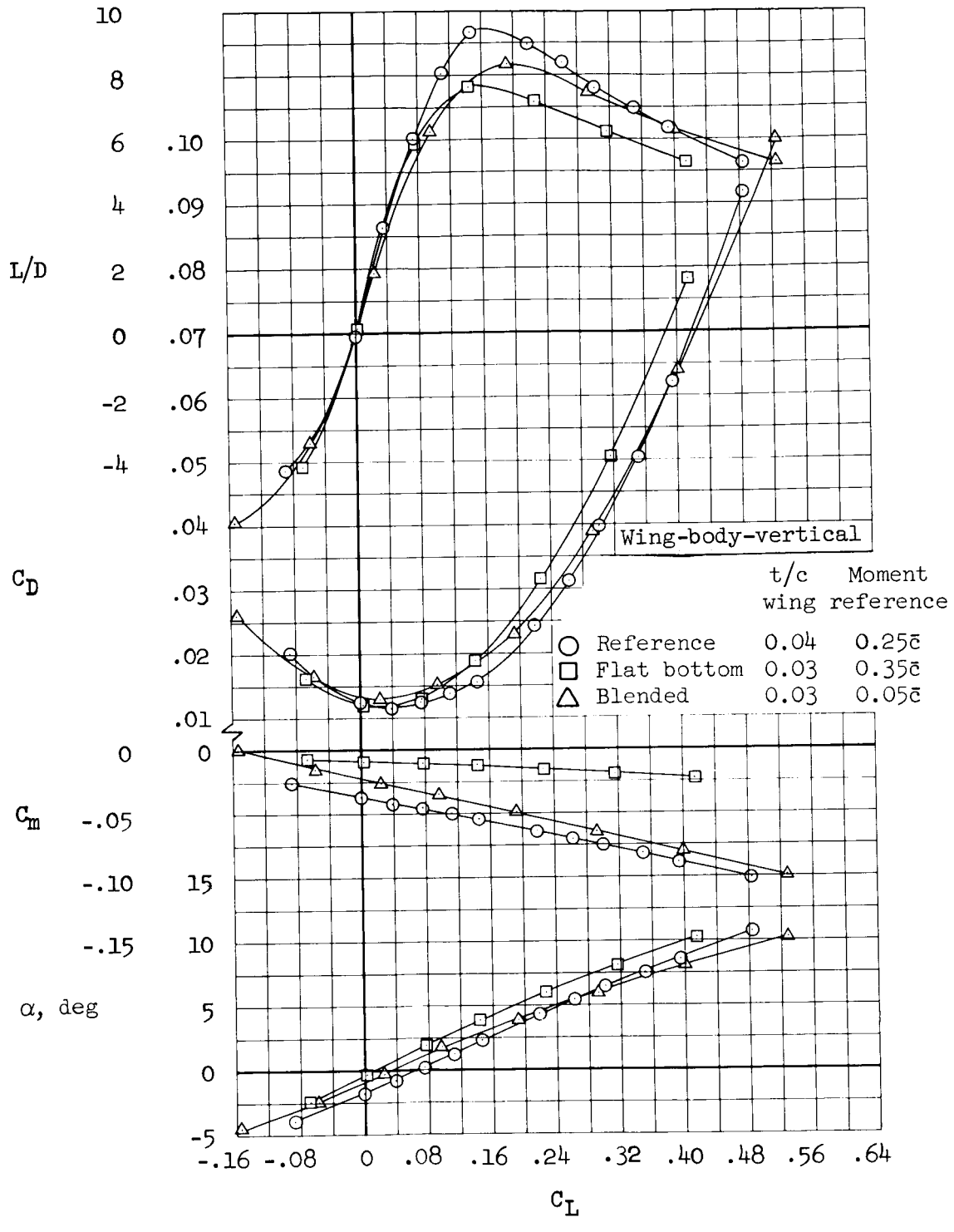


(a) M = 0.65

Figure 4.- Longitudinal aerodynamic characteristics of the wing-body-vertical tail configurations.

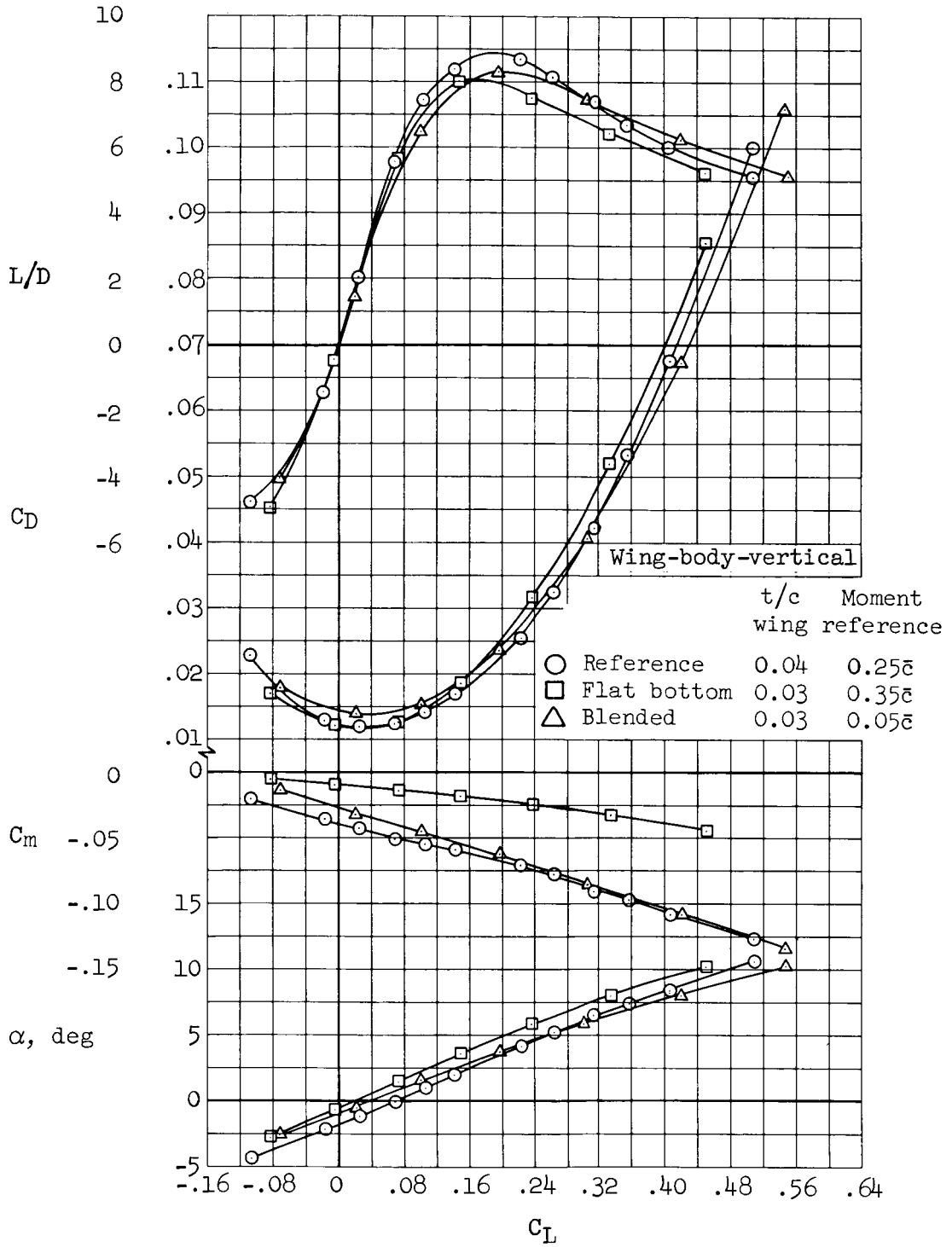


(b) M = 0.90

Figure 4.- Continued.

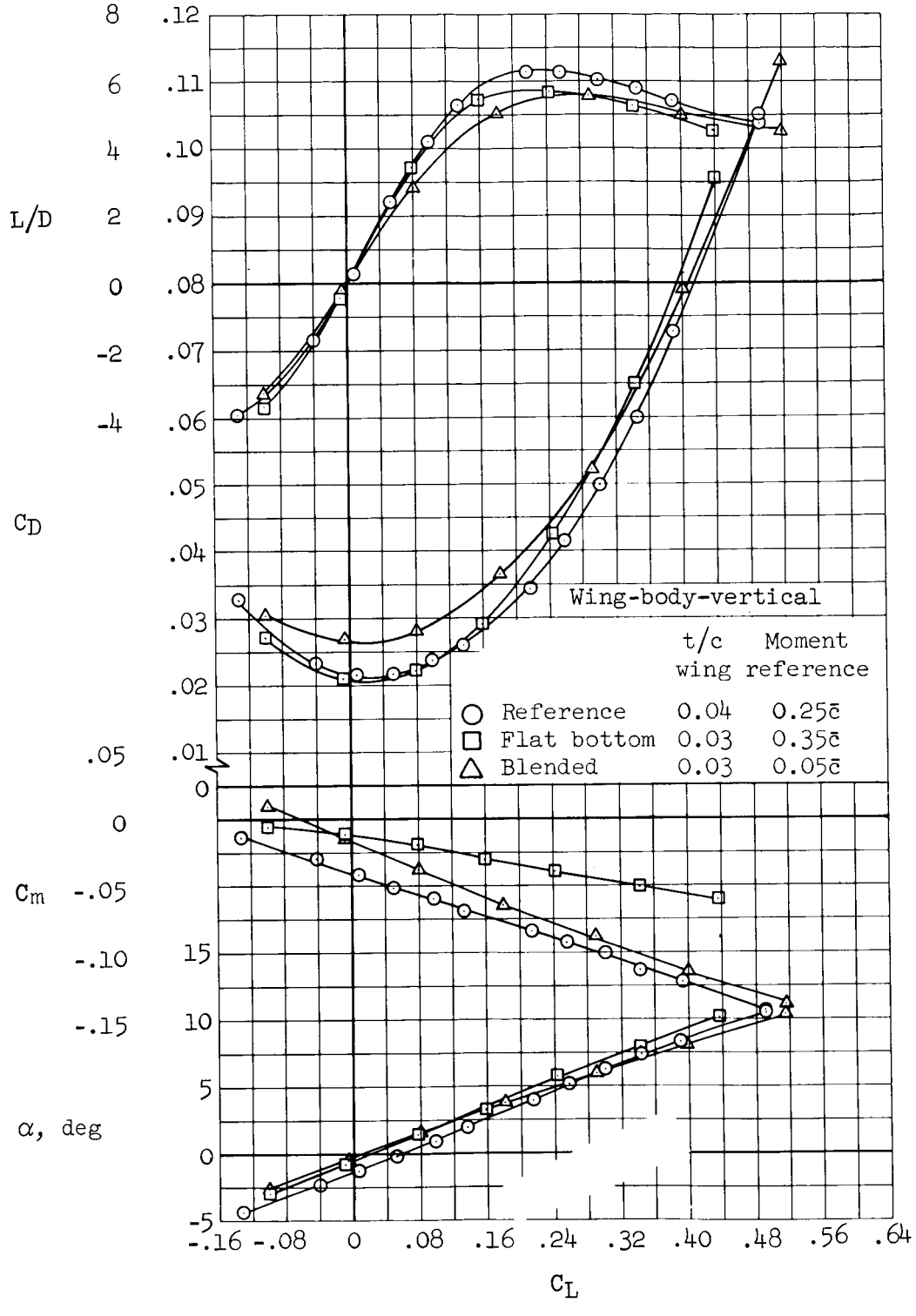


(c) M = 1.10

Figure 4.- Continued.

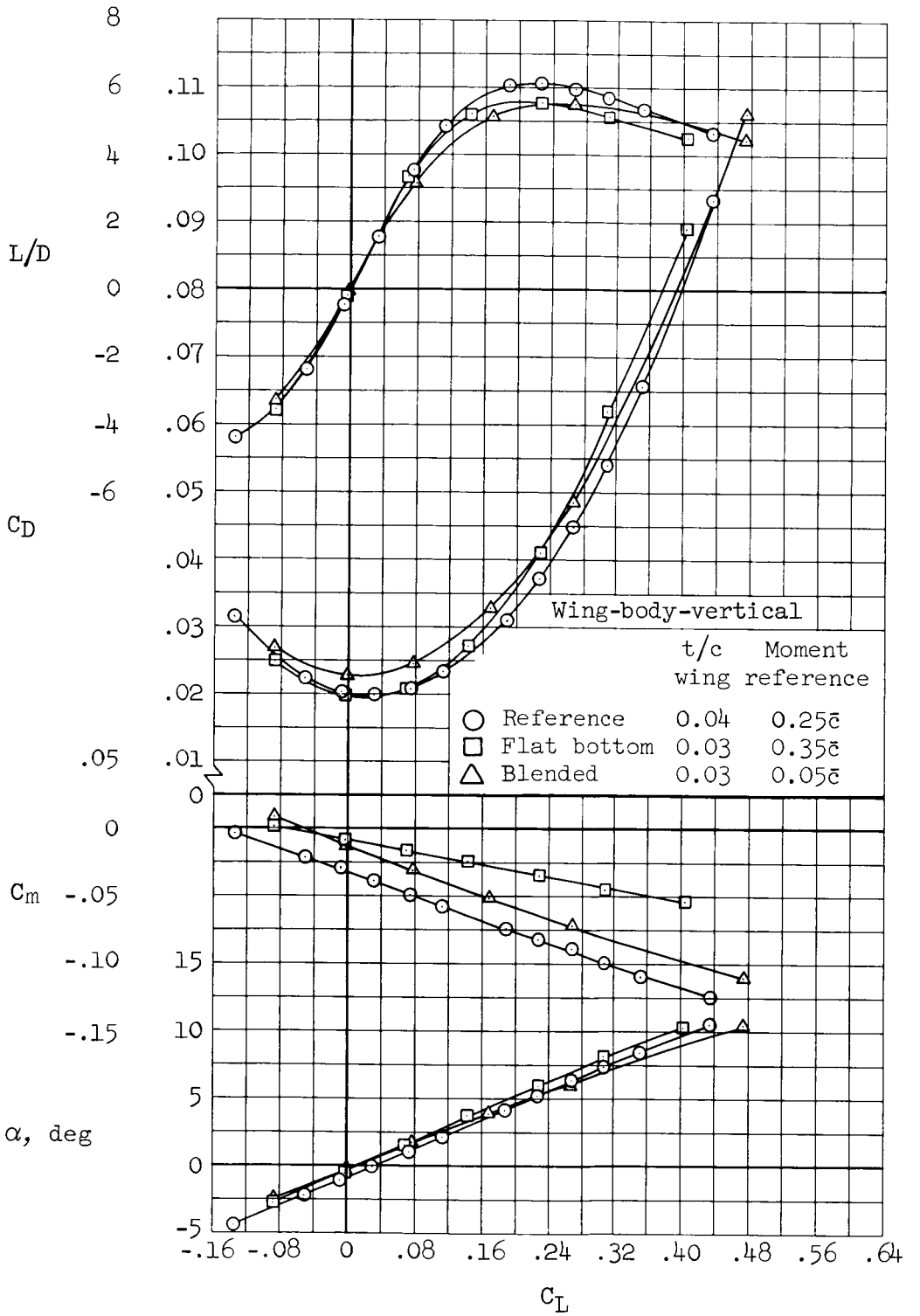


(d) M = 1.30

Figure 4. Continued.

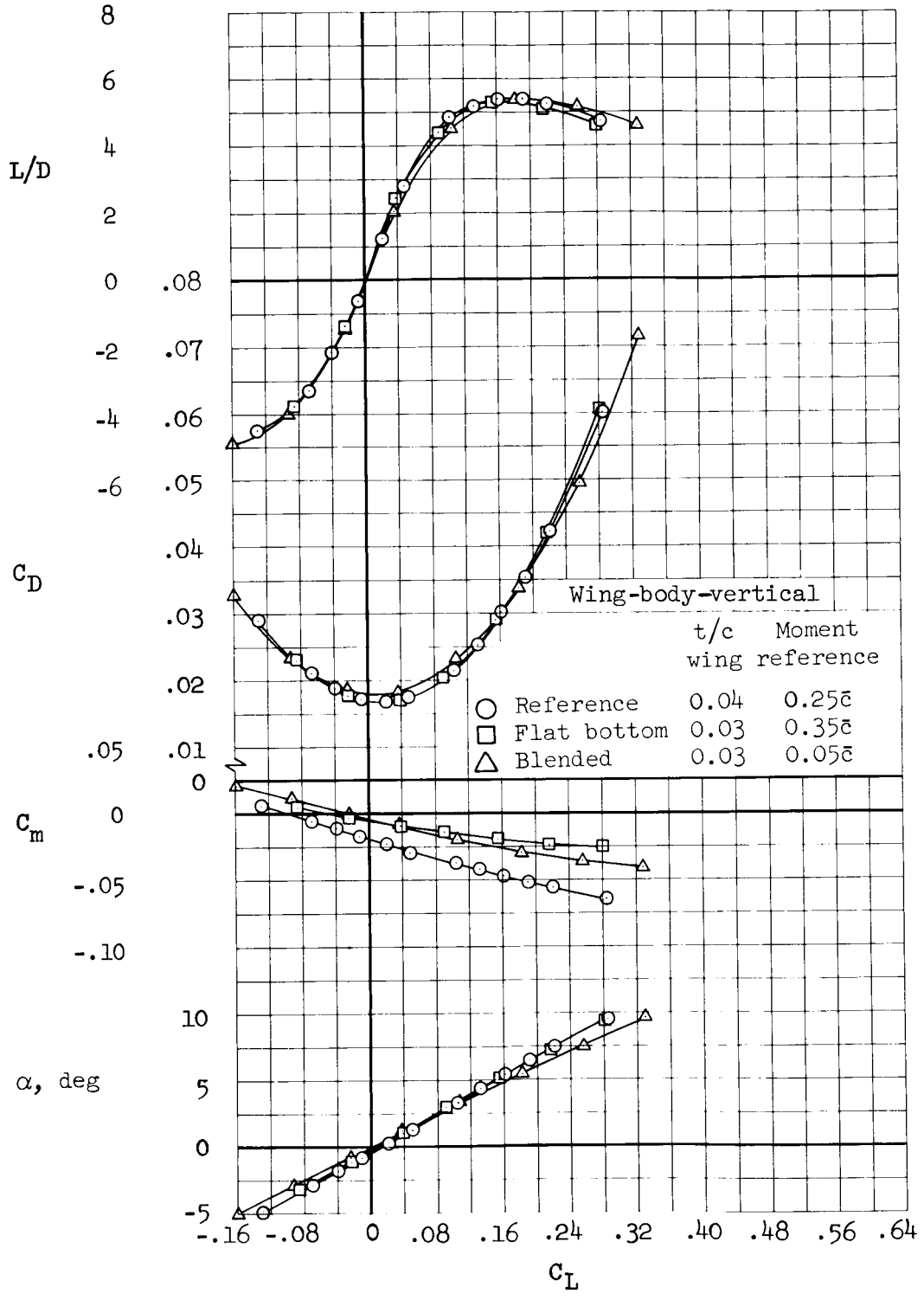


(e) M = 1.99

Figure 4.- Continued.

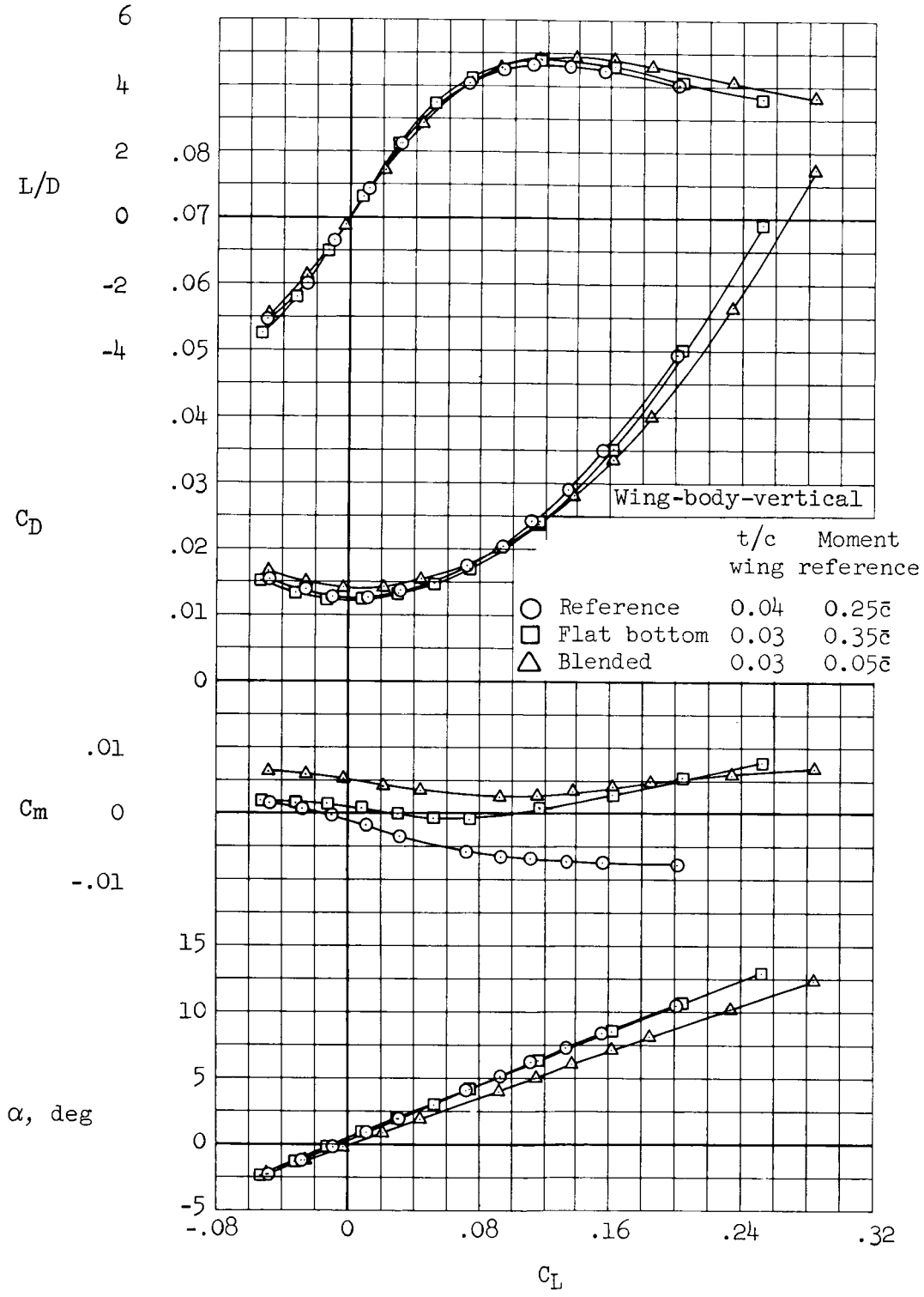


(f) M = 3.88

Figure 4.- Continued.

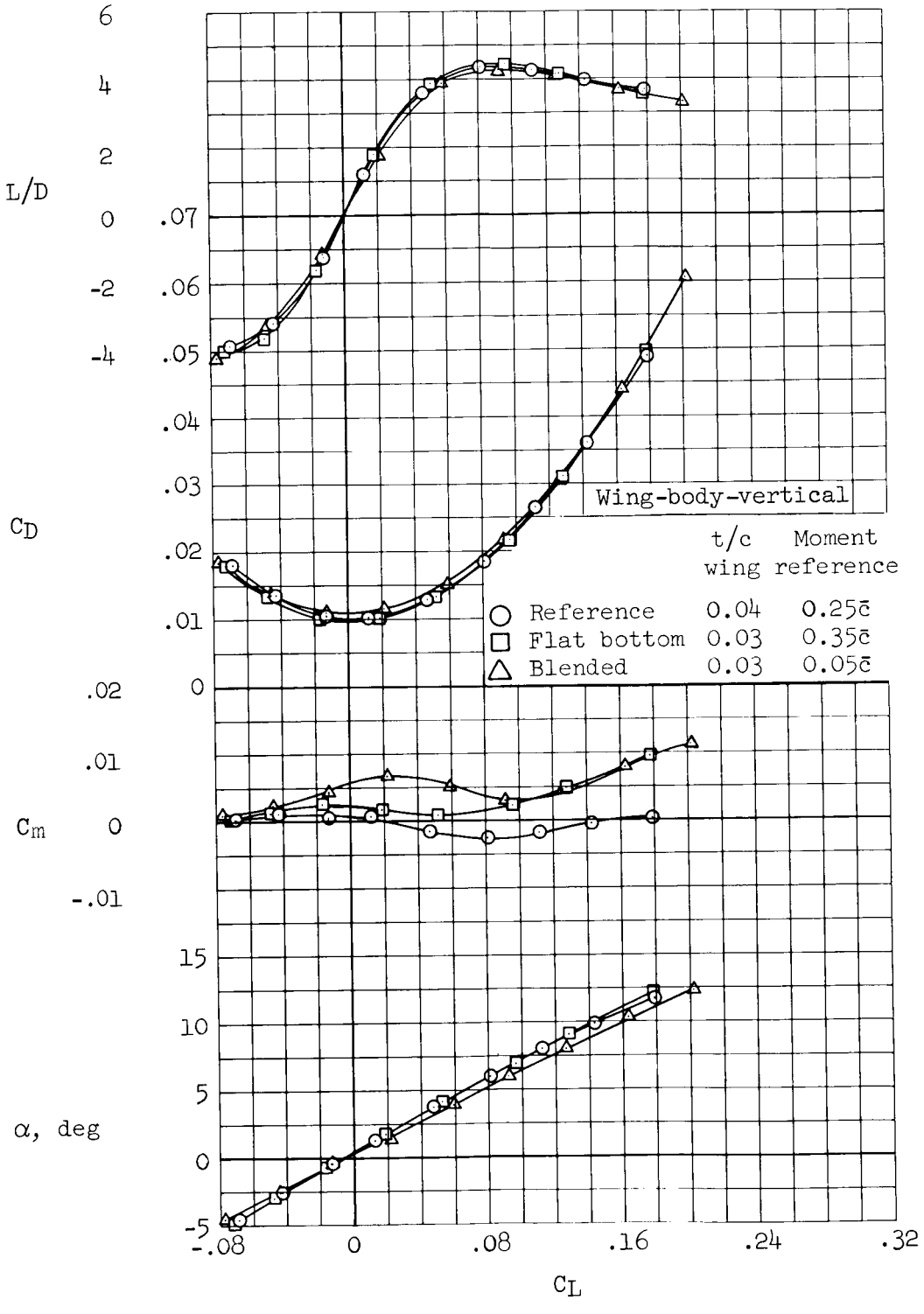


(g) M = 5.31

Figure 4.- Continued.

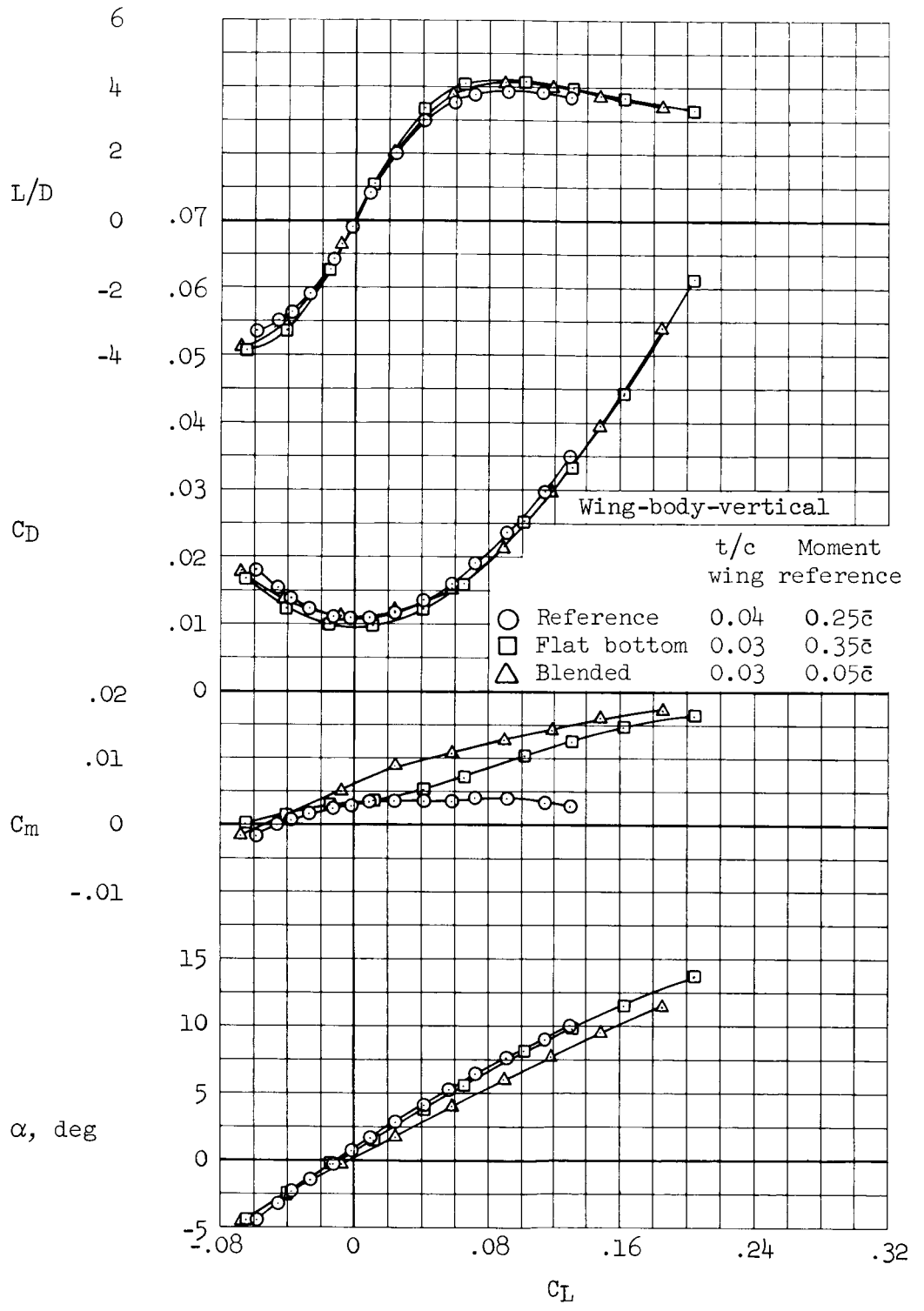


(h) M = 7.42

Figure 4.- Continued.

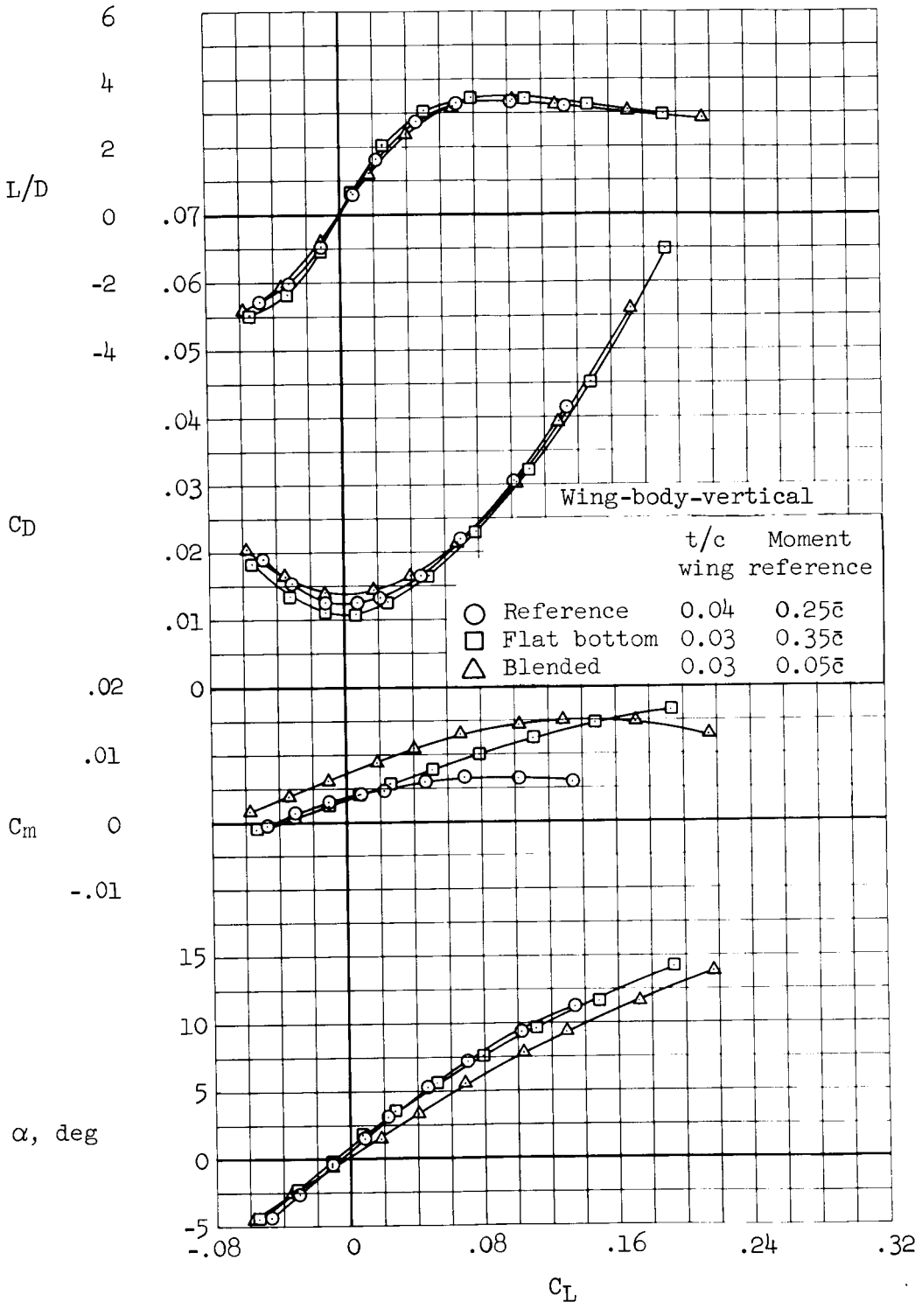


(i) M = 10.70

Figure 4.- Concluded.

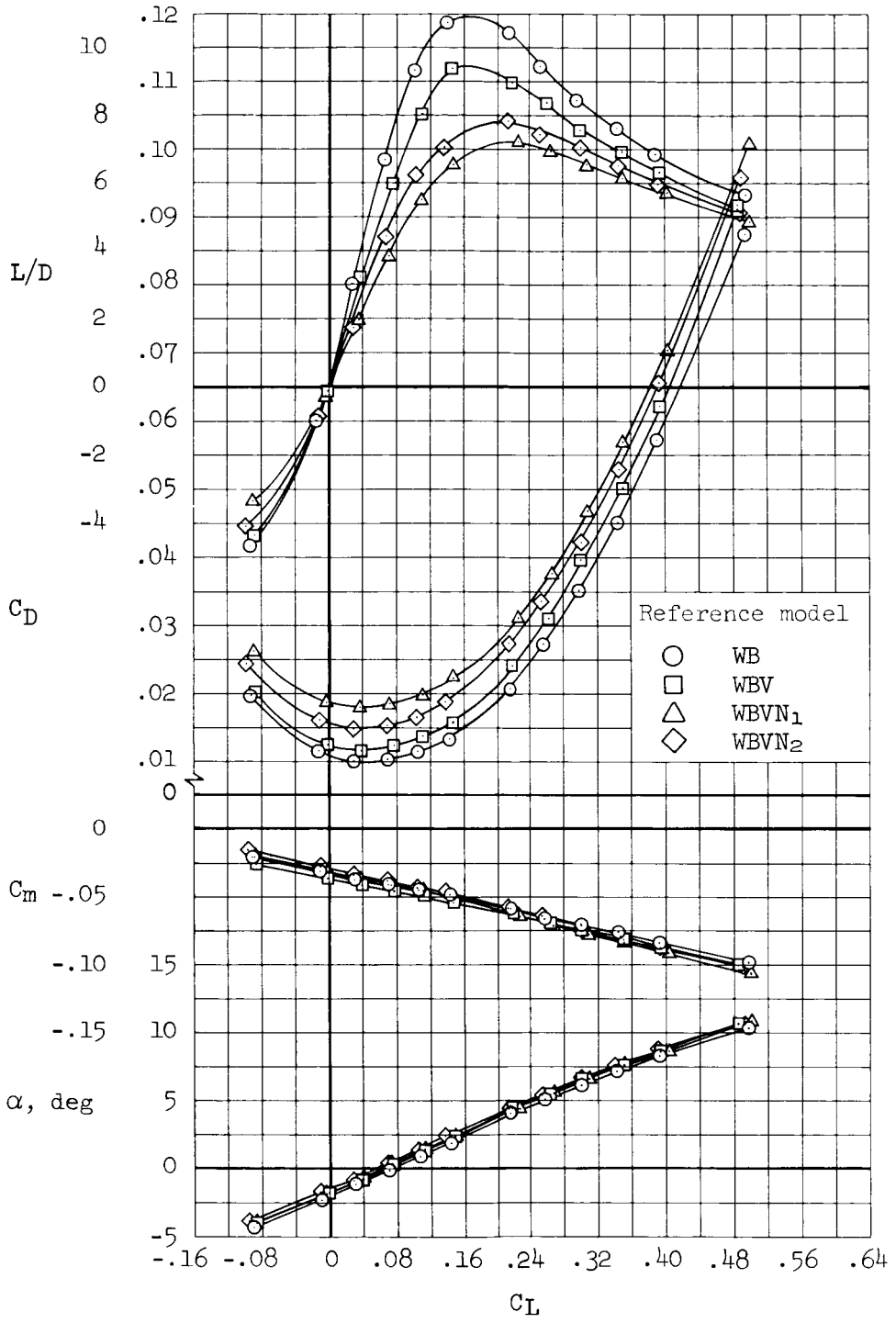


(a) M = 0.65

Figure 5.- Longitudinal aerodynamic characteristics of the reference configuration; uncorrected for nacelle stream-tube drag and nacelle base drag; moment reference at 0.25$\bar{c}$.

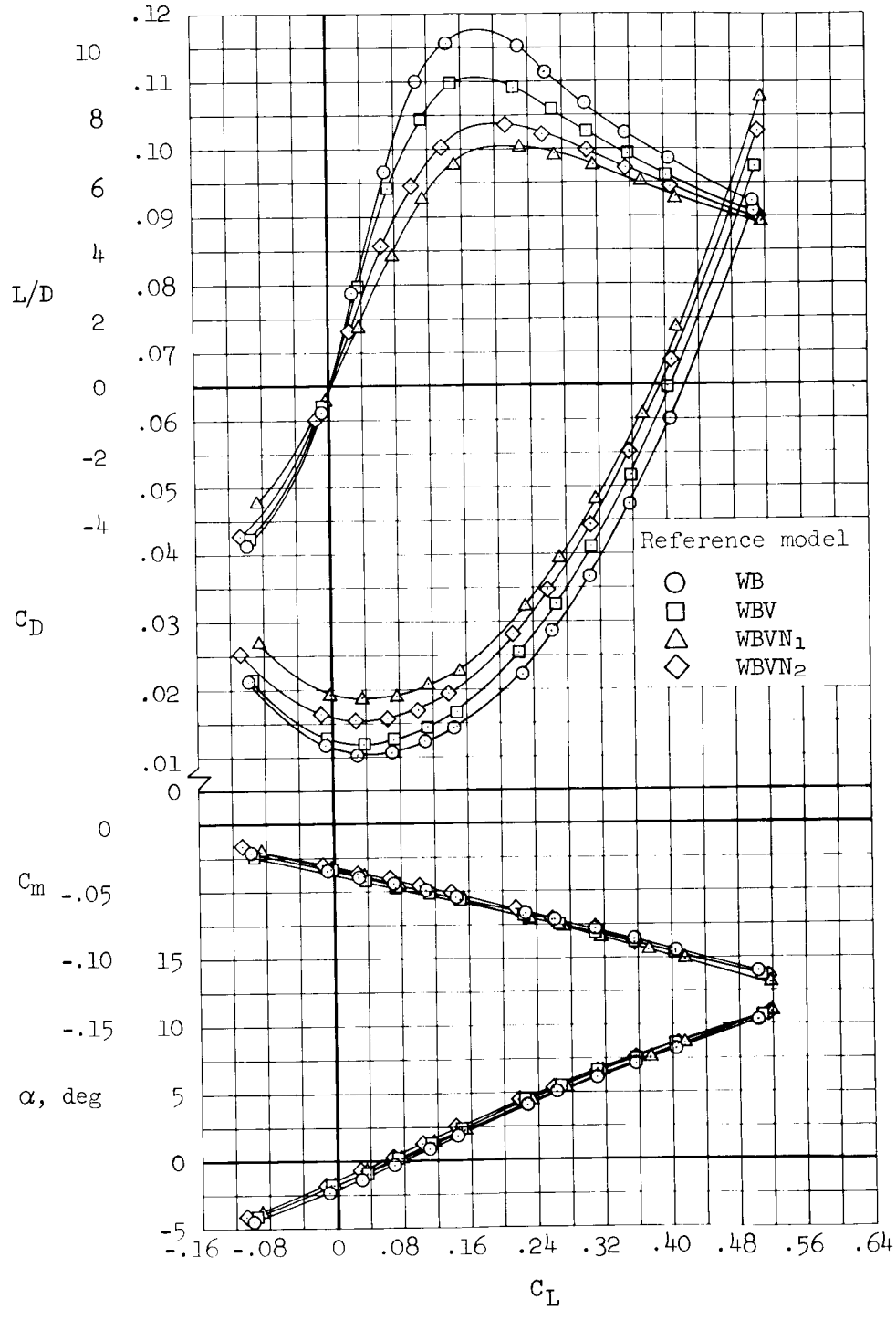


(b) M = 0.80

Figure 5.- Continued.

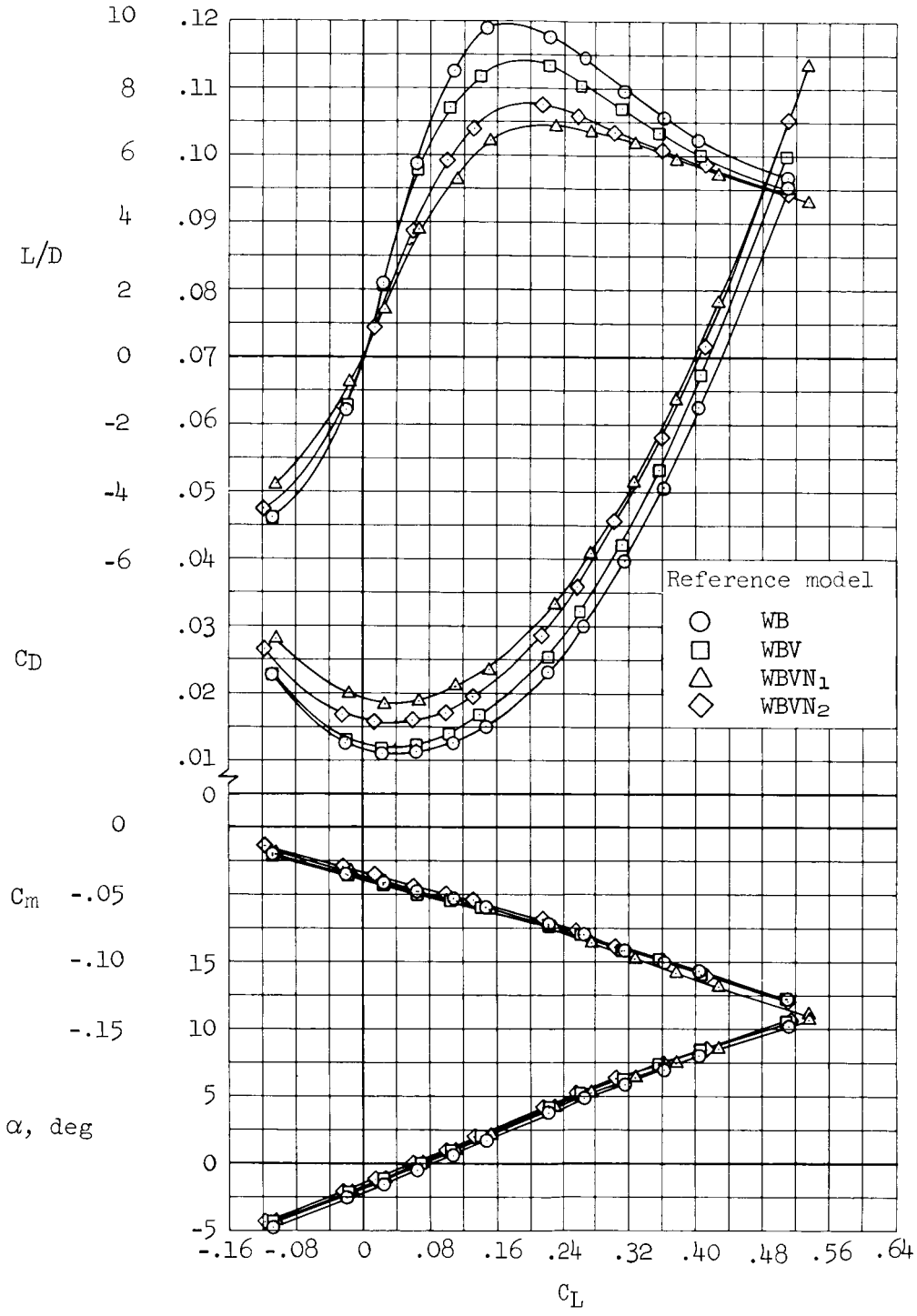


(c) M = 0.90

Figure 5.- Continued.

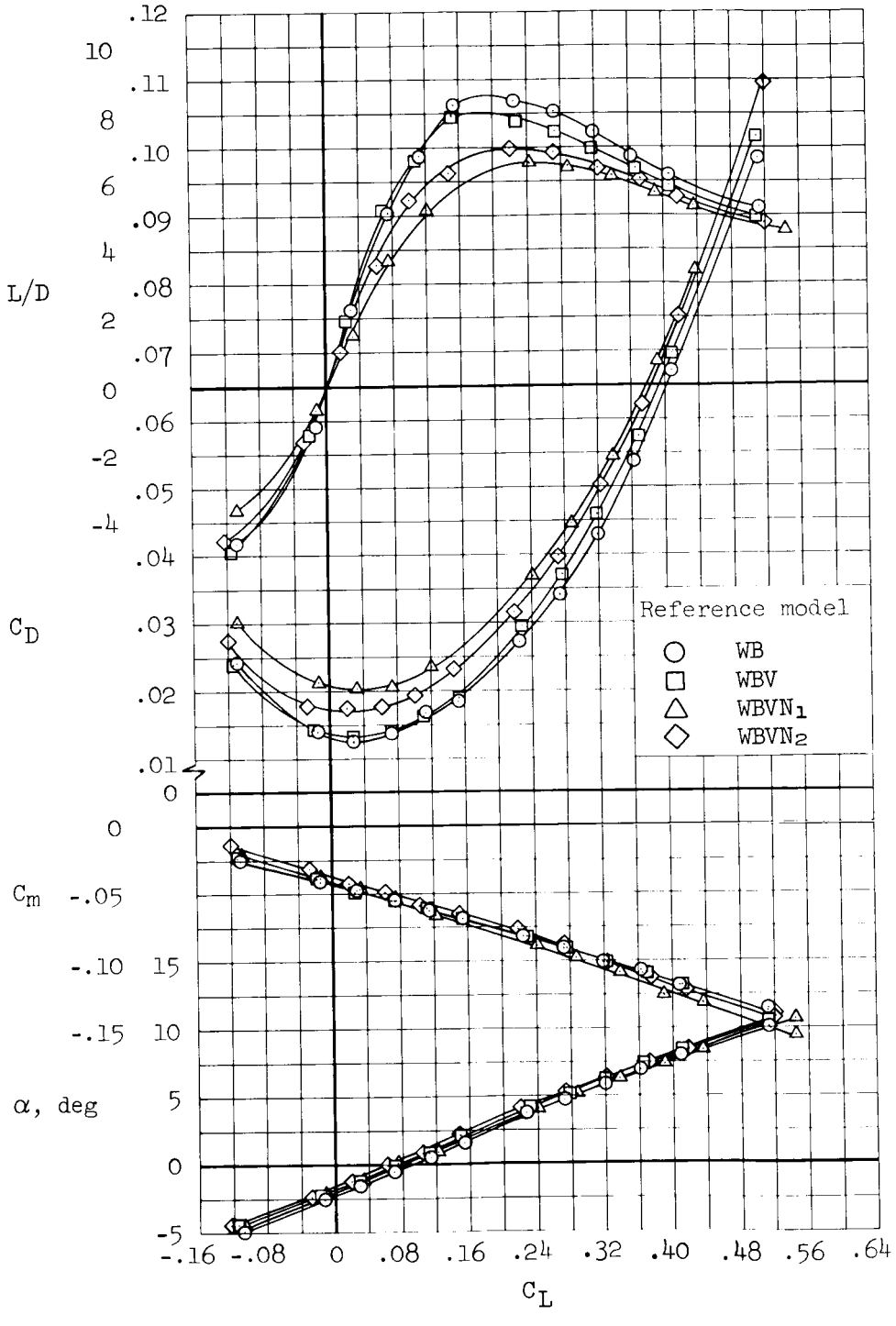


(d) M = 0.95

Figure 5.- Continued.

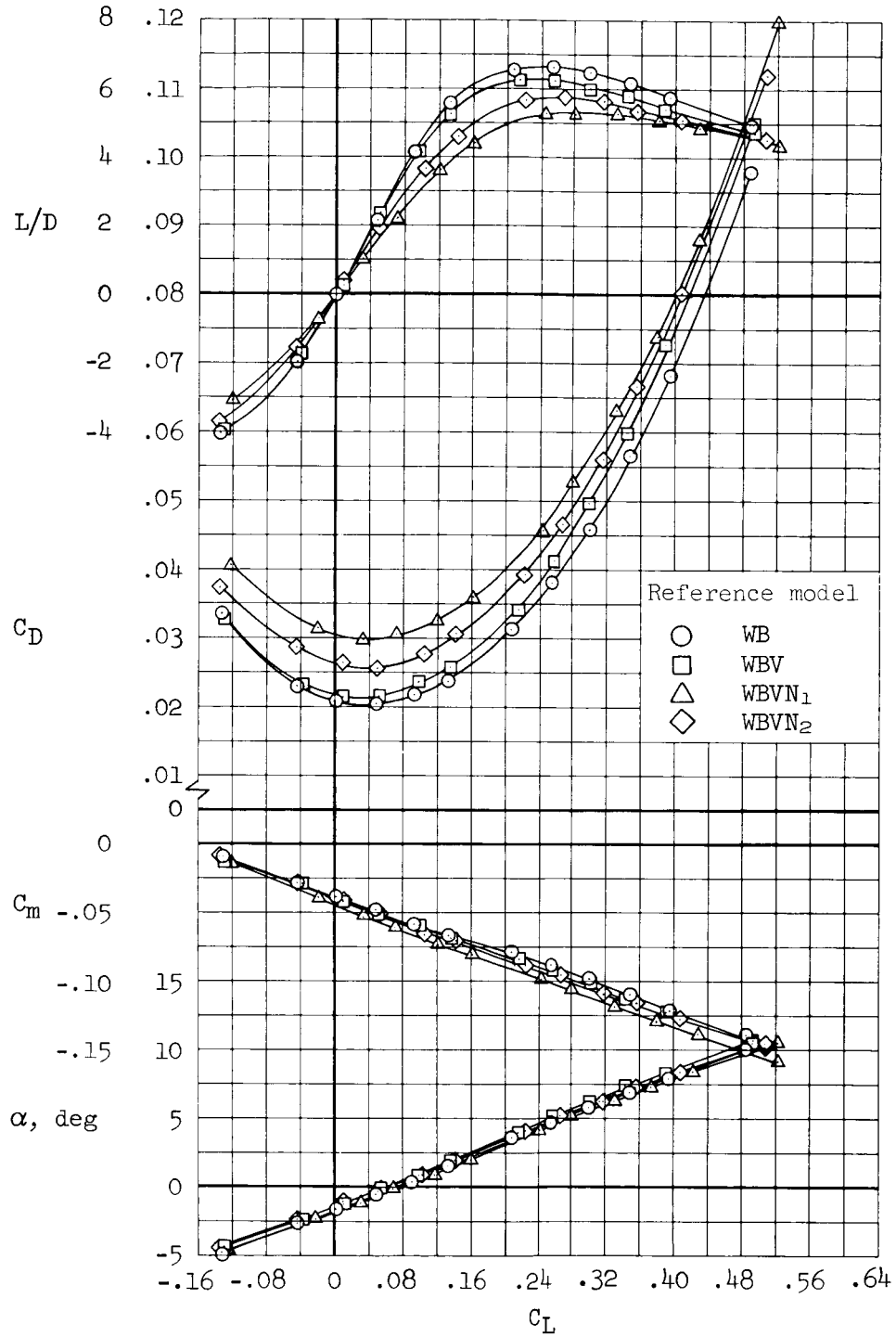


(e) M = 1.10

Figure 5.- Continued.

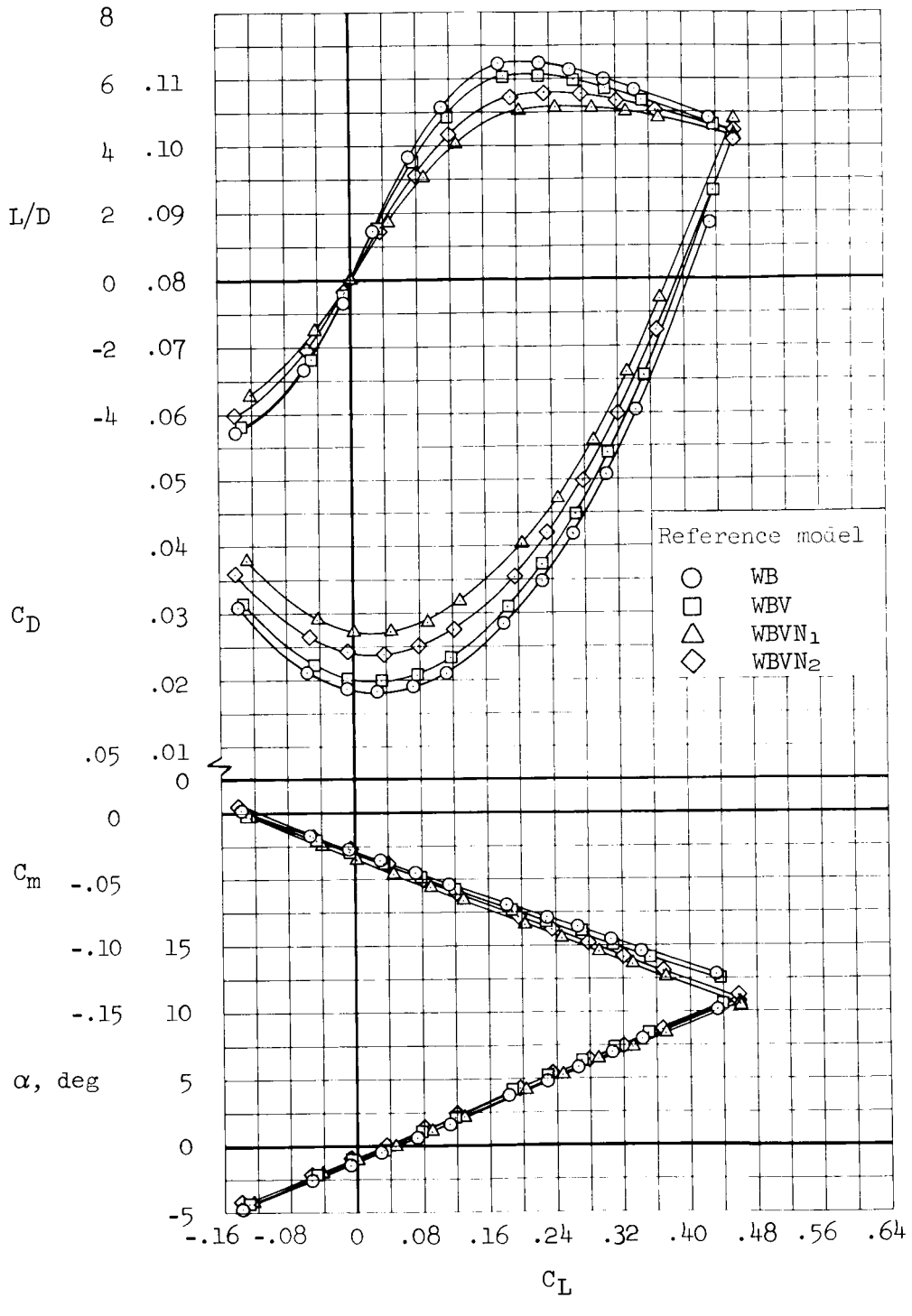


(f) M = 1.30

Figure 5.- Continued.

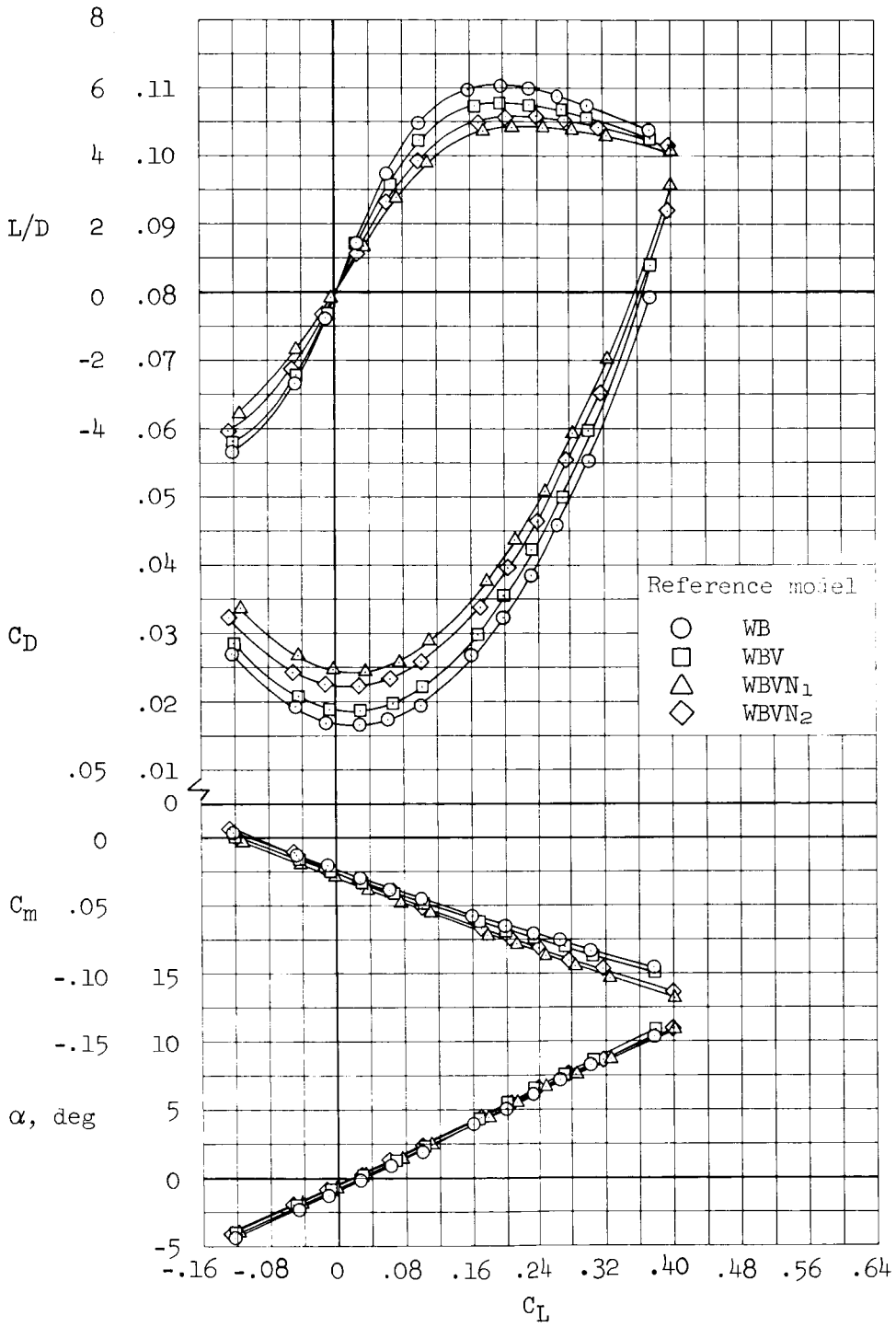


(g) M = 1.59

Figure 5.- Continued.

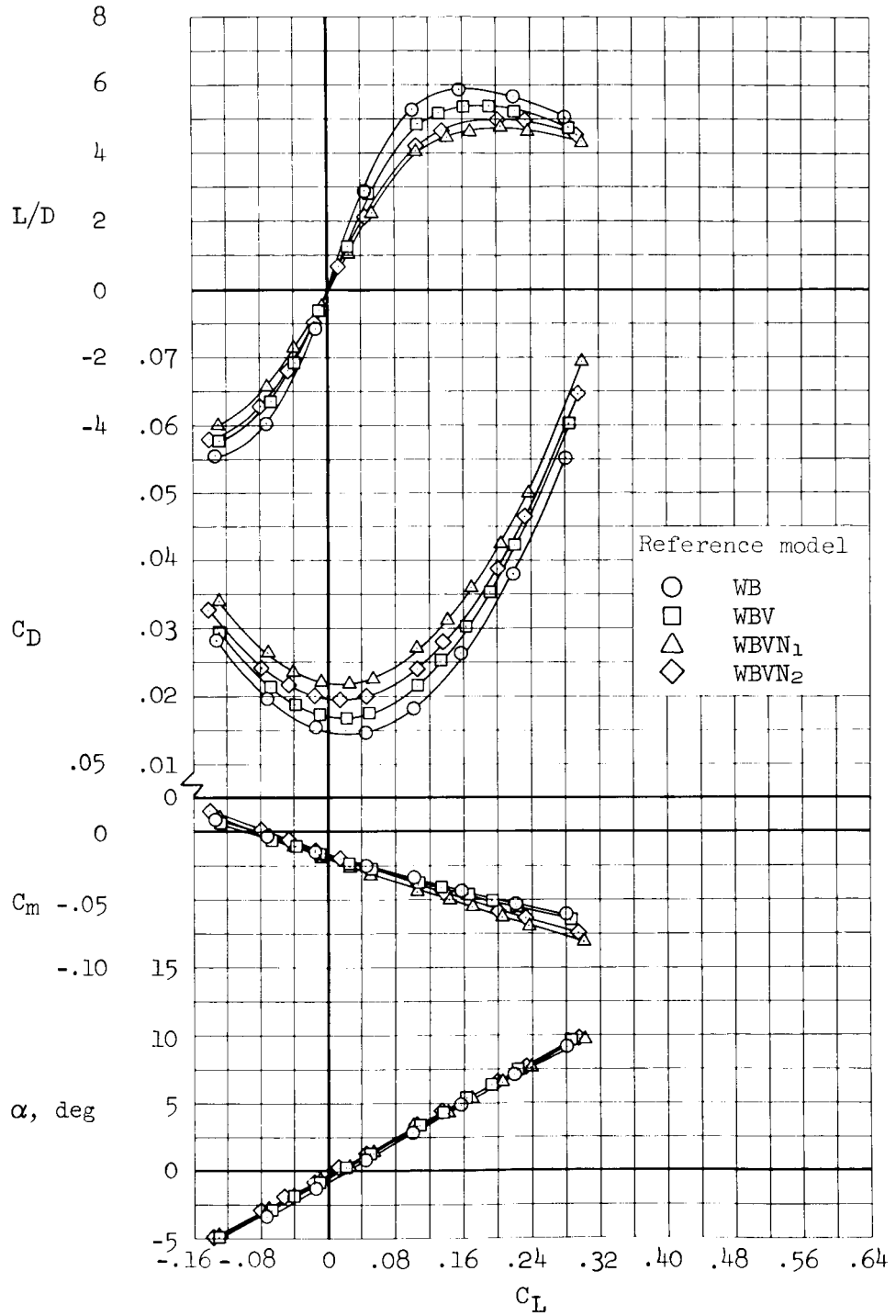


(h) M = 1.99

Figure 5.- Continued.

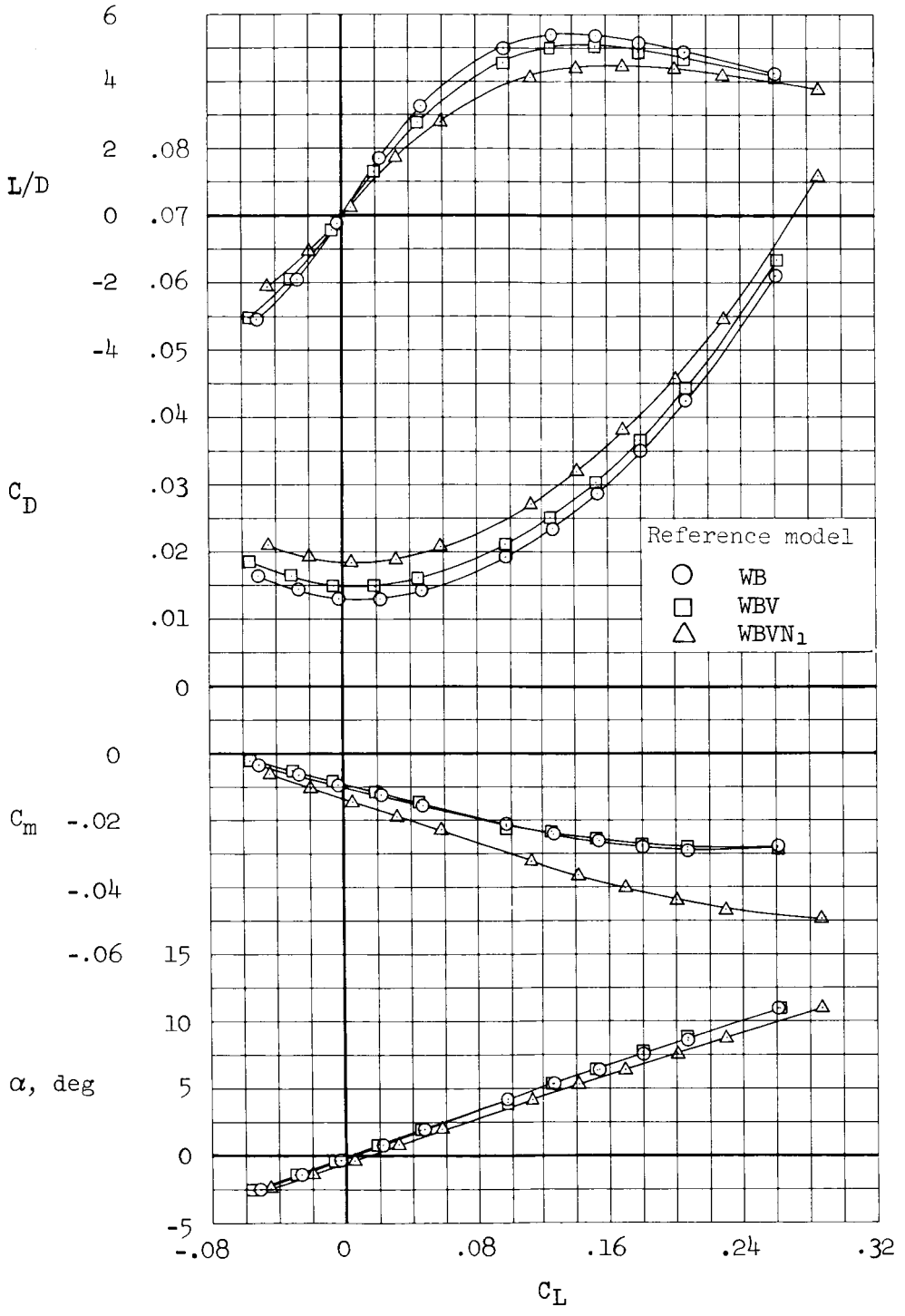


(i) M = 2.93

Figure 5.- Continued.

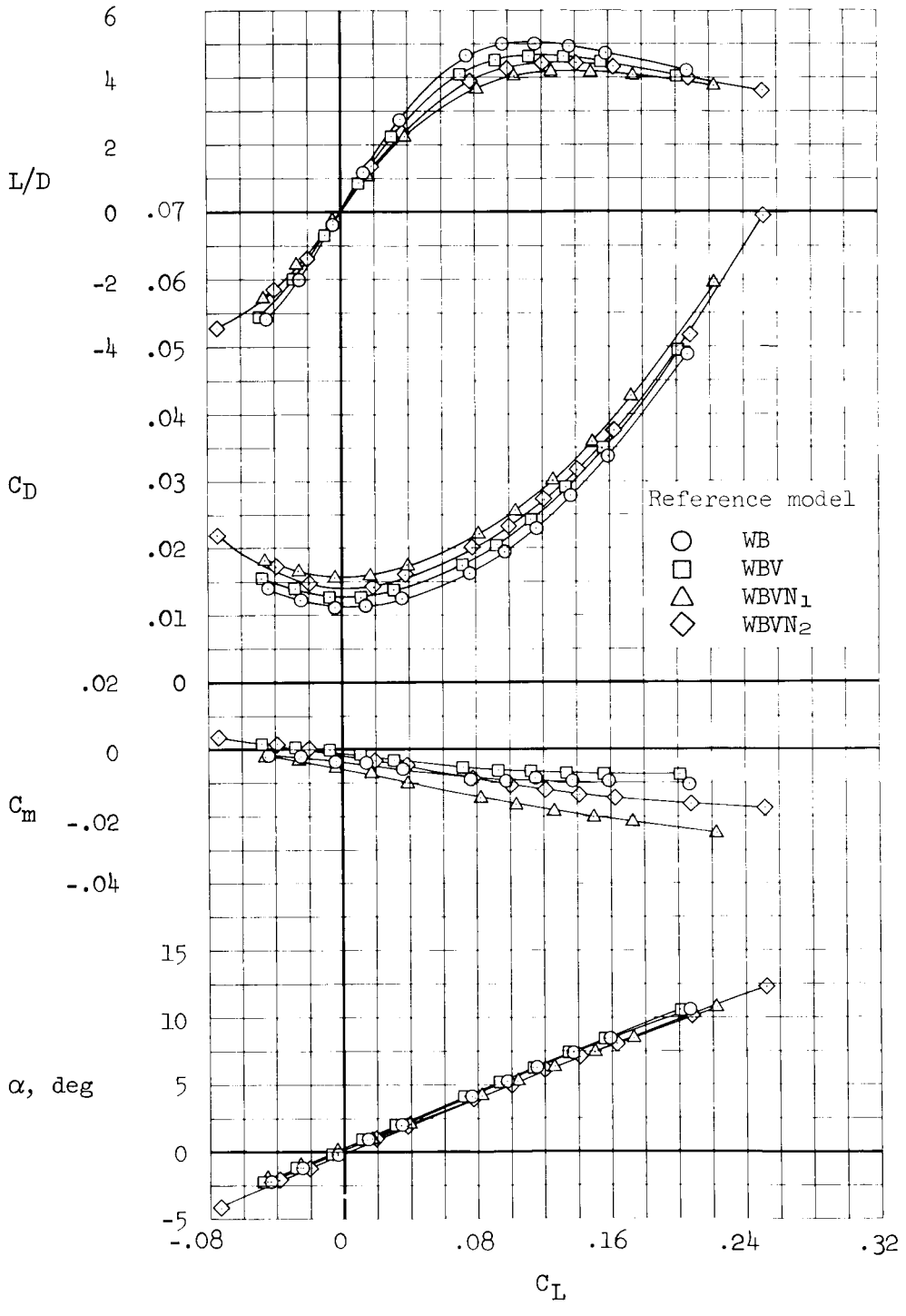


(j) M = 3.88

Figure 5.- Continued.

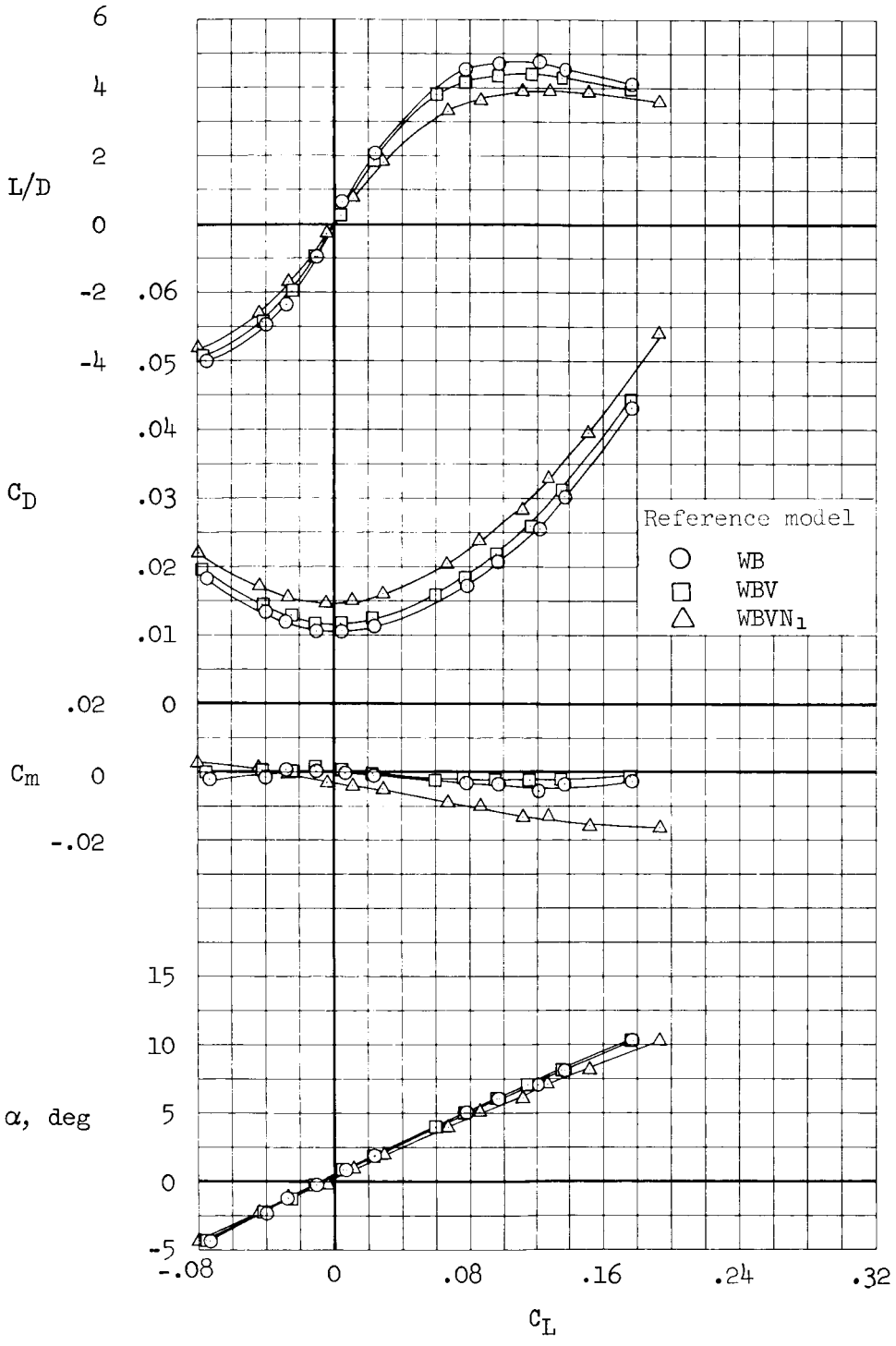


(k) M = 4.81

Figure 5.- Continued.

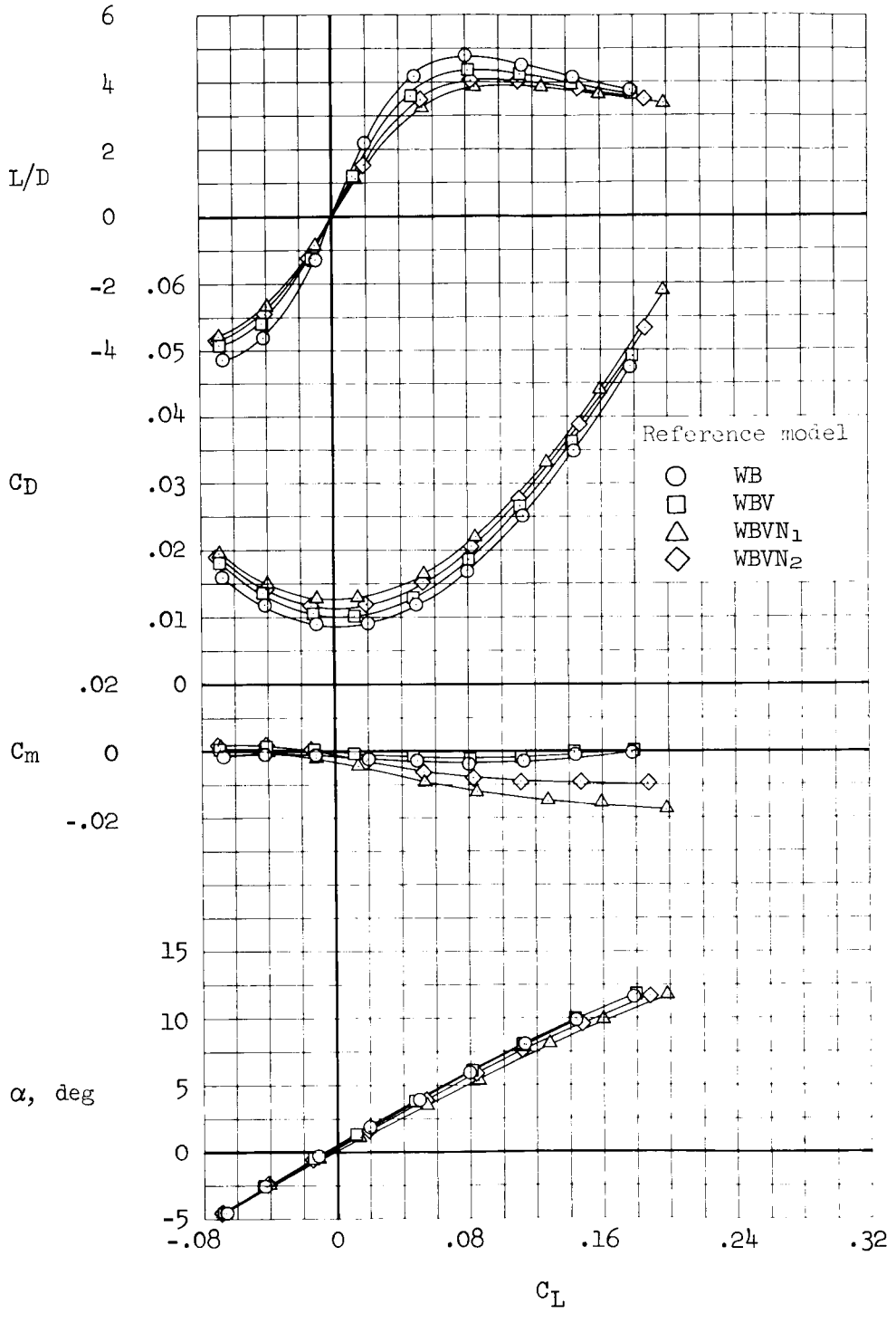


(1) M = 5.31

Figure 5.- Continued.

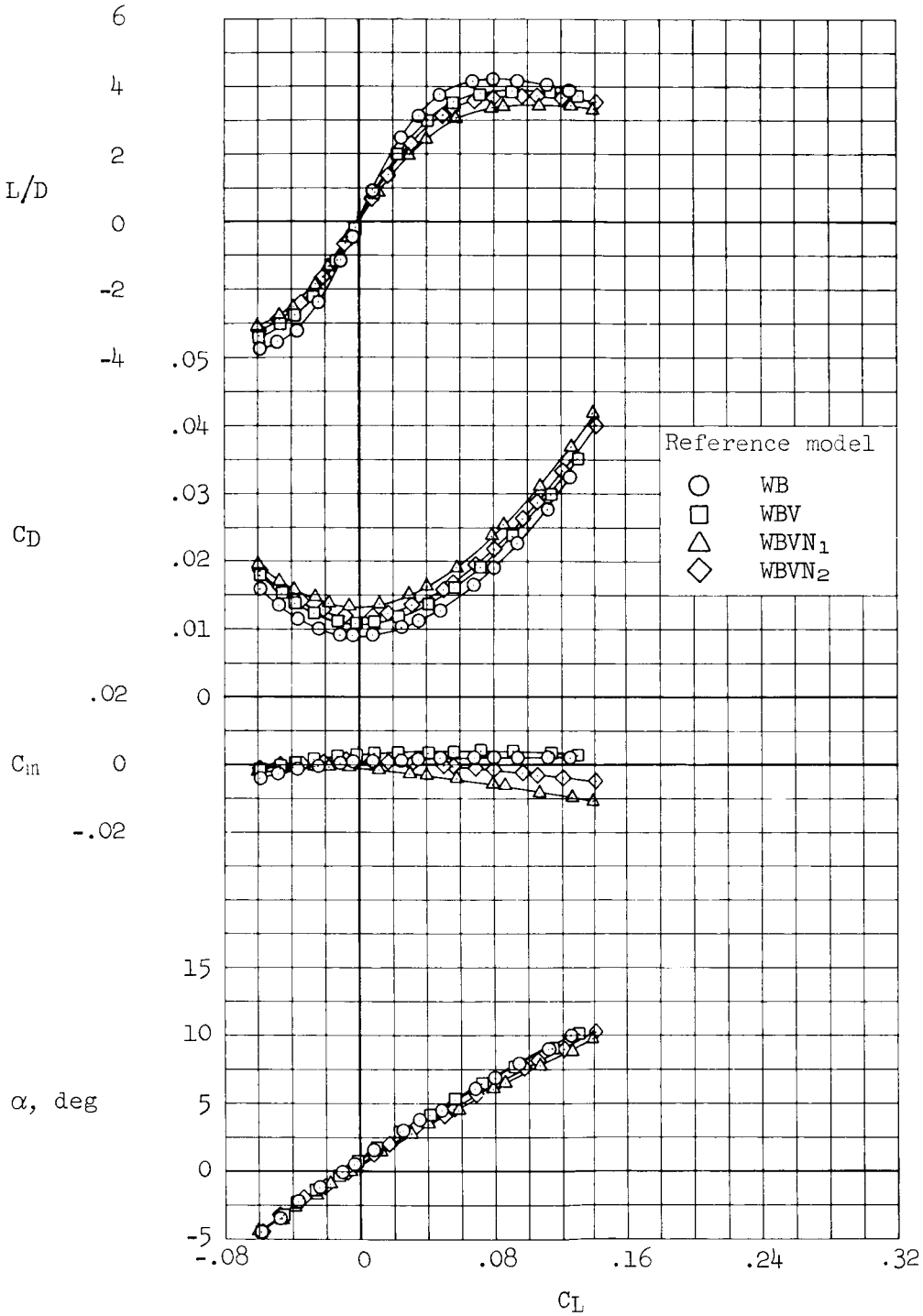


(m) M = 7.42

Figure 5.- Continued.

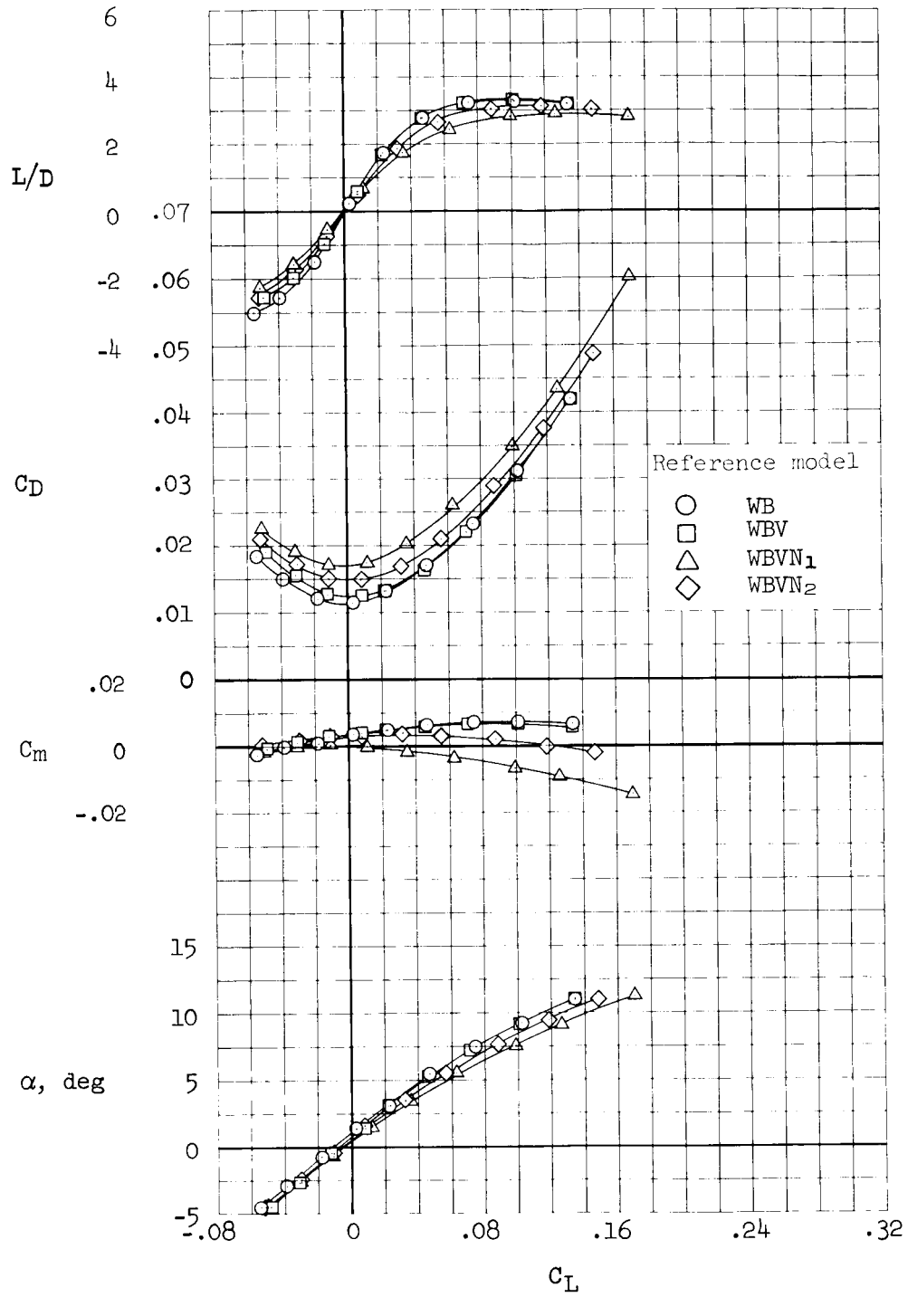


(n) M = 10.70

Figure 5.- Concluded.

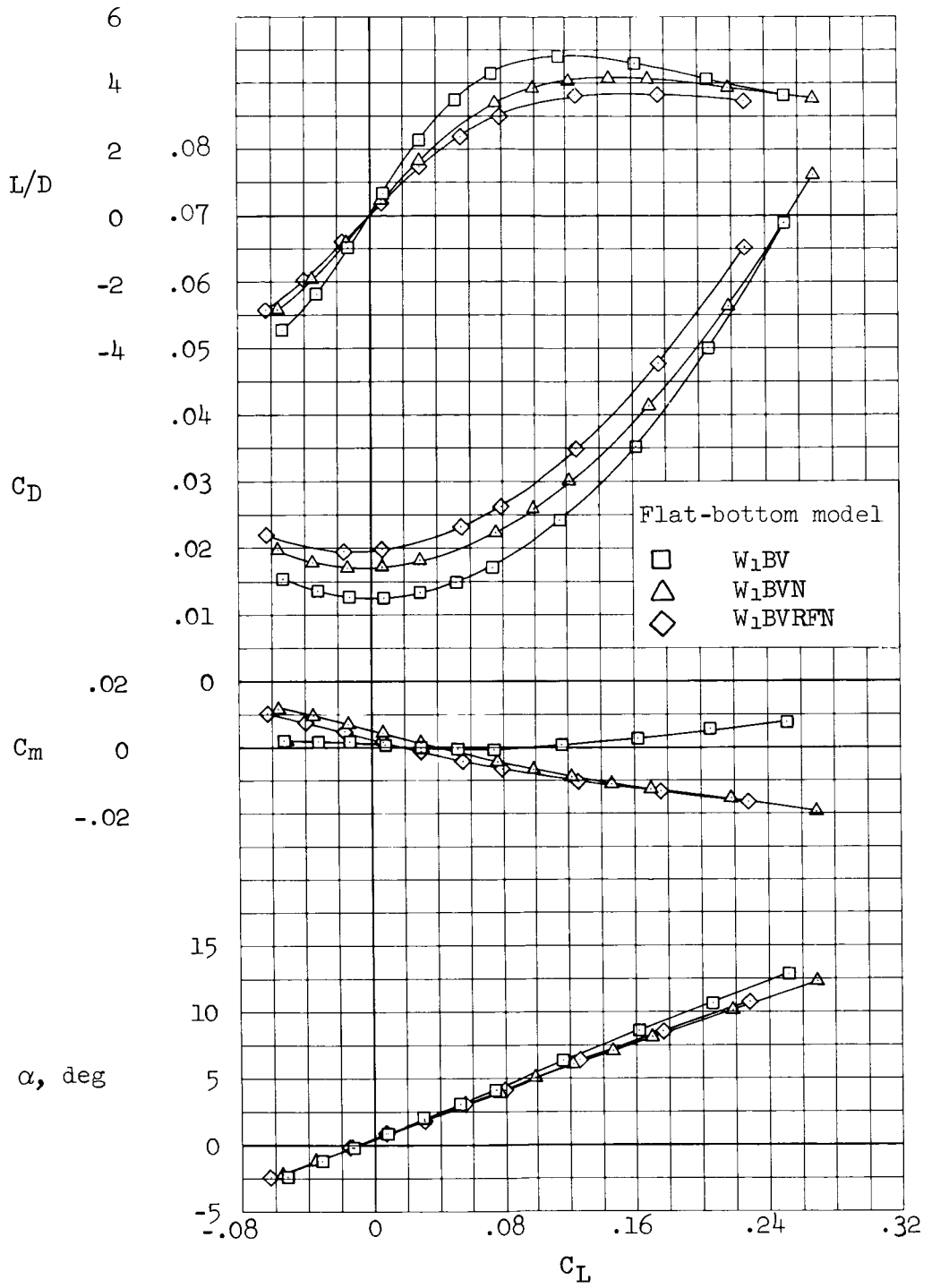


(a) M = 3.88

Figure 6.- Longitudinal aerodynamic characteristics of the flat-bottom configuration; wing t/c = 0.03; uncorrected for nacelle stream-tube drag; moment reference to 0.35$\bar{c}$.

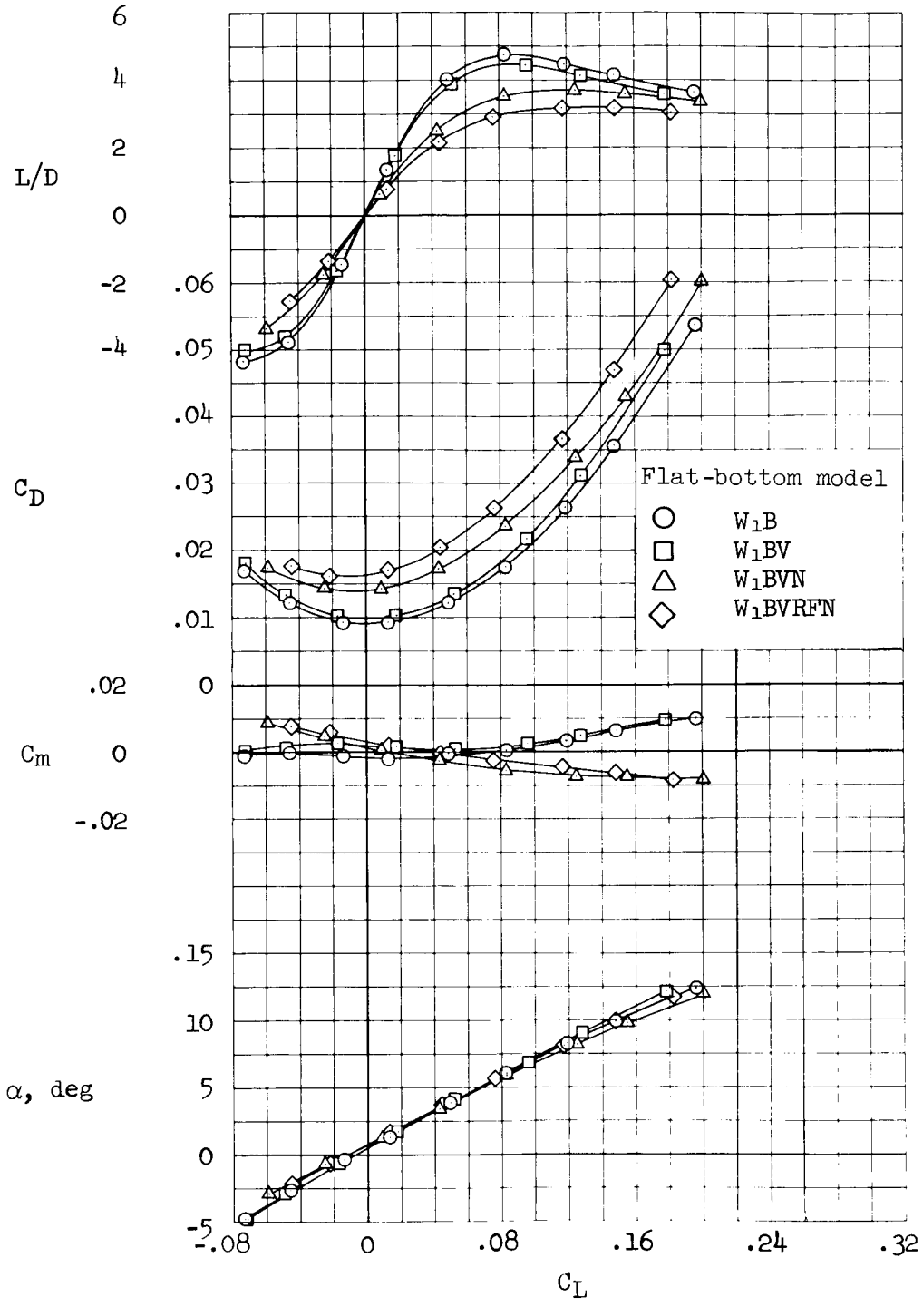


(b) M = 5.31

Figure 6.- Continued.

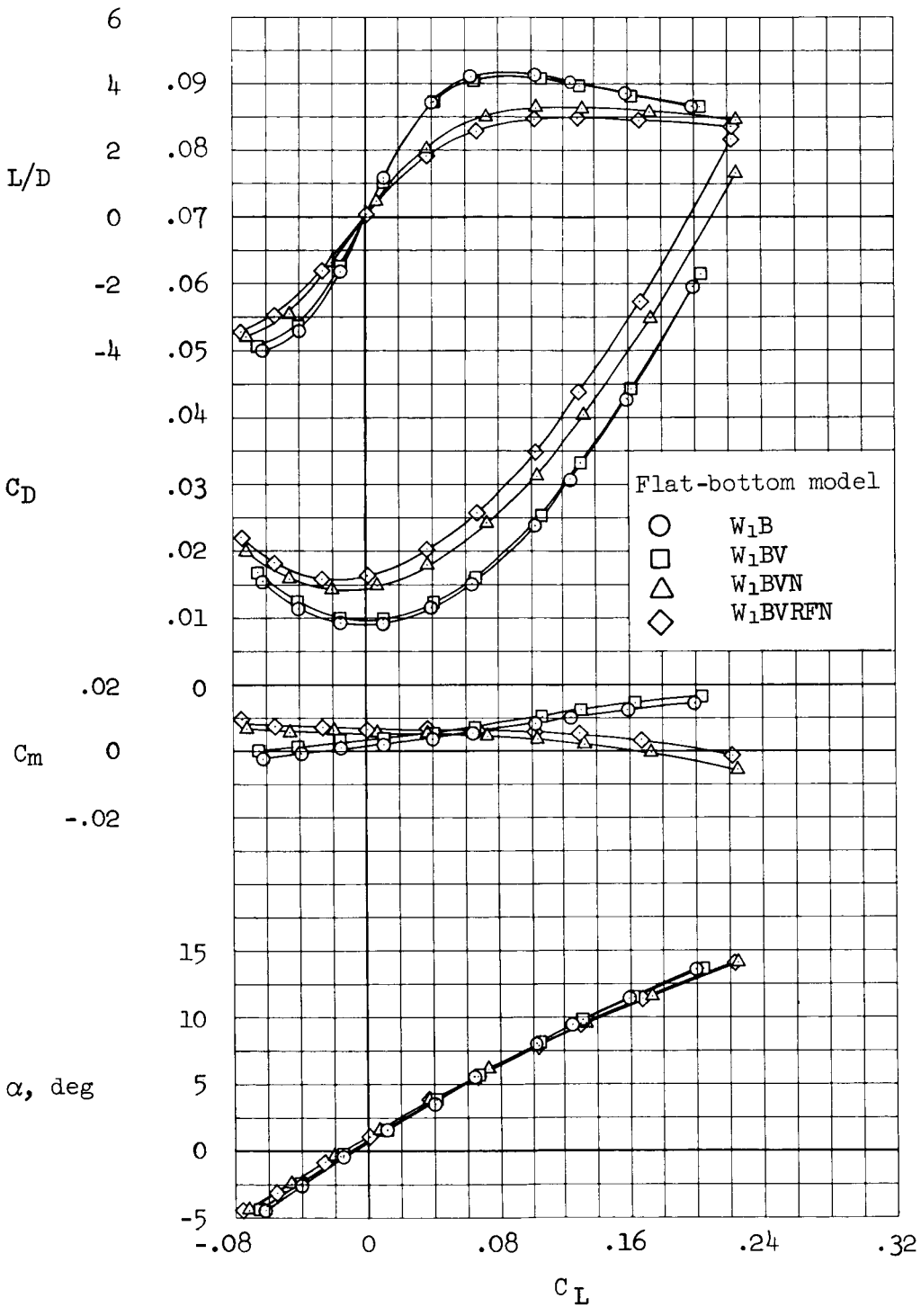


(c) M = 7.42

Figure 6.- Concluded.

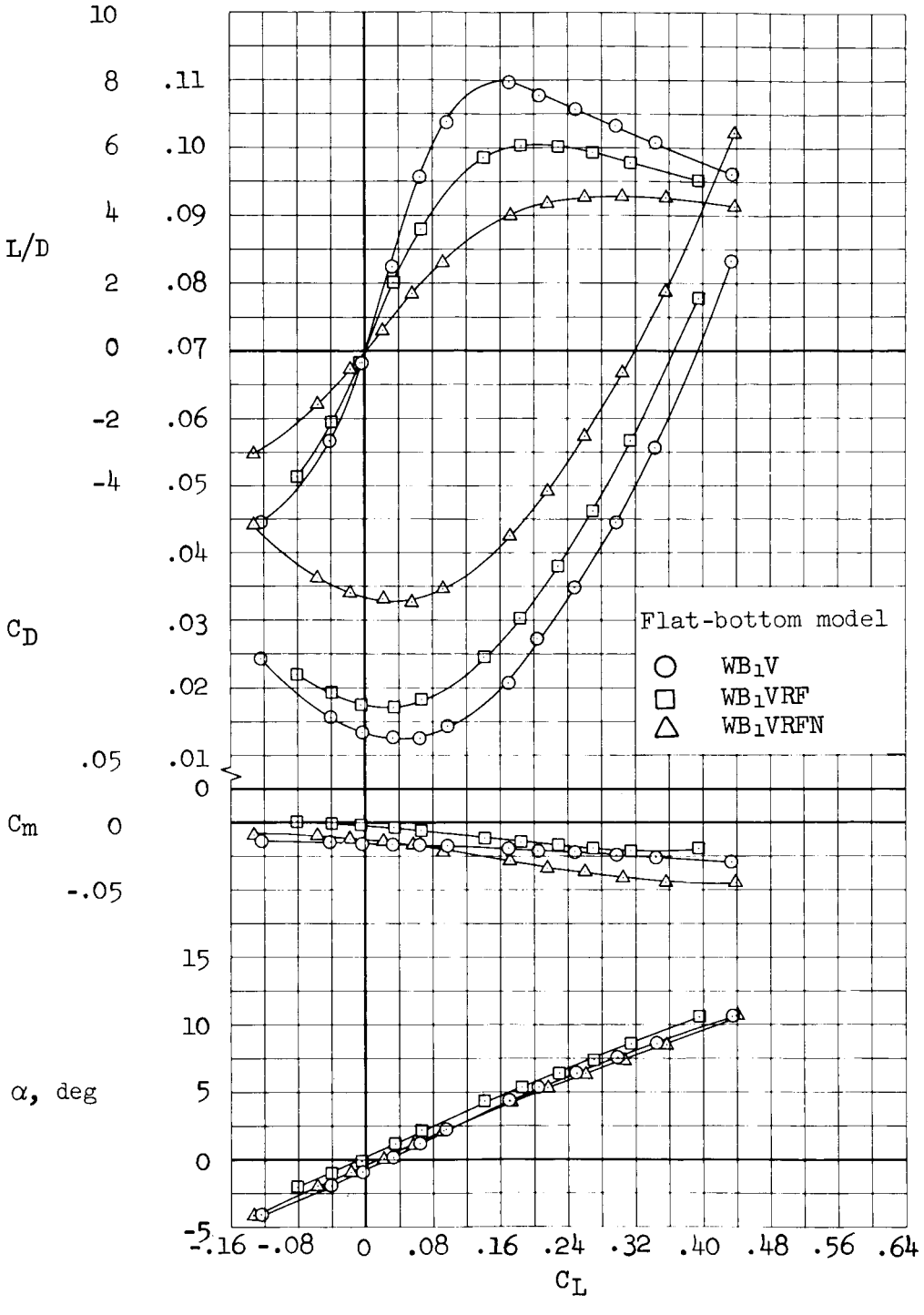


(a) M = 0.65

Figure 7.- Longitudinal aerodynamic characteristics of the flat-bottom configuration with a drooped nose; wing t/c = 0.04; uncorrected for nacelle stream-tube drag; moment reference at 0.35$\bar{c}$.

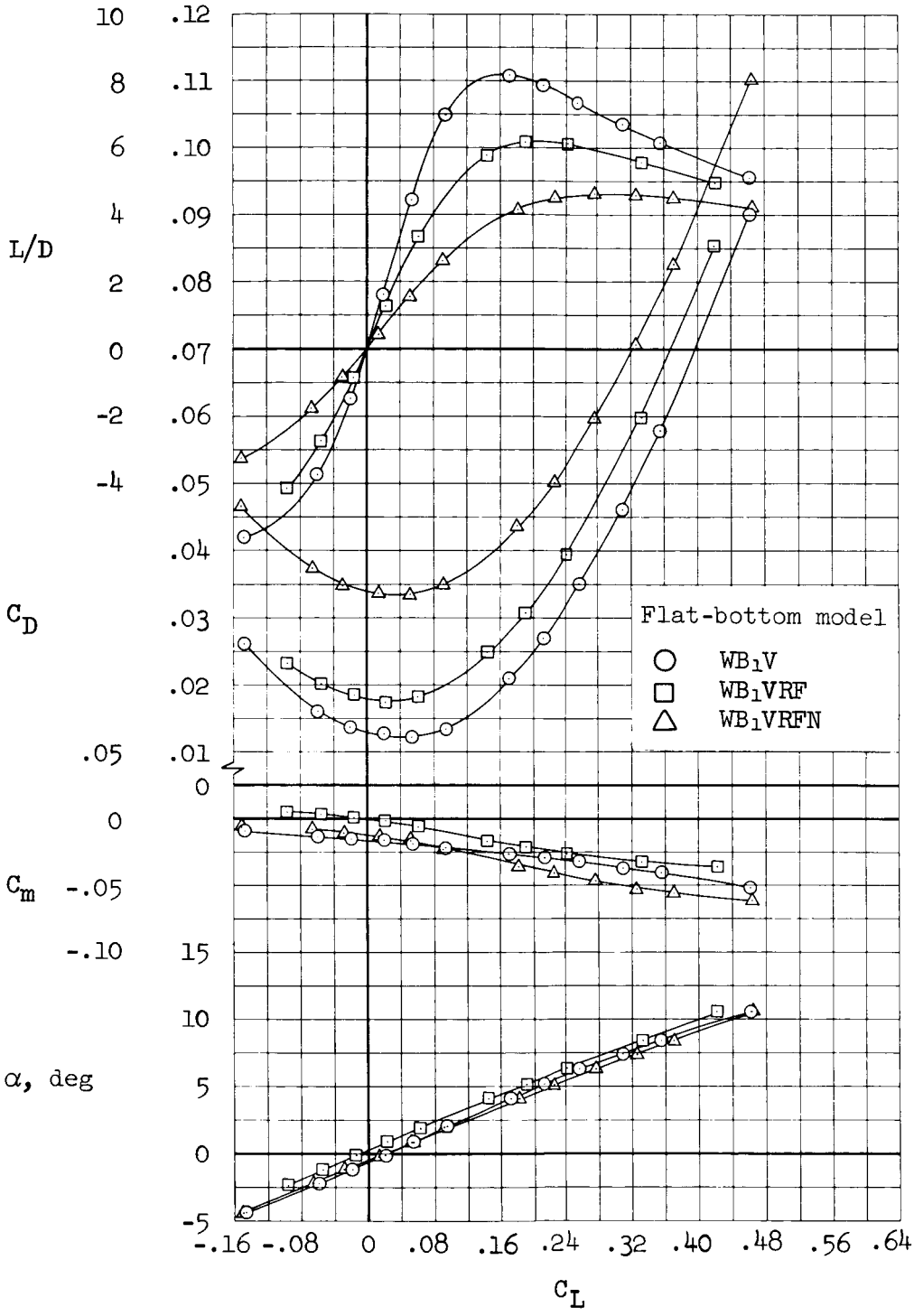


(b) M = 0.90

Figure 7.- Continued.

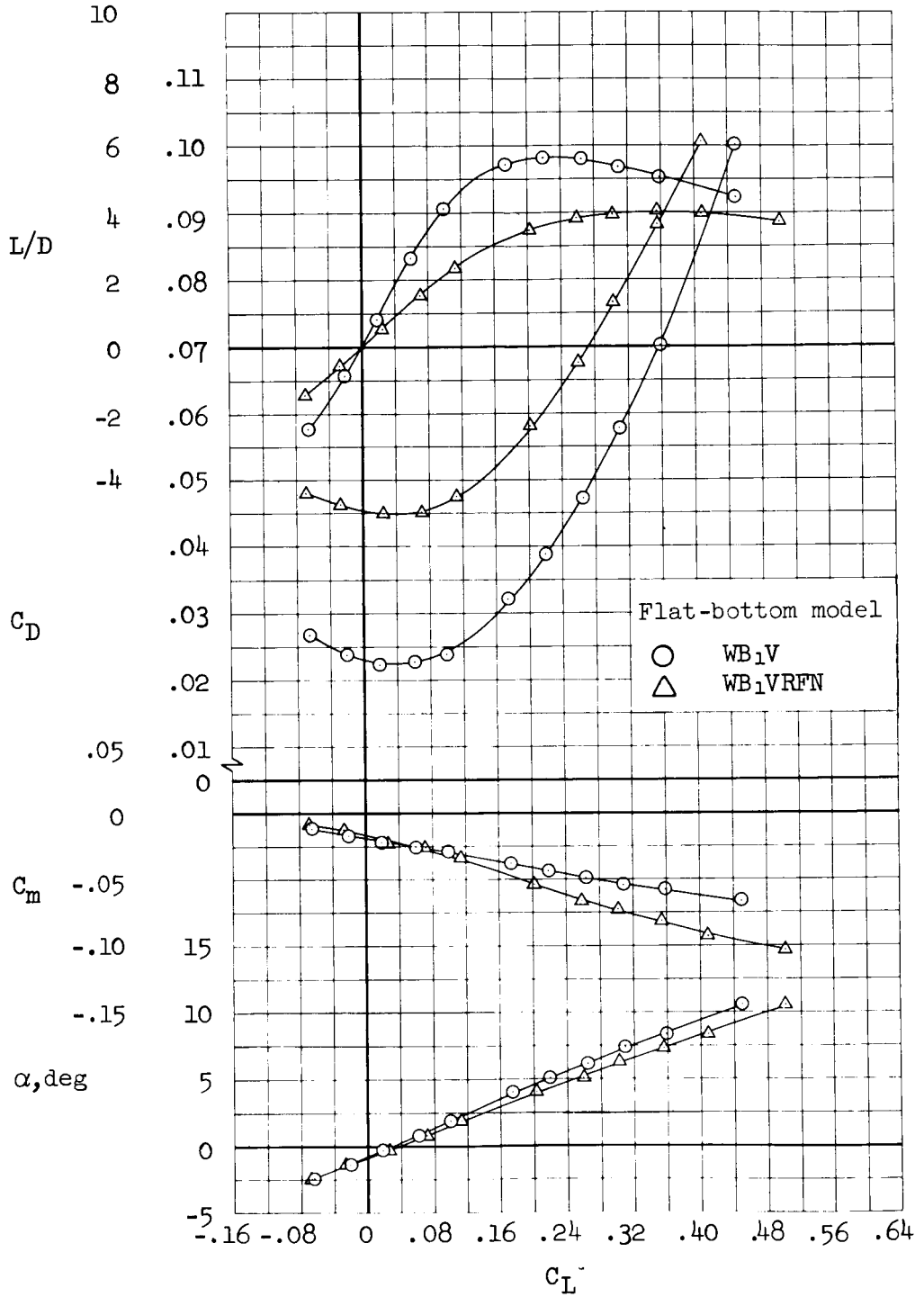


(c) M = 1.10

Figure 7.- Continued.

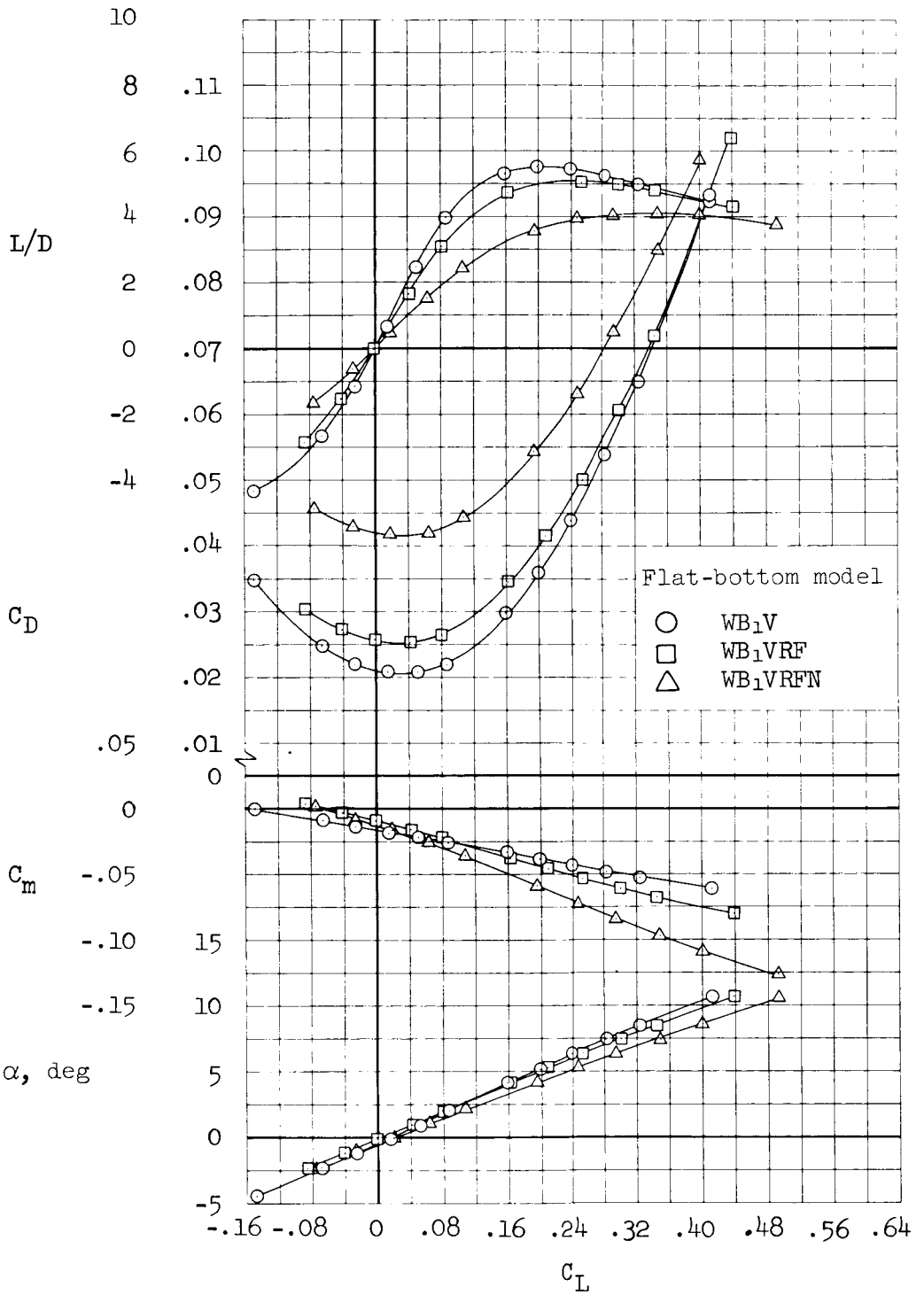


(d) M = 1.30

Figure 7.- Continued.

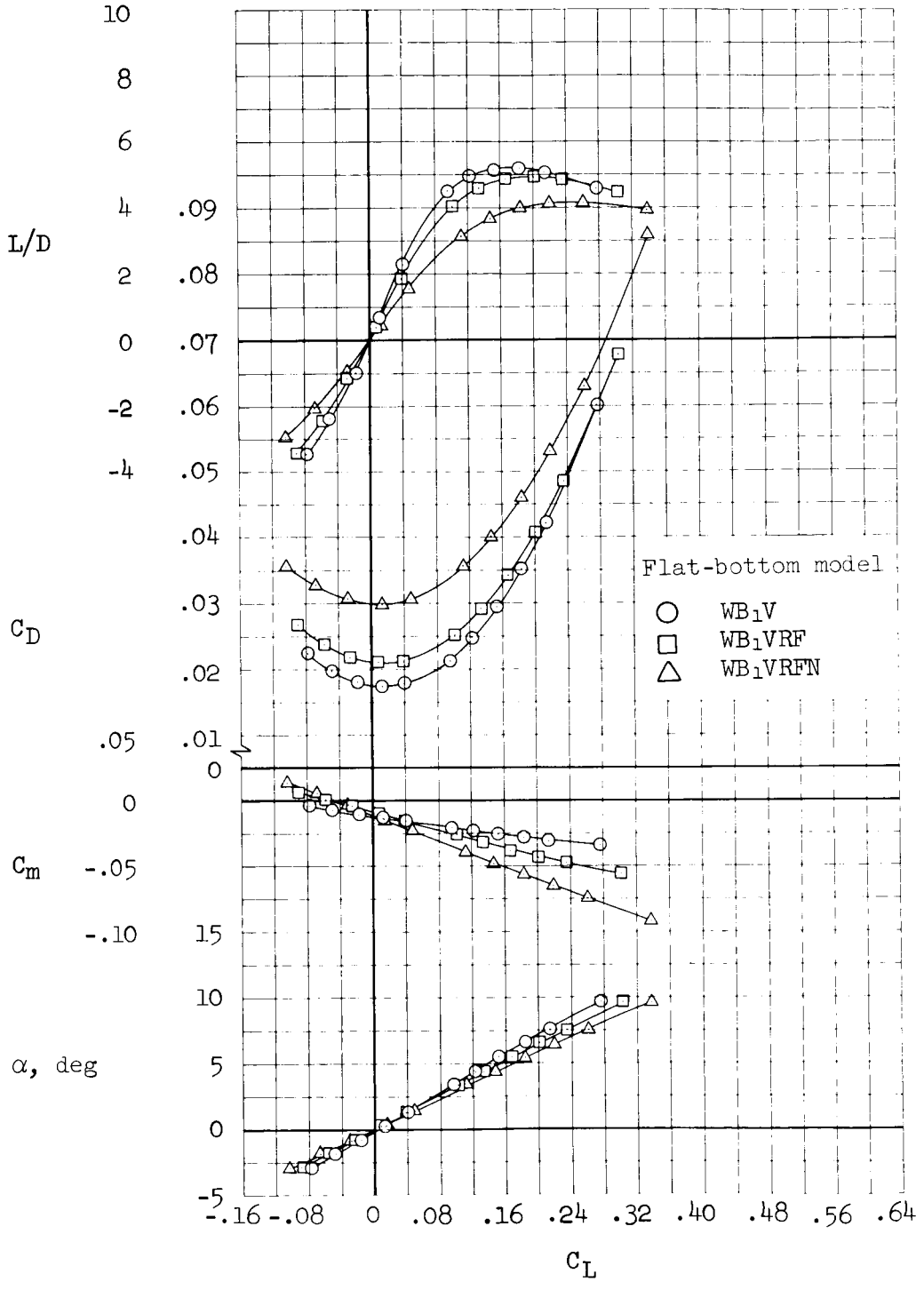


(e) M = 1.99

Figure 7.- Continued.

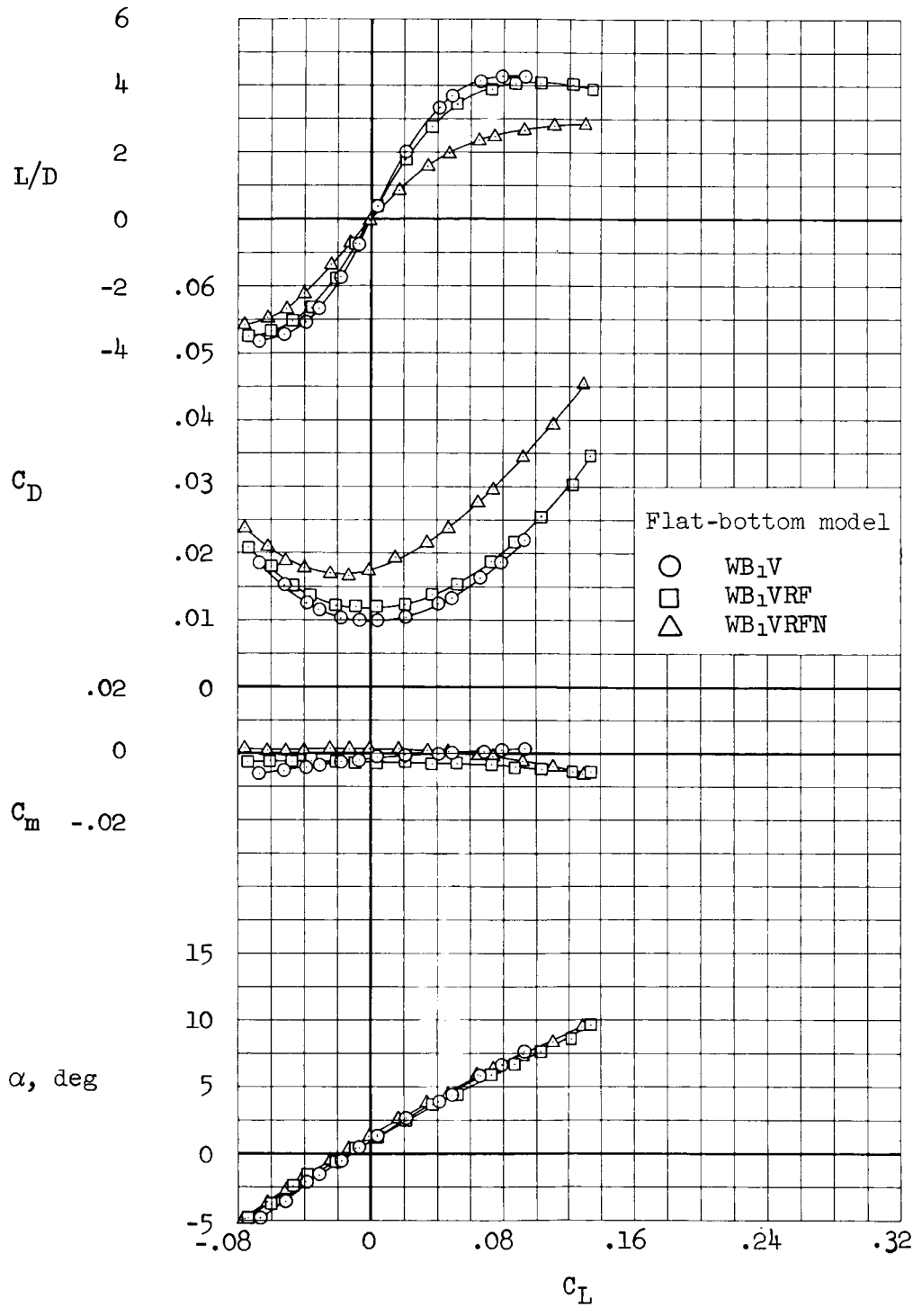


(f) M = 7.42

Figure 7.- Concluded.

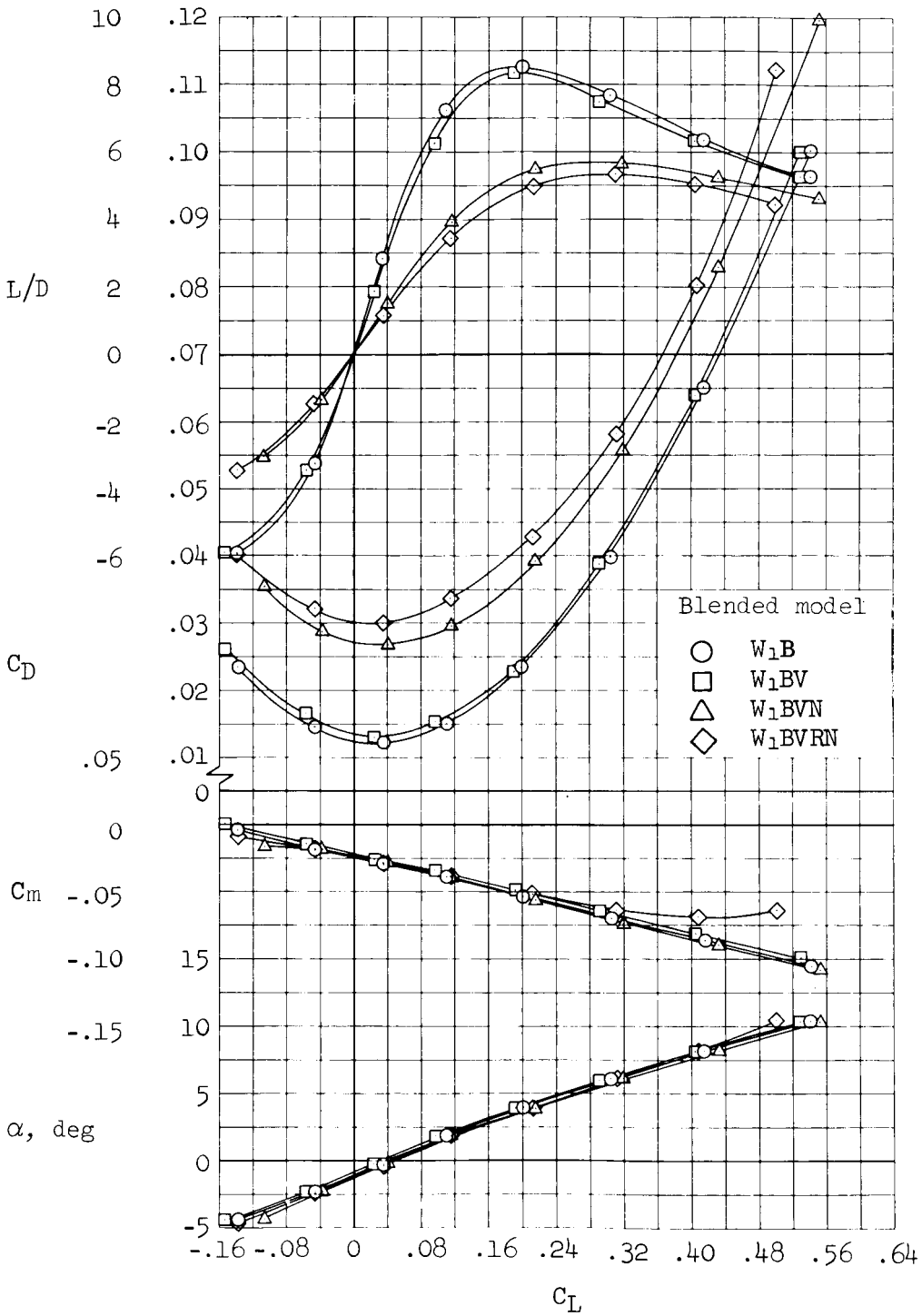


(a) M = 0.65

Figure 8.- Longitudinal aerodynamic characteristics of the blended configuration; uncorrected for nacelle stream-tube drag; moment reference at 0.05$\bar{c}$.

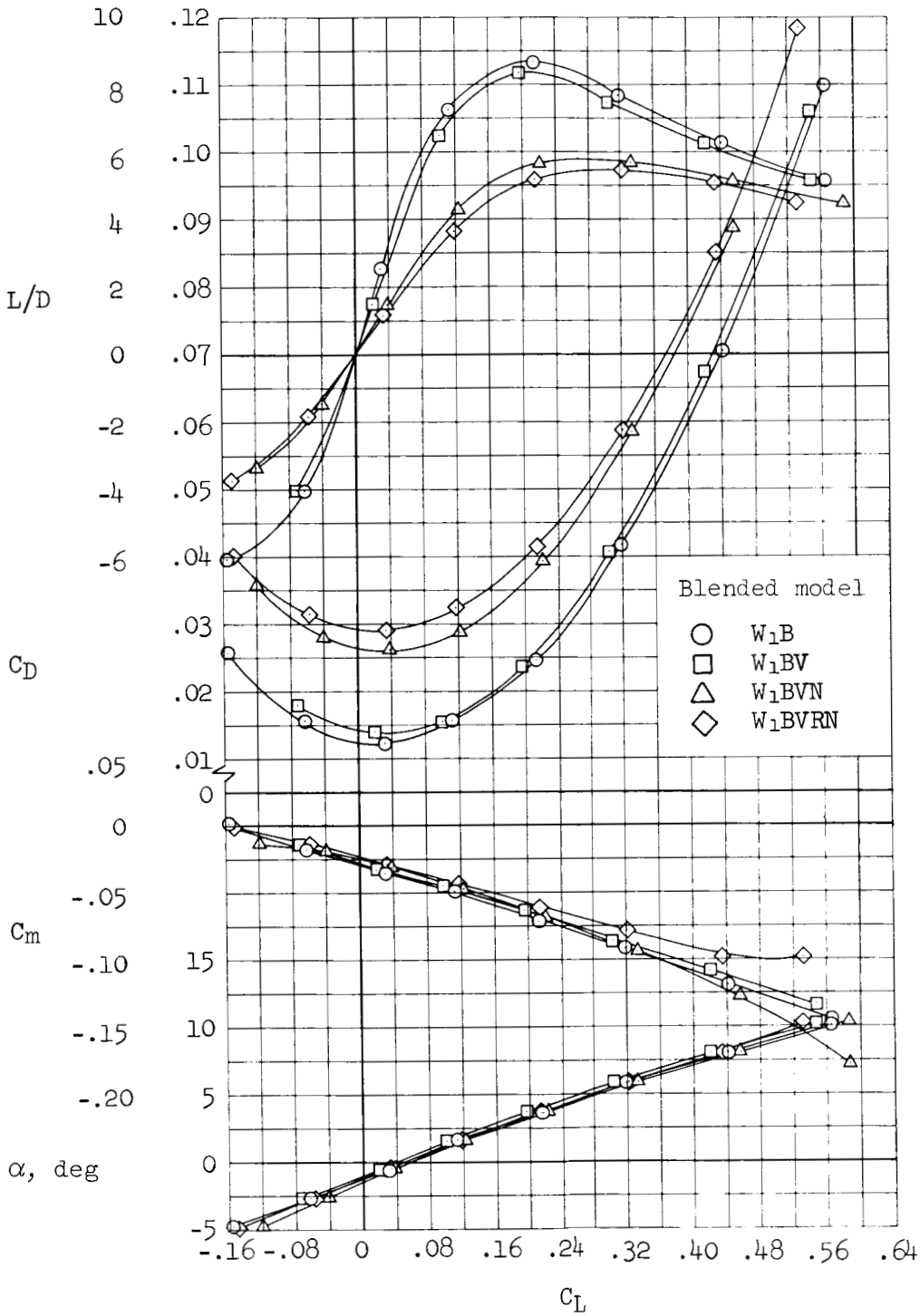


(b) M = 0.90

Figure 8.- Continued.

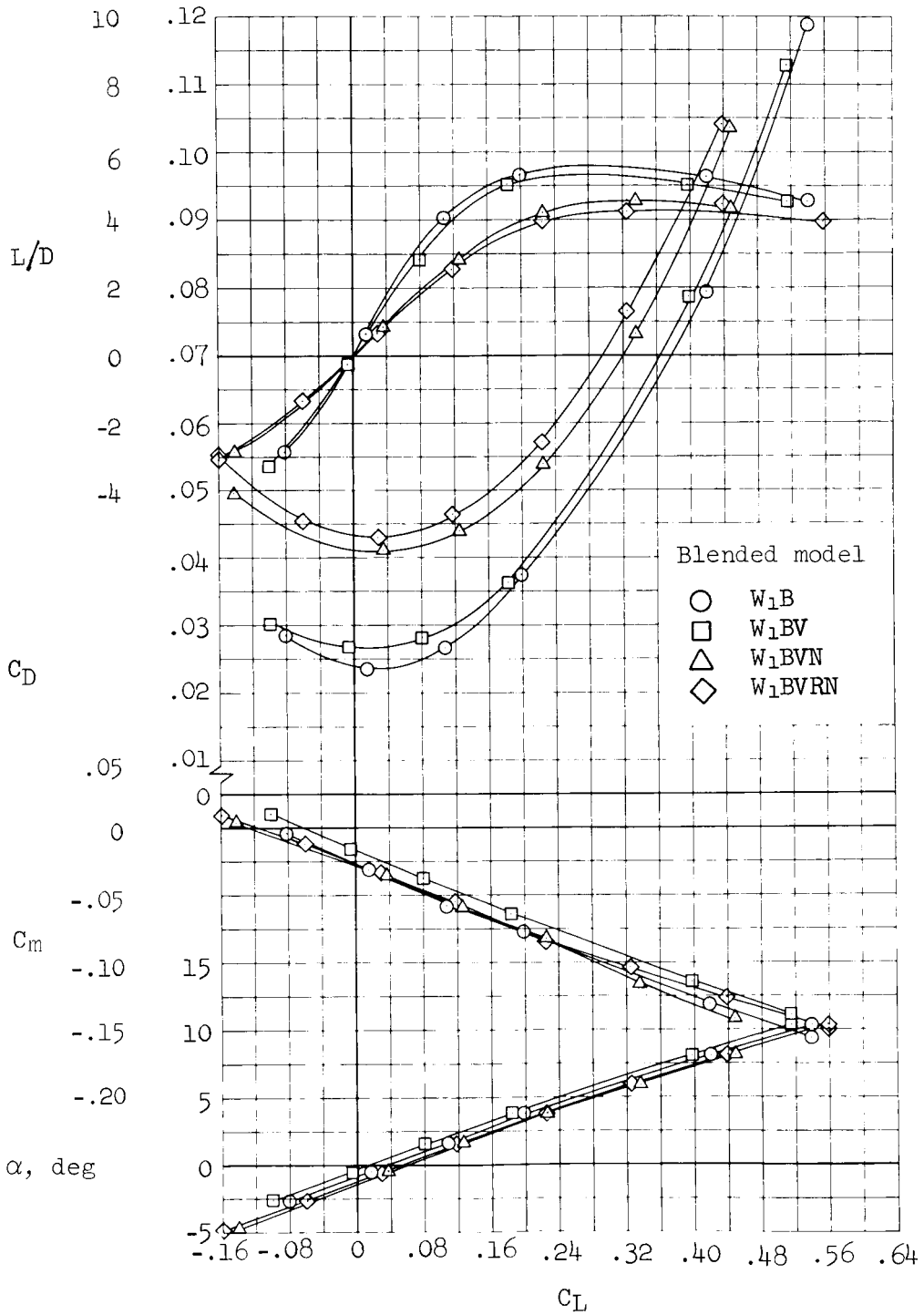


(c) M = 1.10

Figure 8.- Continued.

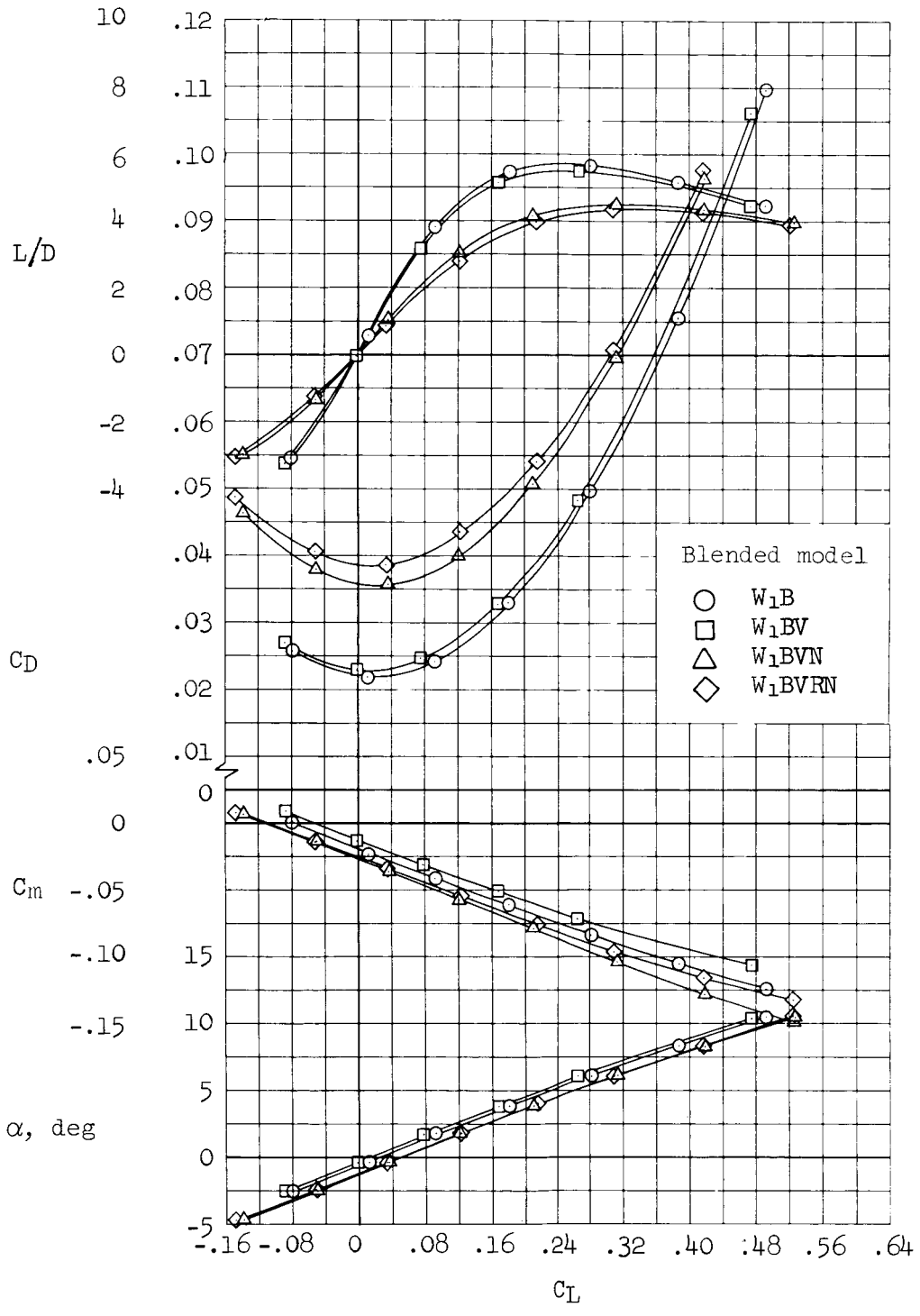


(d) M = 1.30

Figure 8.- Continued.

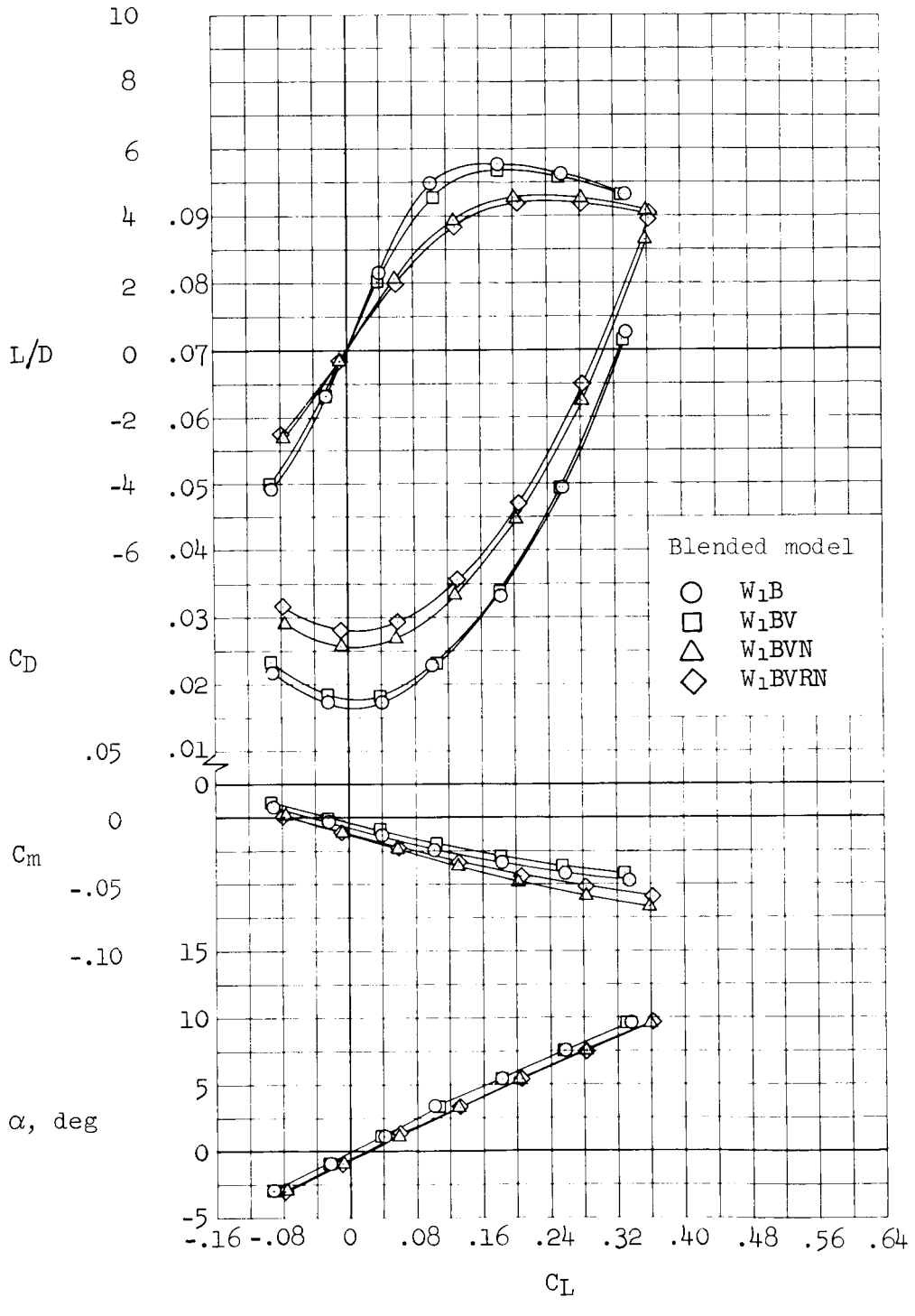


(e) M = 1.99

Figure 8.- Continued.

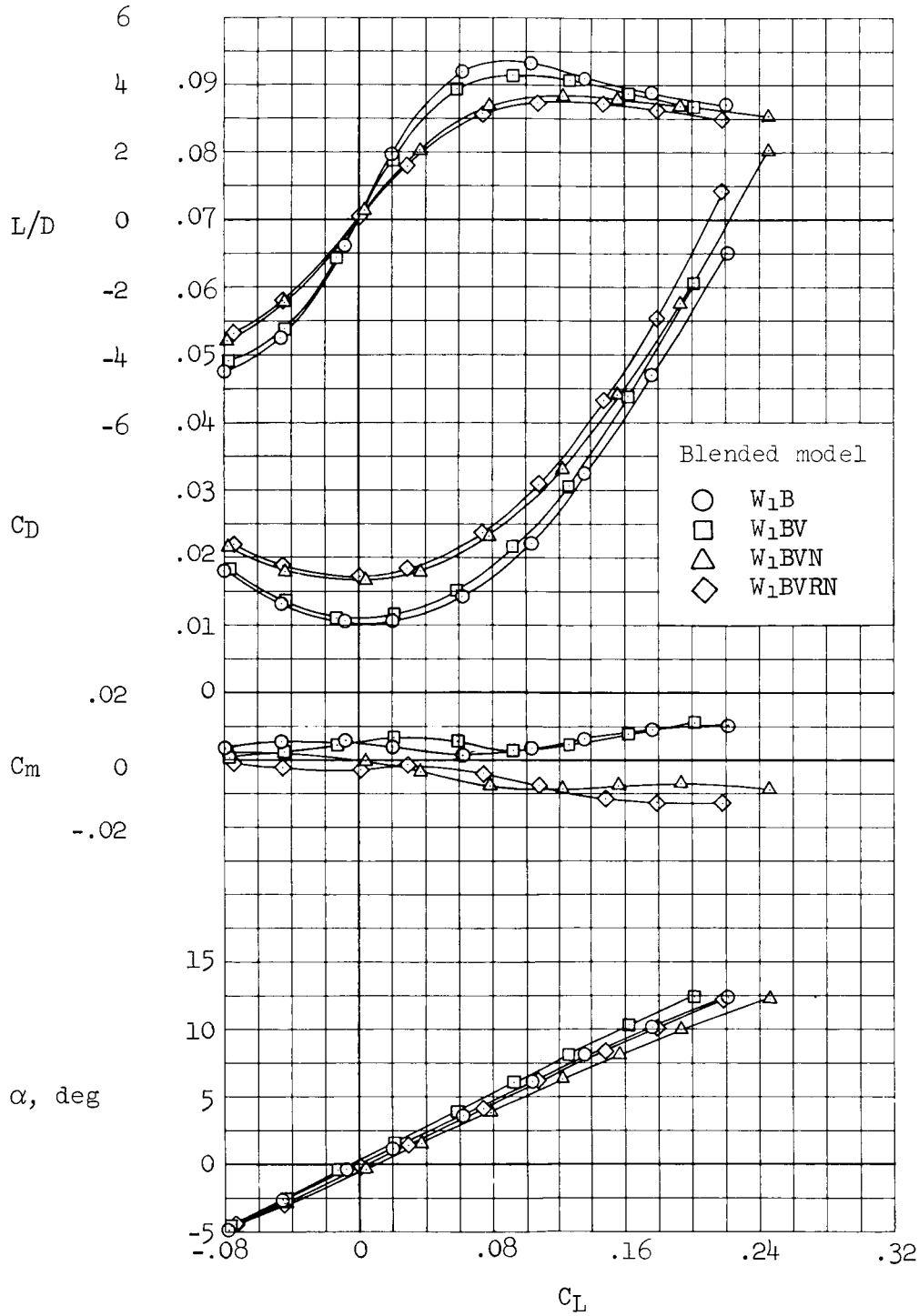


(f) M = 5.31

Figure 8.- Continued.

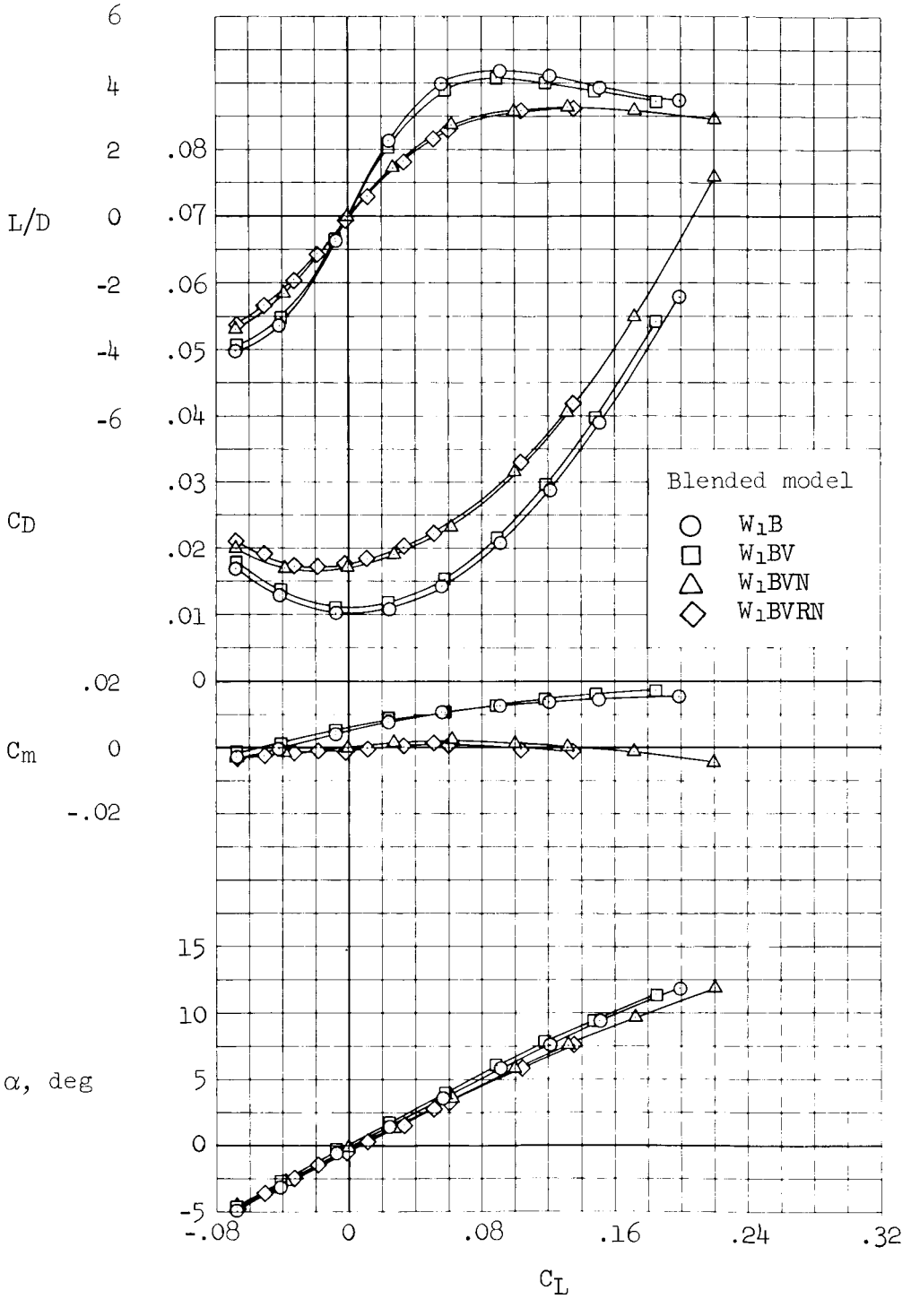


(g) M = 7.42

Figure 8.- Continued.

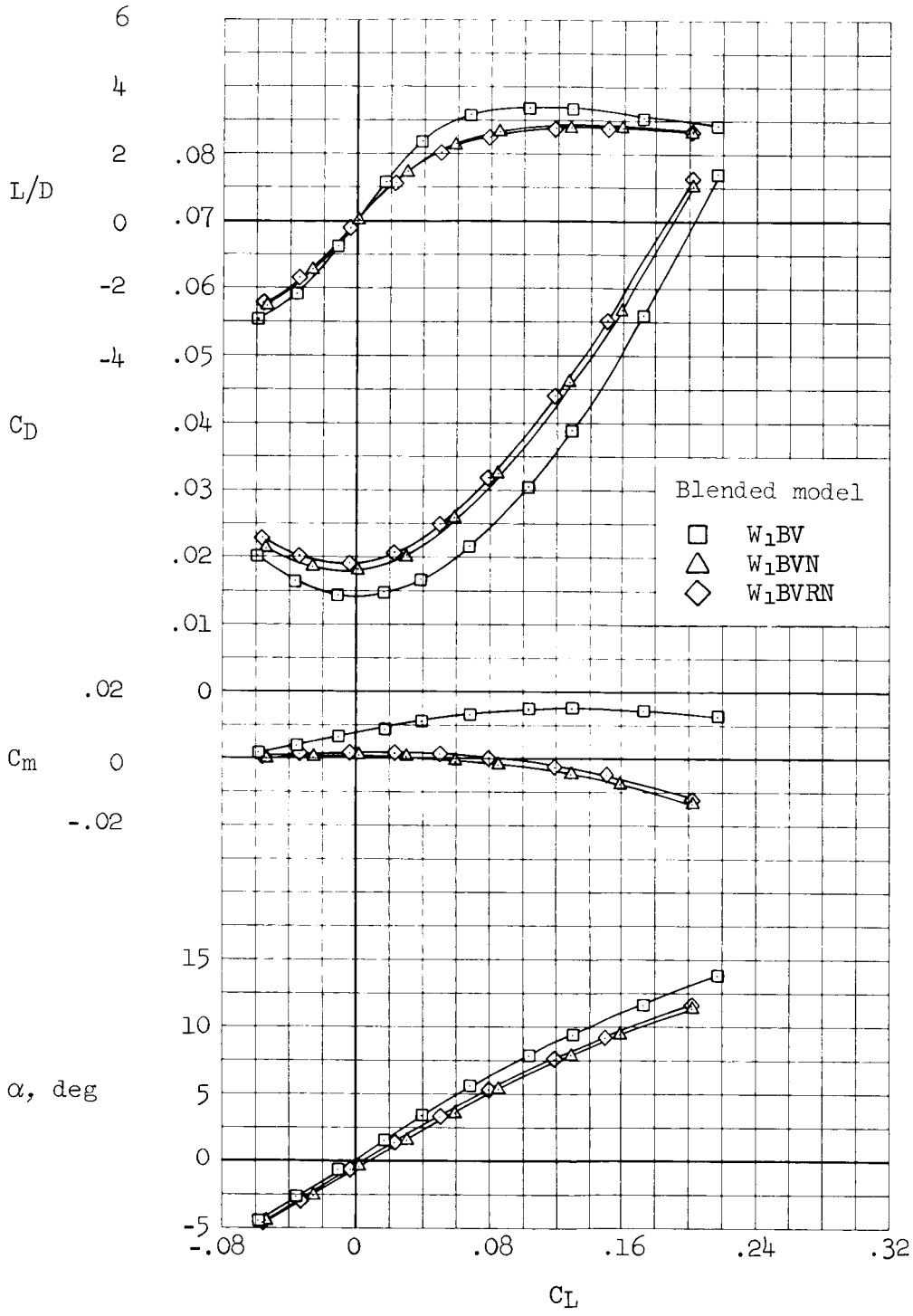


(h) M = 10.70

Figure 8.- Concluded.

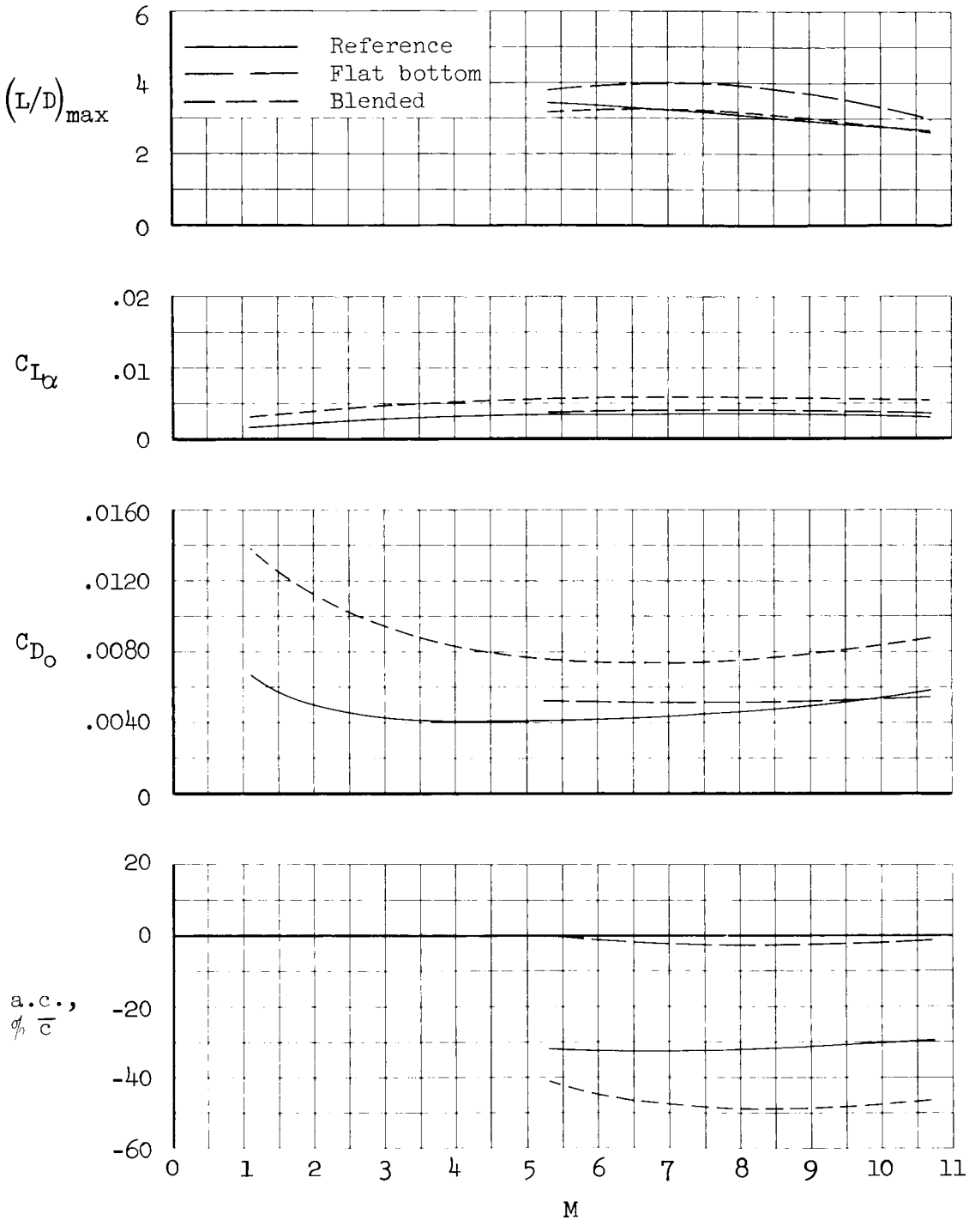


Figure 9.- Variation with Mach number of the longitudinal aerodynamic characteristics of the body alone configurations.

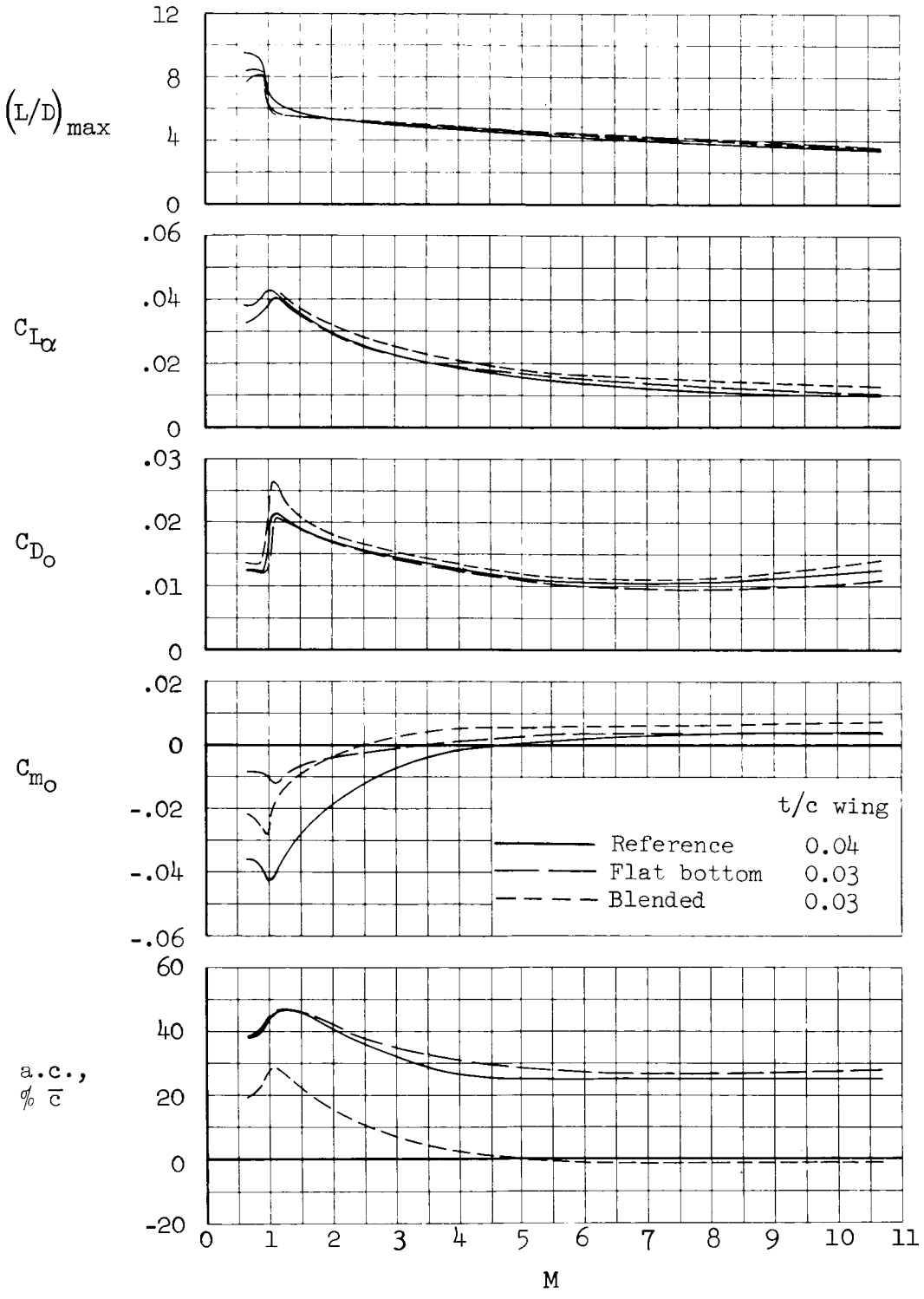


Figure 10.- Variation with Mach number of the longitudinal aerodynamic characteristics of the wing-body-vertical tail configurations.

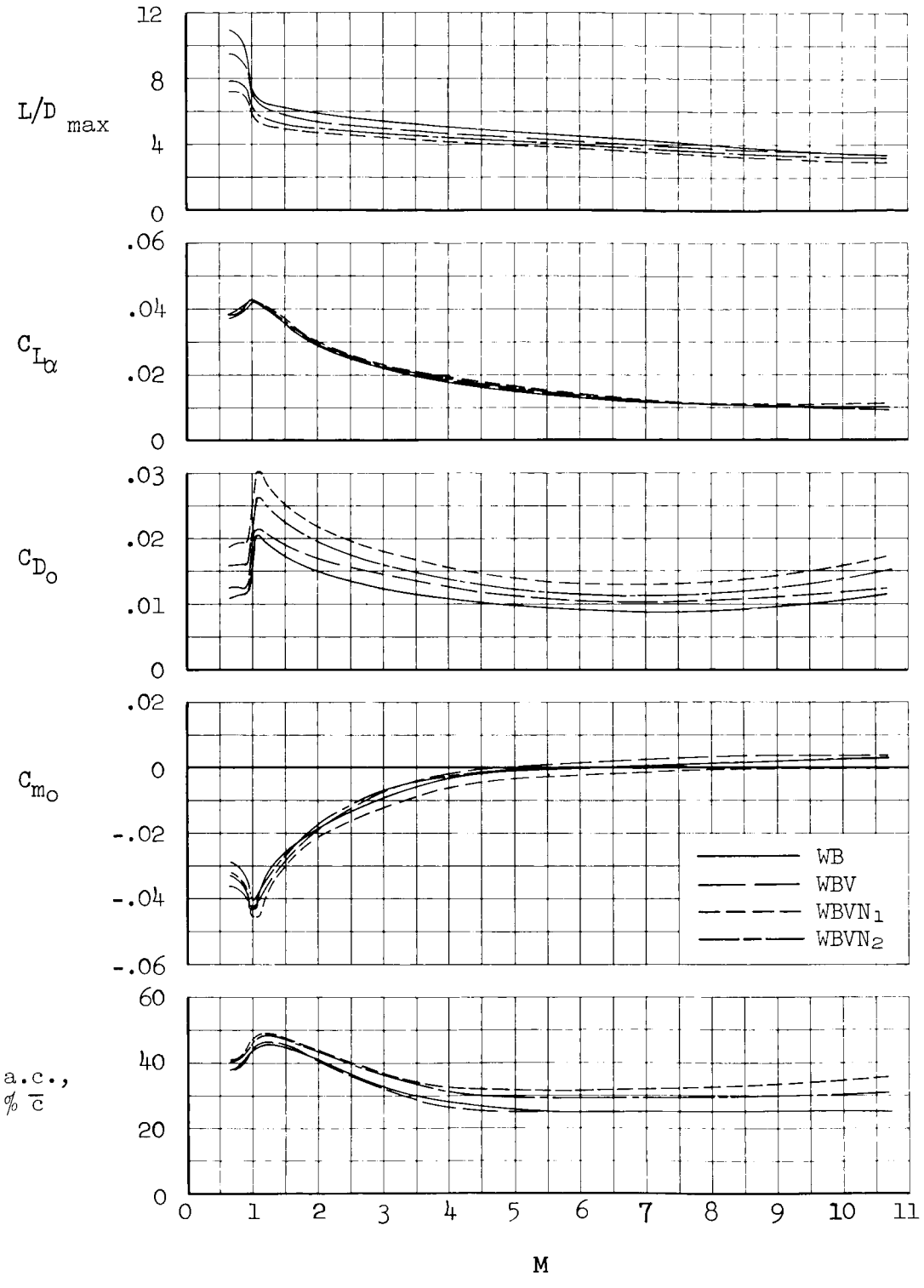


Figure 11.- Variation with Mach number of the longitudinal aerodynamic characteristics of the reference configuration; uncorrected for nacelle stream-tube drag and nacelle base drag.

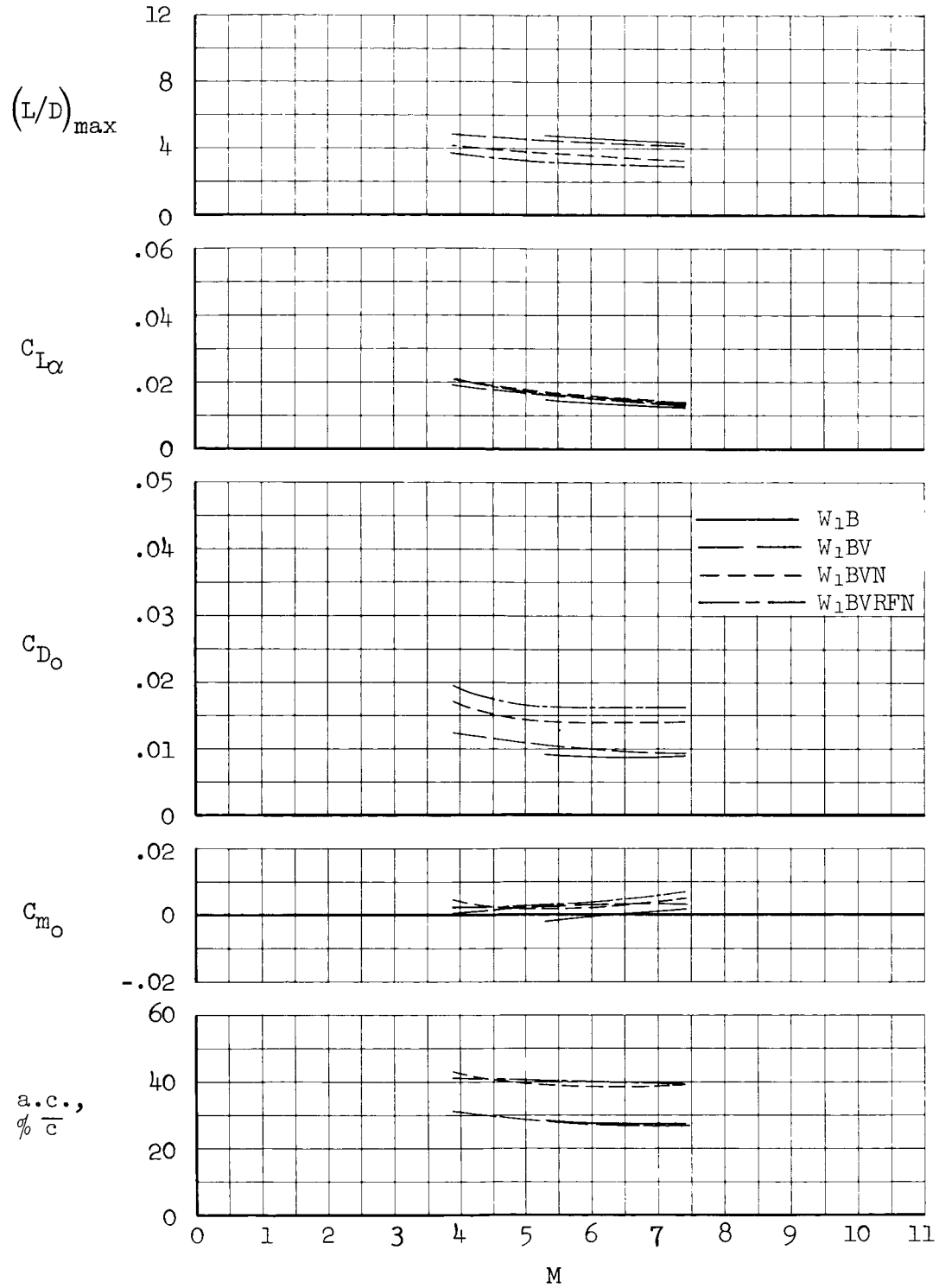


Figure 12.- Variation with Mach number of the longitudinal aerodynamic characteristics of the flat-bottom configuration; wing t/c = 0.03; uncorrected for nacelle stream-tube drag.

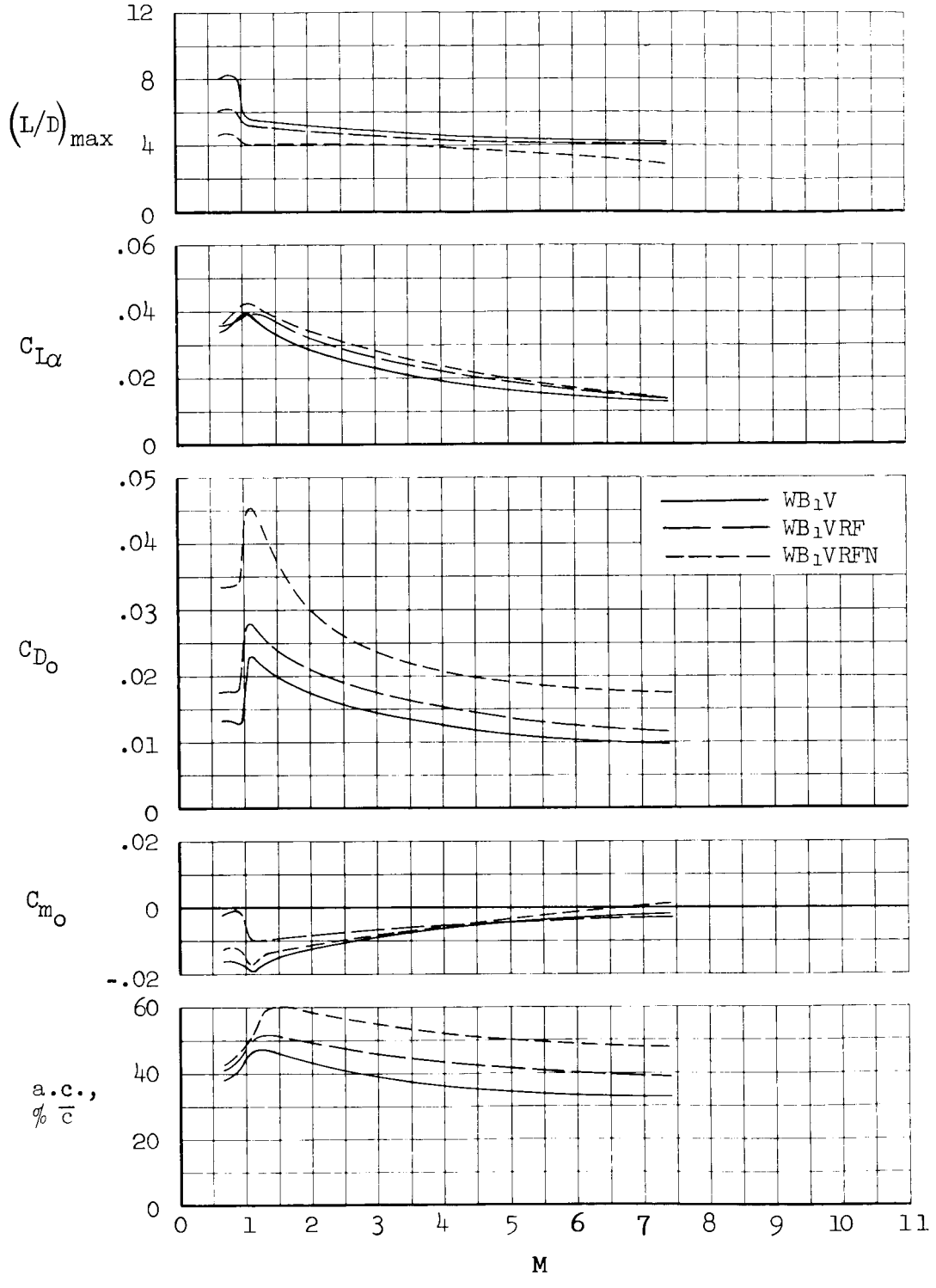


Figure 13.- Variation with Mach number of the longitudinal aerodynamic characteristics of the flat-bottom configuration with a drooped nose; wing t/c = 0.04; uncorrected for nacelle stream-tube drag.

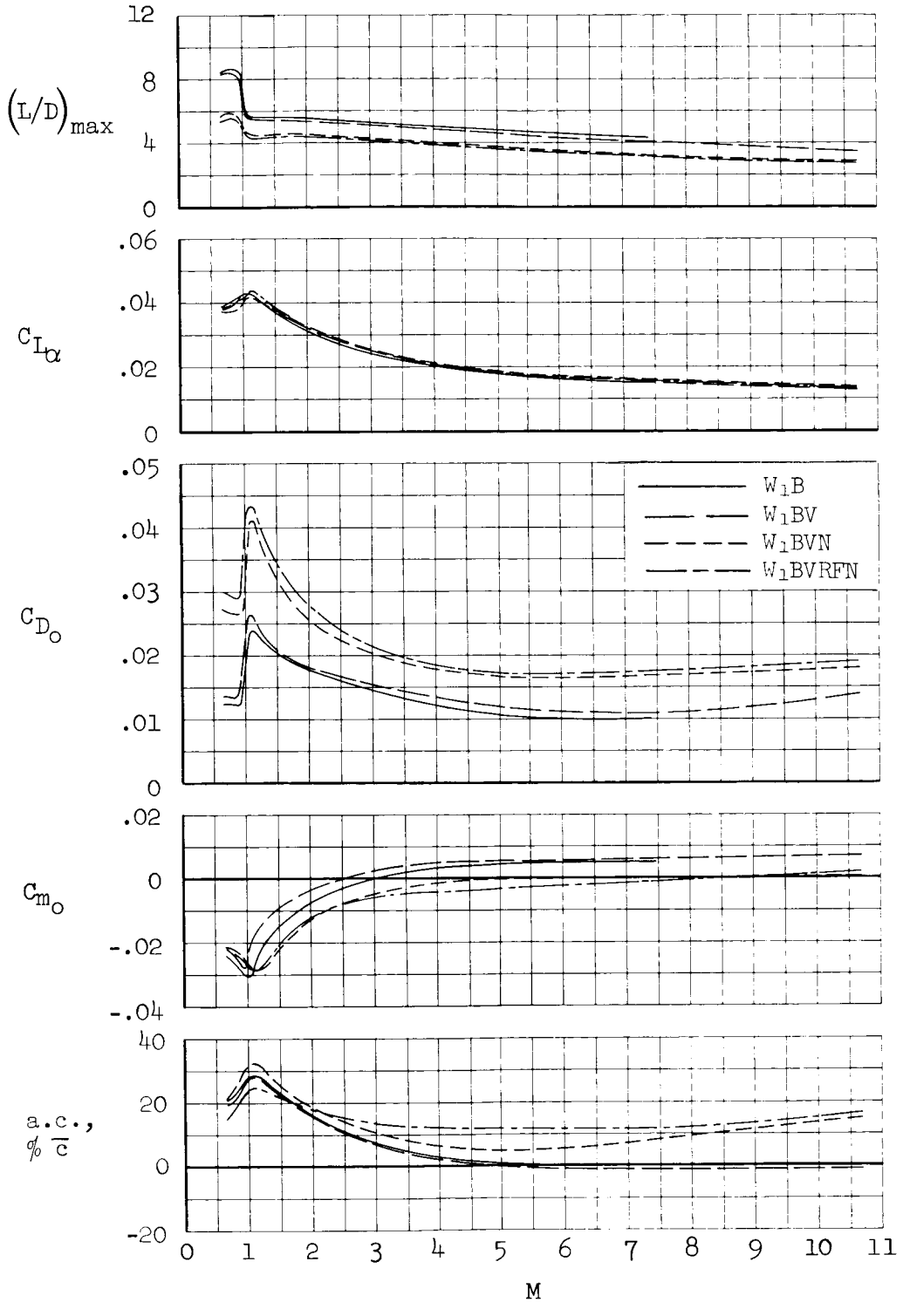


Figure 14.- Variation with Mach number of the longitudinal aerodynamic characteristics of the blended configuration; uncorrected for nacelle stream-tube drag.

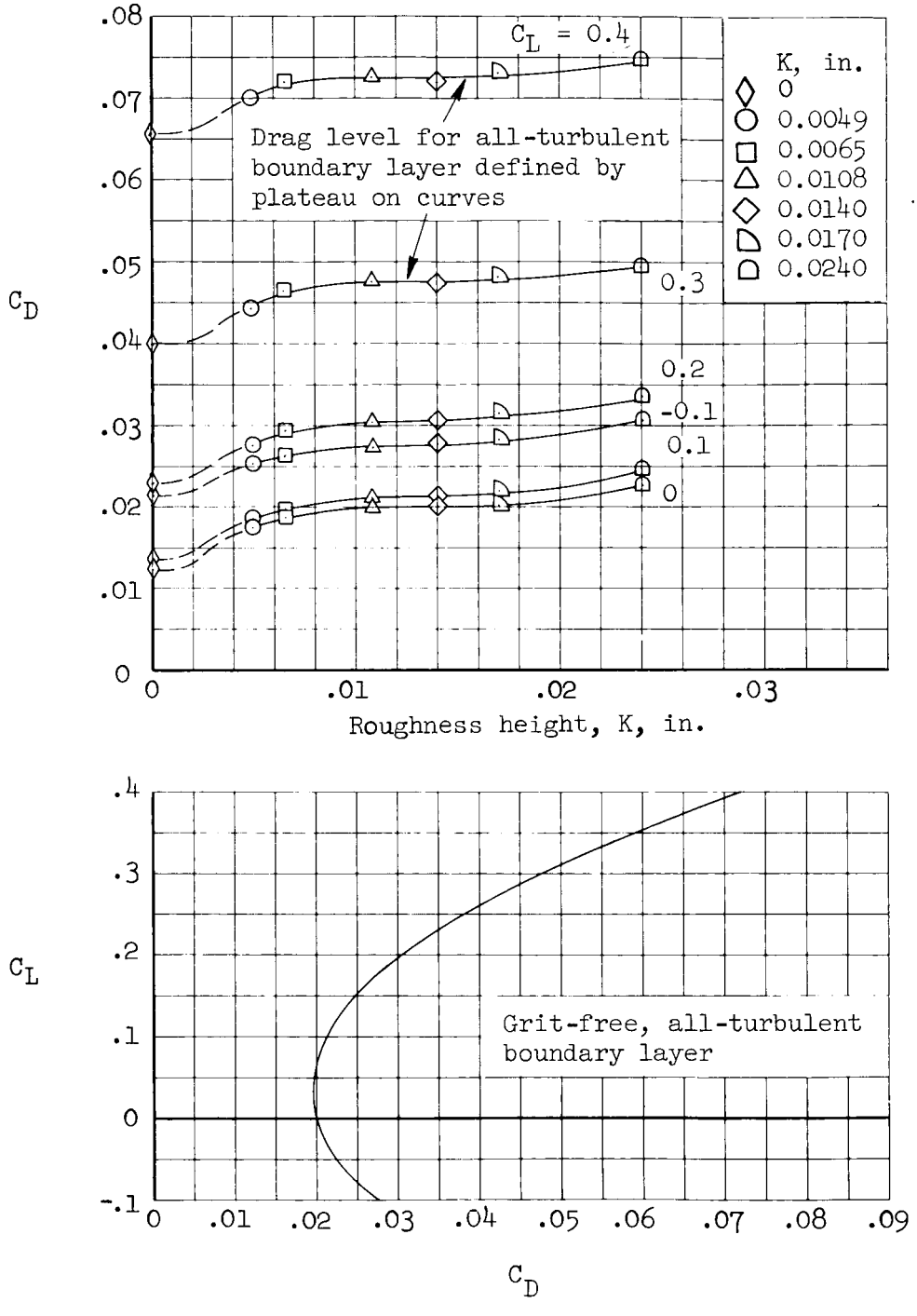


(a) M = 0.90

Figure 15.- Determination of the drag level for an all-turbulent boundary layer using variable size roughness; reference configuration; wing-body-vertical tail combination.

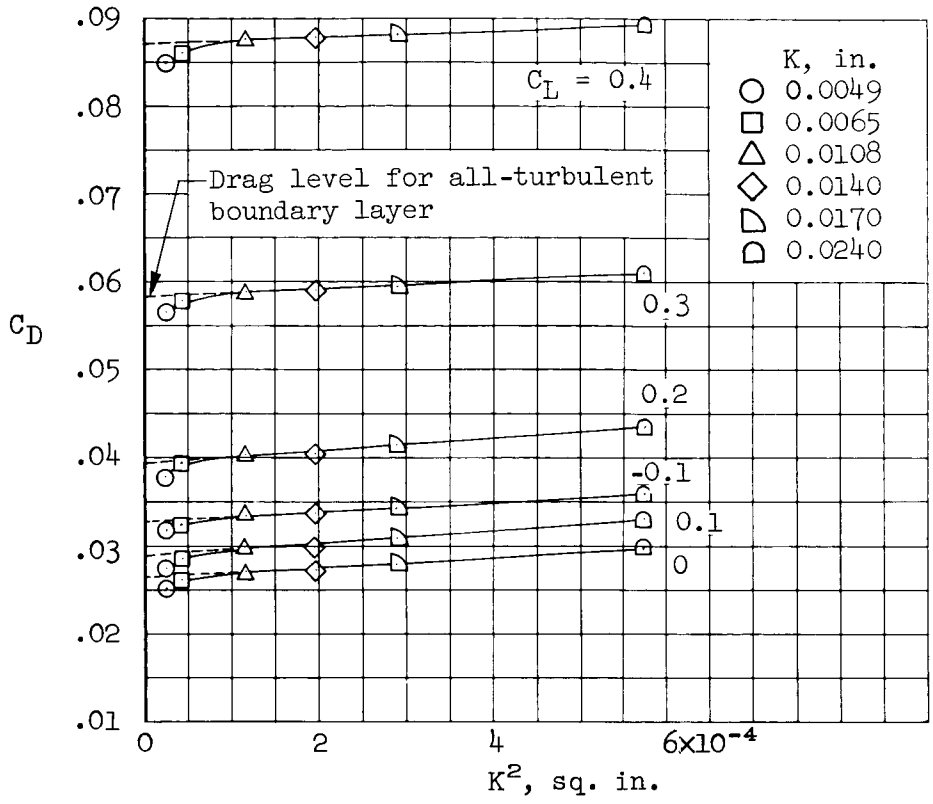


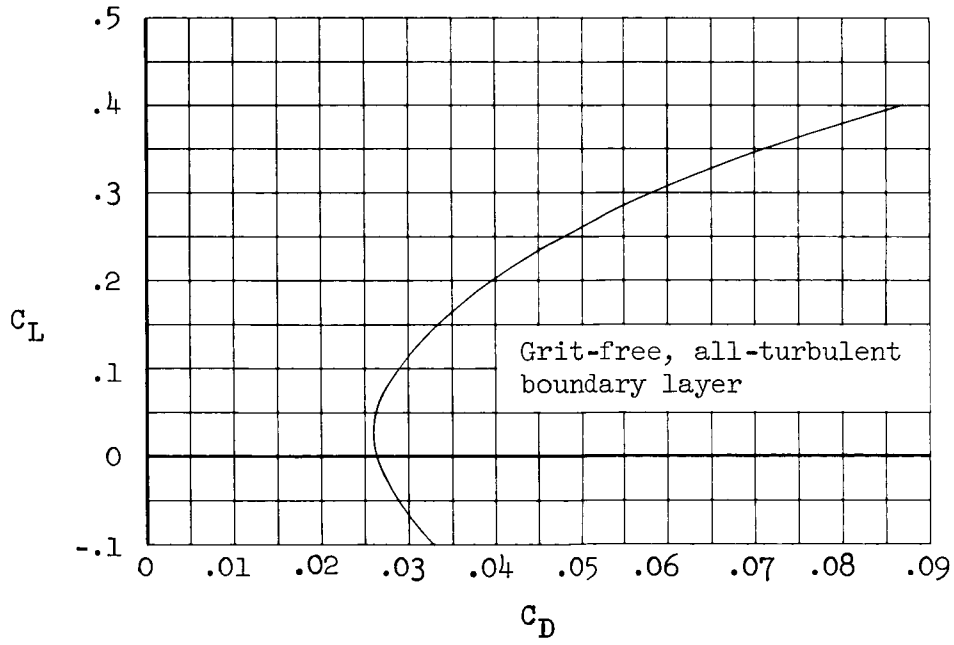


(b) M = 1.30

Figure 15.- Continued.

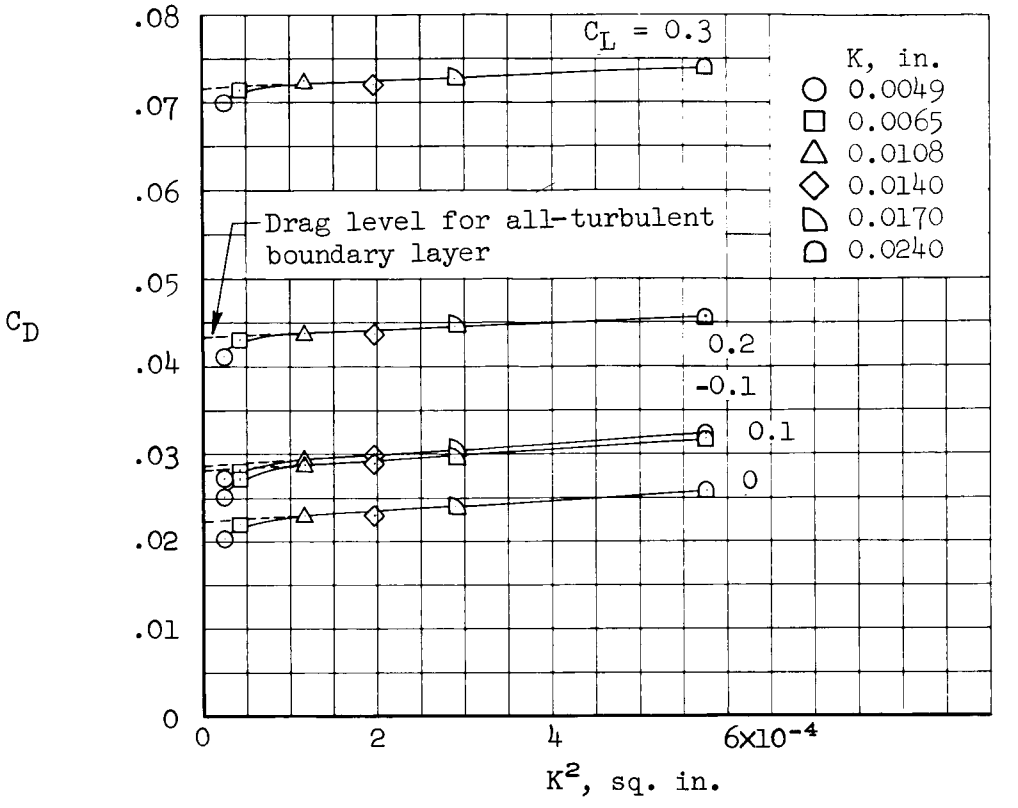


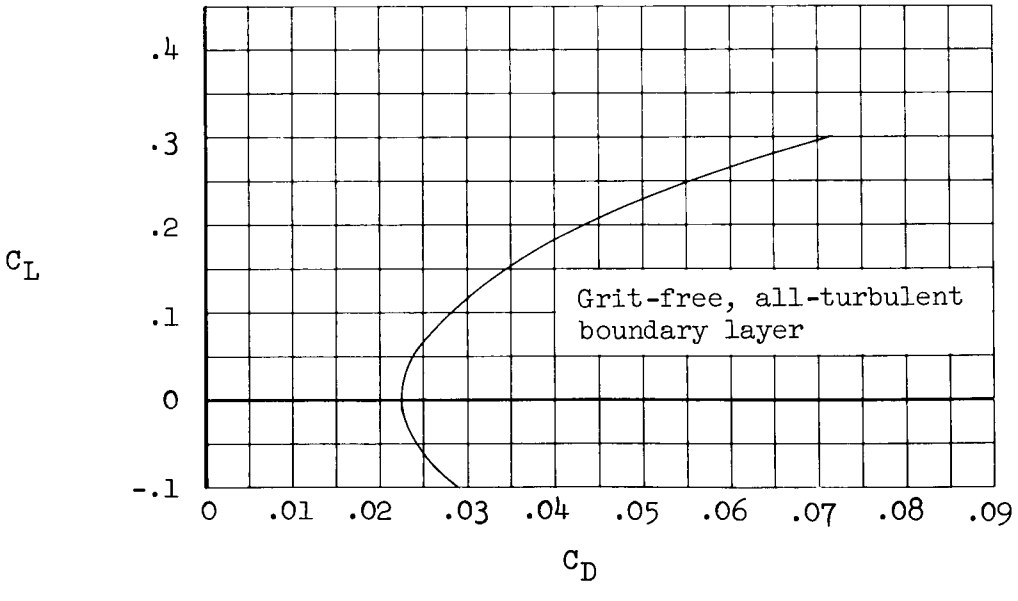


(c) M = 1.99

Figure 15.- Continued.

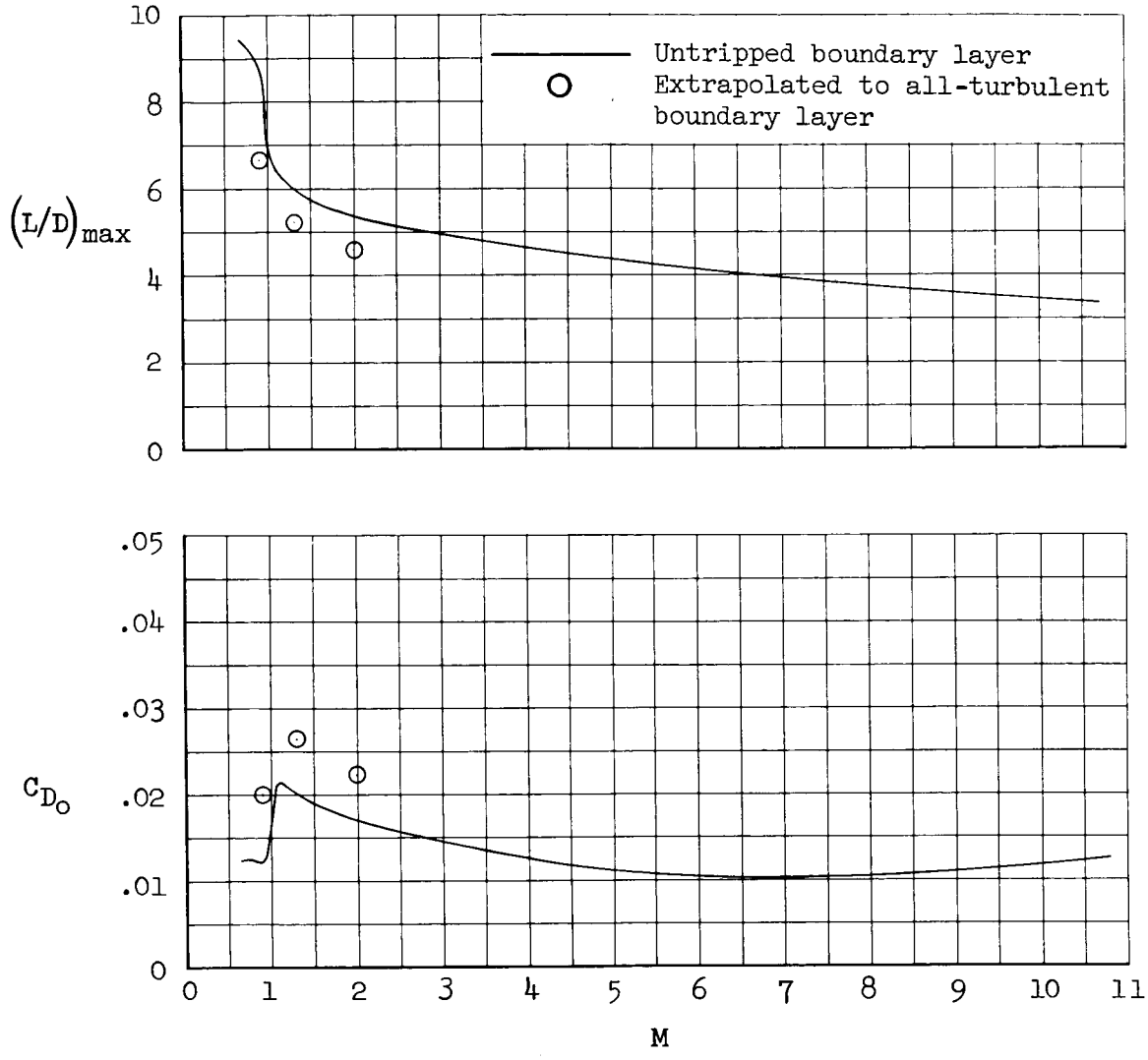


(d) Summary

Figure 15.- Concluded.

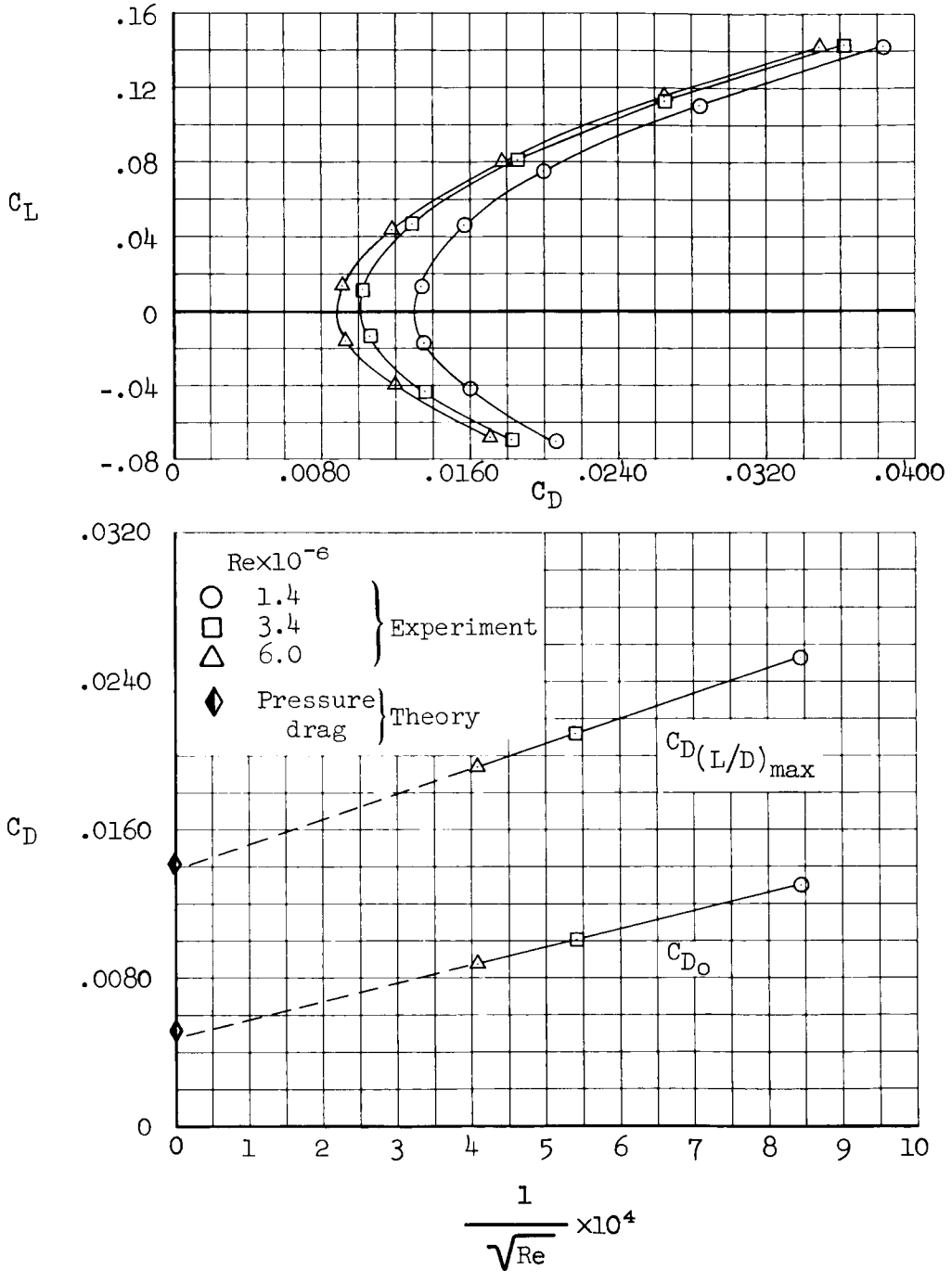


(a) M = 5.31

Figure 16.- Effects of variation in Reynolds number on drag coefficient; reference configuration; wing-body-vertical tail combination.

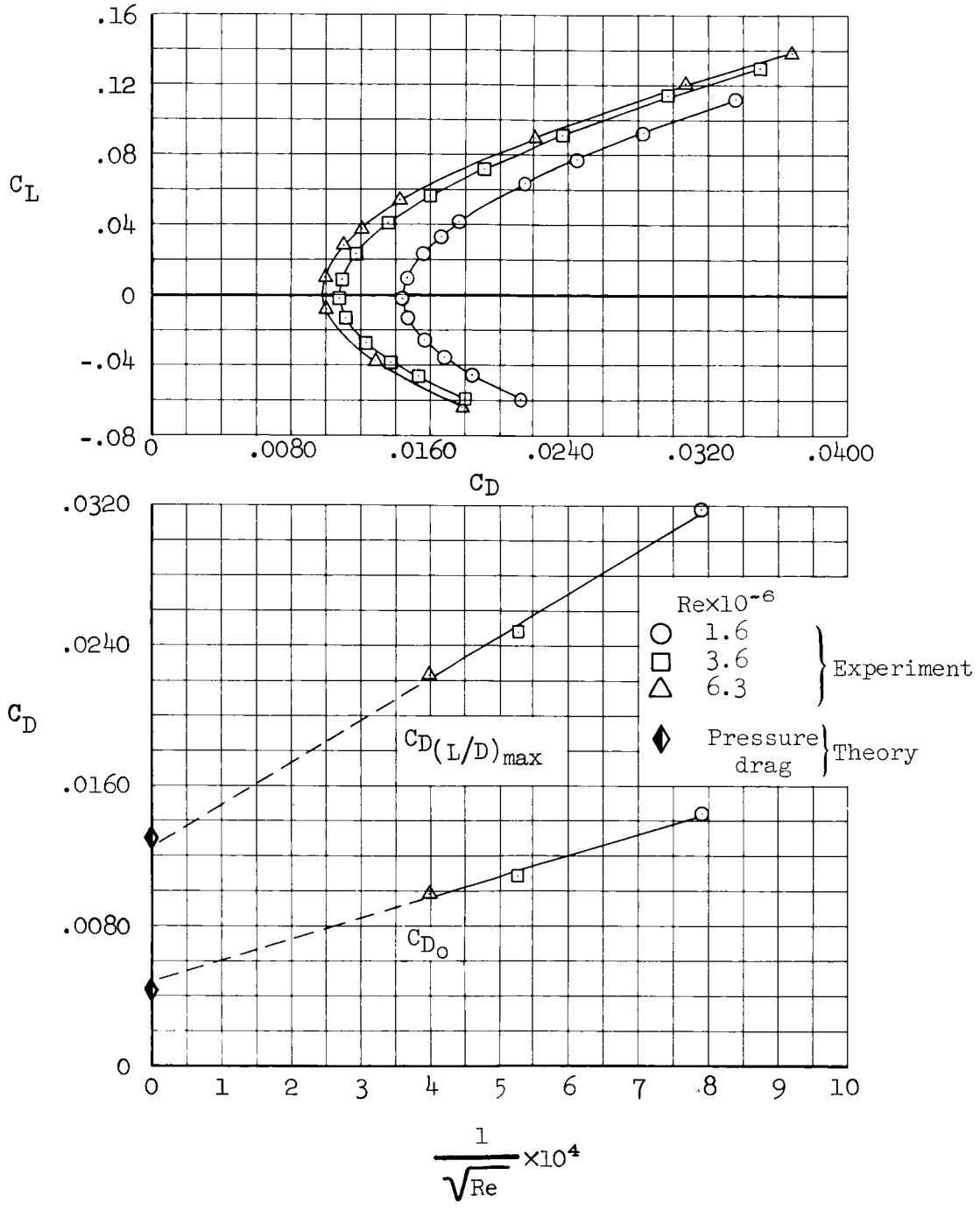


(b) M = 7.42

Figure 16.- Continued.

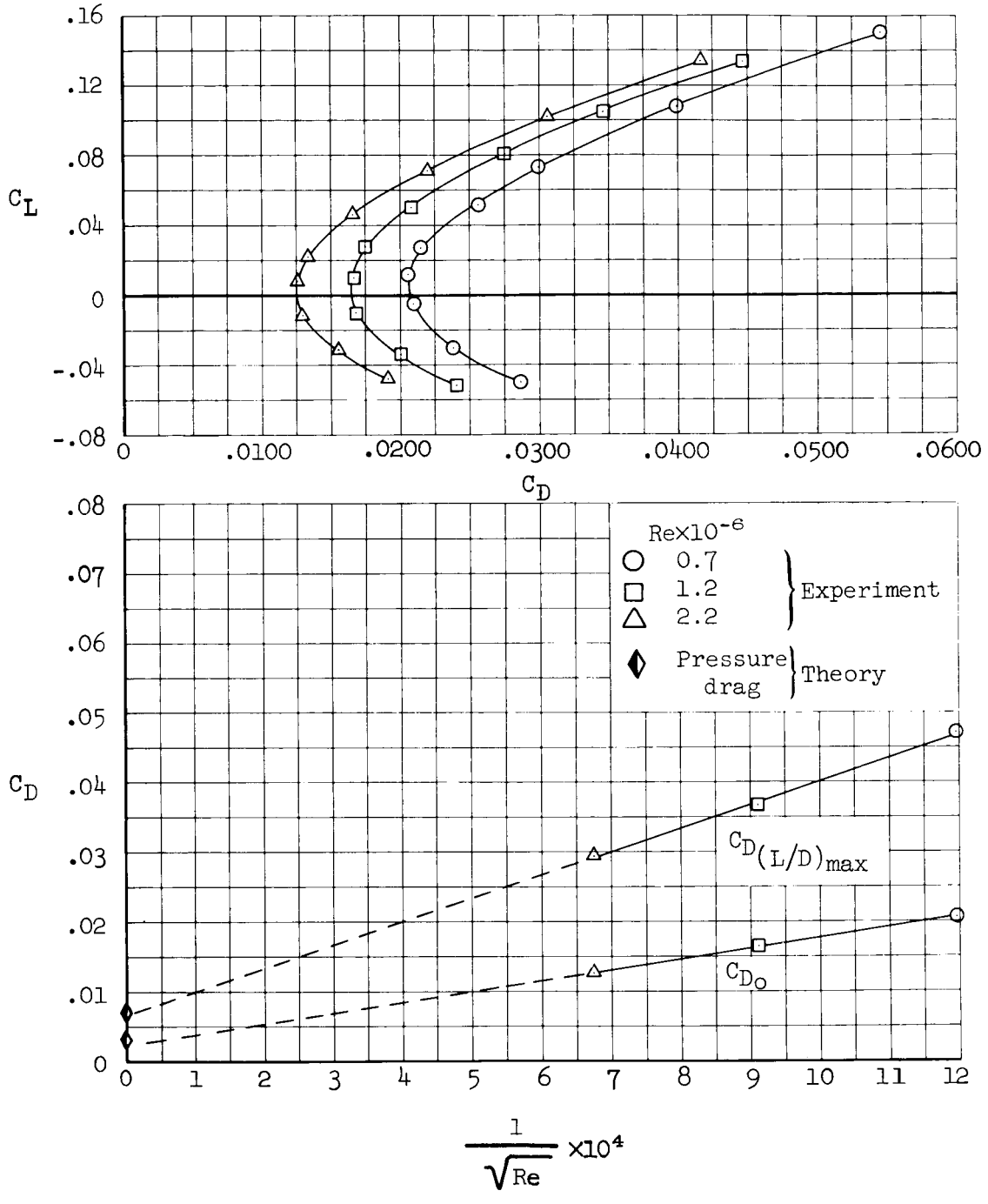


(c) M = 10.70

Figure 16.- Concluded.

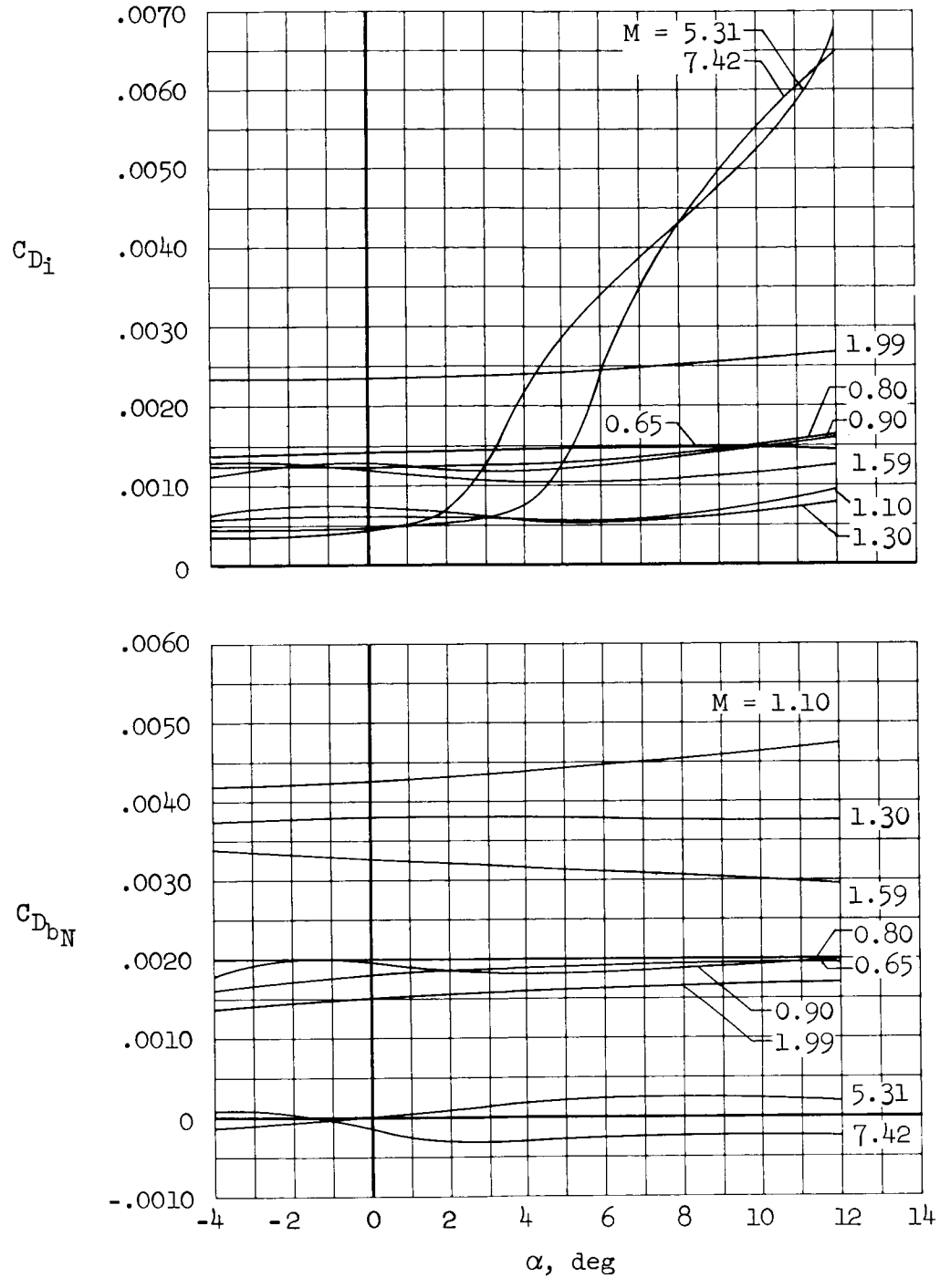


(a) Reference configuration with wing-mounted nacelles ($N_1$); nacelle stream-tube drag coefficients and nacelle base drag coefficients

Figure 17.- Nacelle stream-tube drag coefficients and nacelle base drag coefficients as determined by nacelle pressure survey.

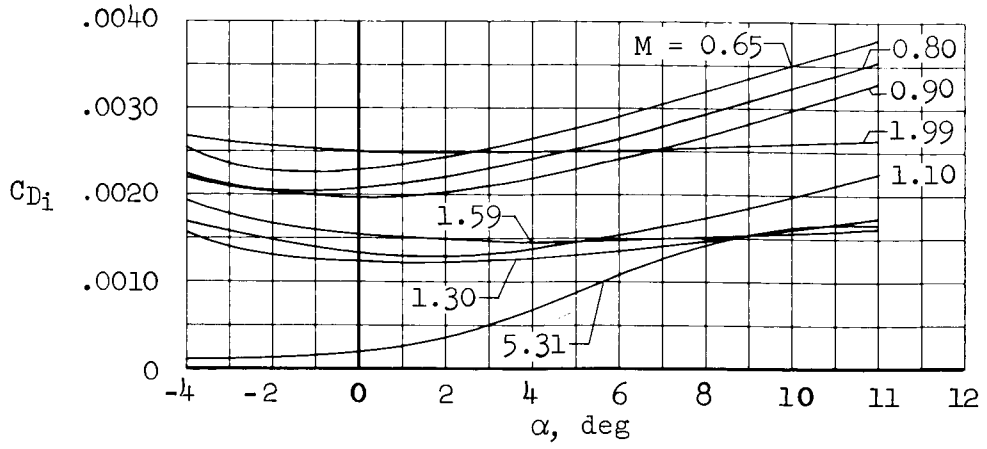


(b) Reference configuration with armpit-mounted nacelles ($N_2$); nacelle stream-tube drag coefficients

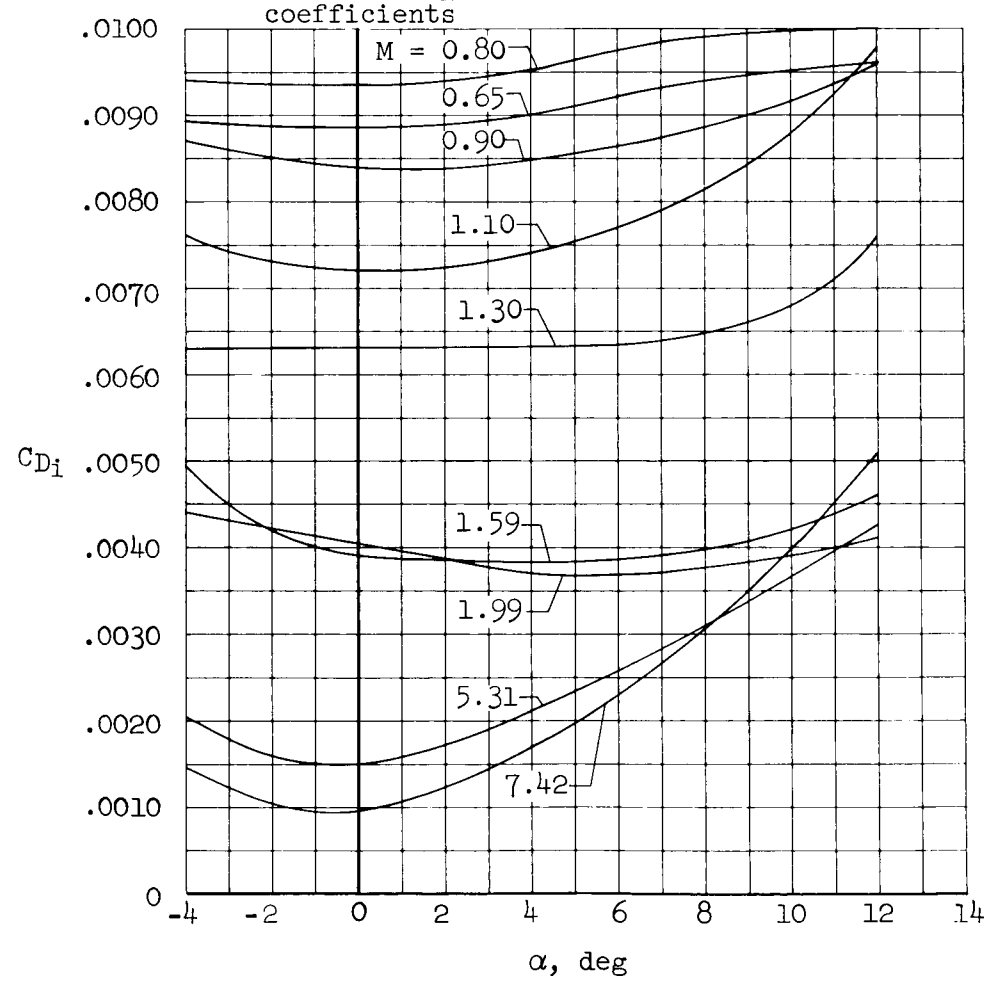


(c) Flat-bottom and blended configurations; nacelle stream-tube drag coefficients

Figure 17.- Concluded.

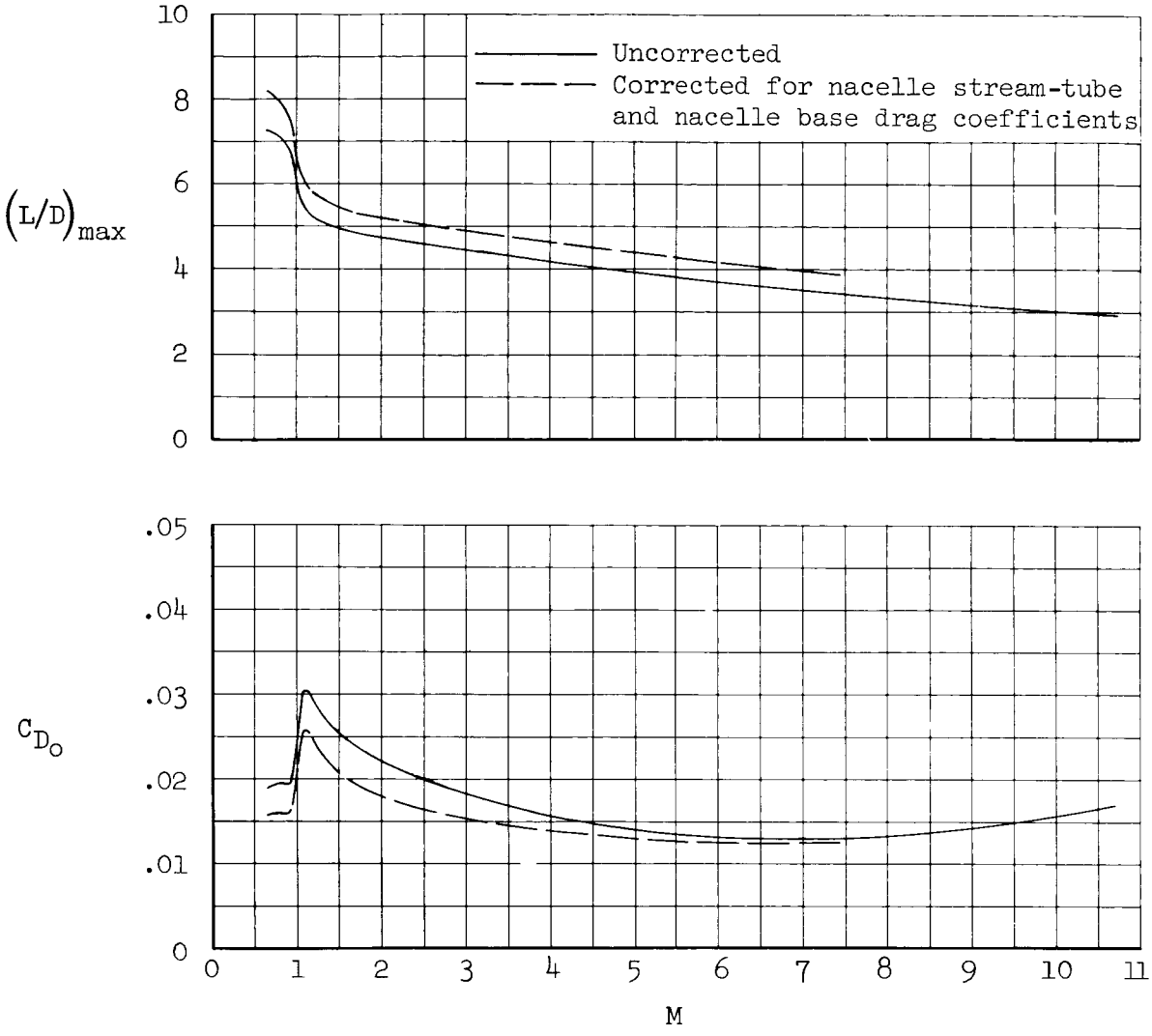


(a) Reference configuration with wing-mounted nacelles ($WBVN_1$)

Figure 18.- The effect of nacelle stream-tube drag coefficients and nacelle base drag coefficients on maximum lift-drag ratio and zero-lift drag coefficient.

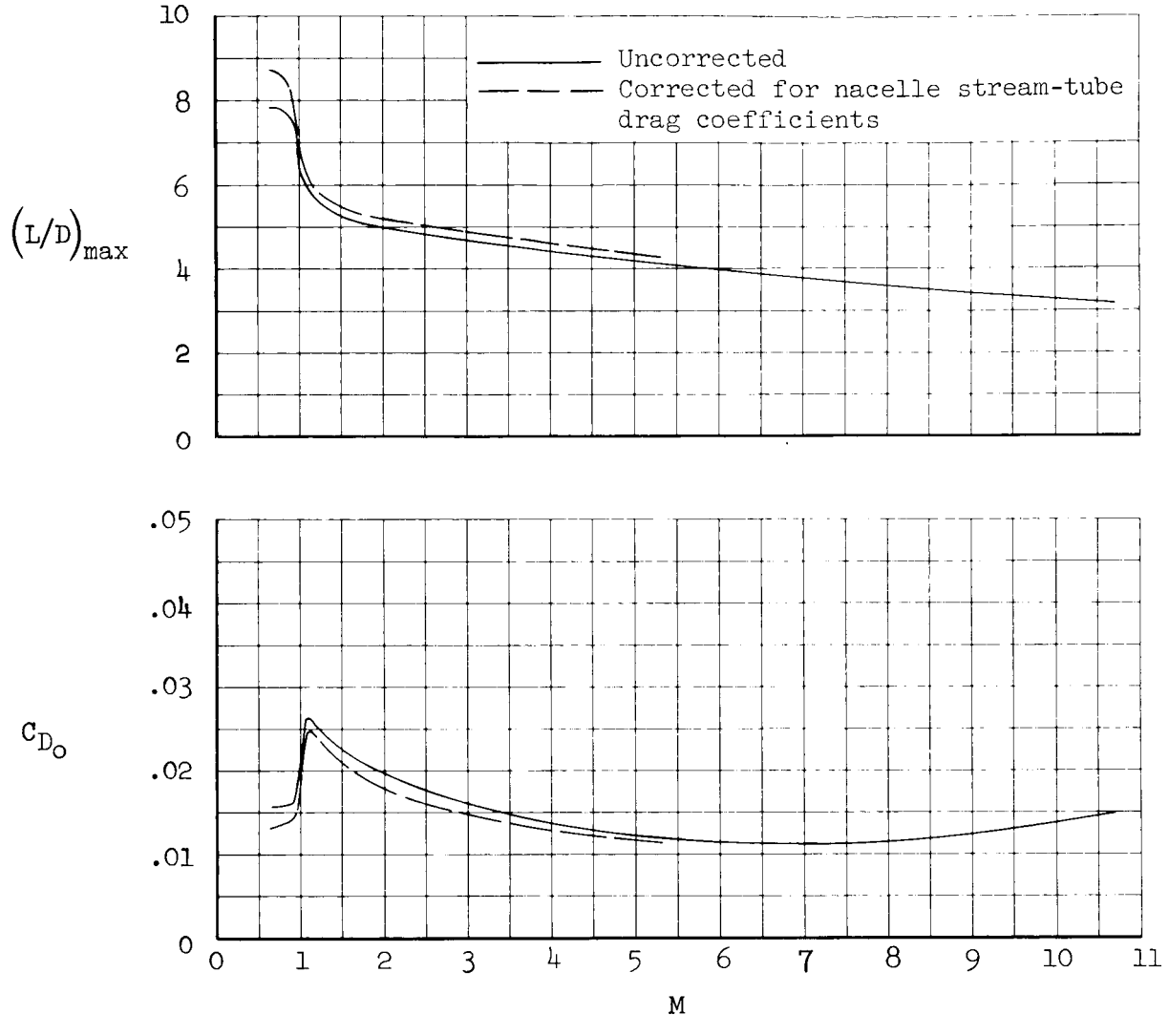


(b) Reference configuration with armpit-mounted nacelles ($WBVN_2$)

Figure 18.- Continued.

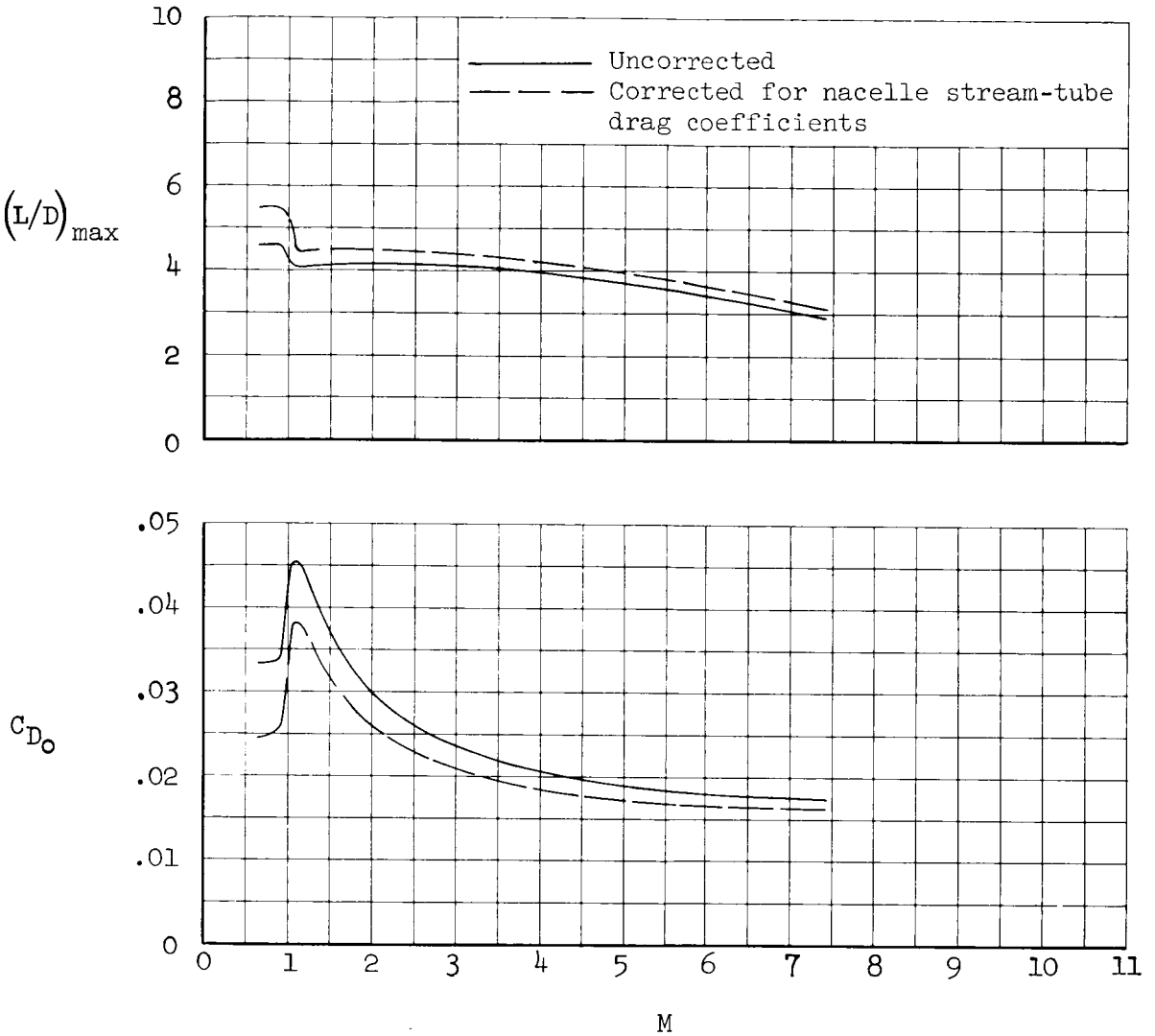


(c) Flat-bottom configuration ($WB_1VRFN$) with a drooped nose; wing t/c = 0.04

Figure 18.- Continued.

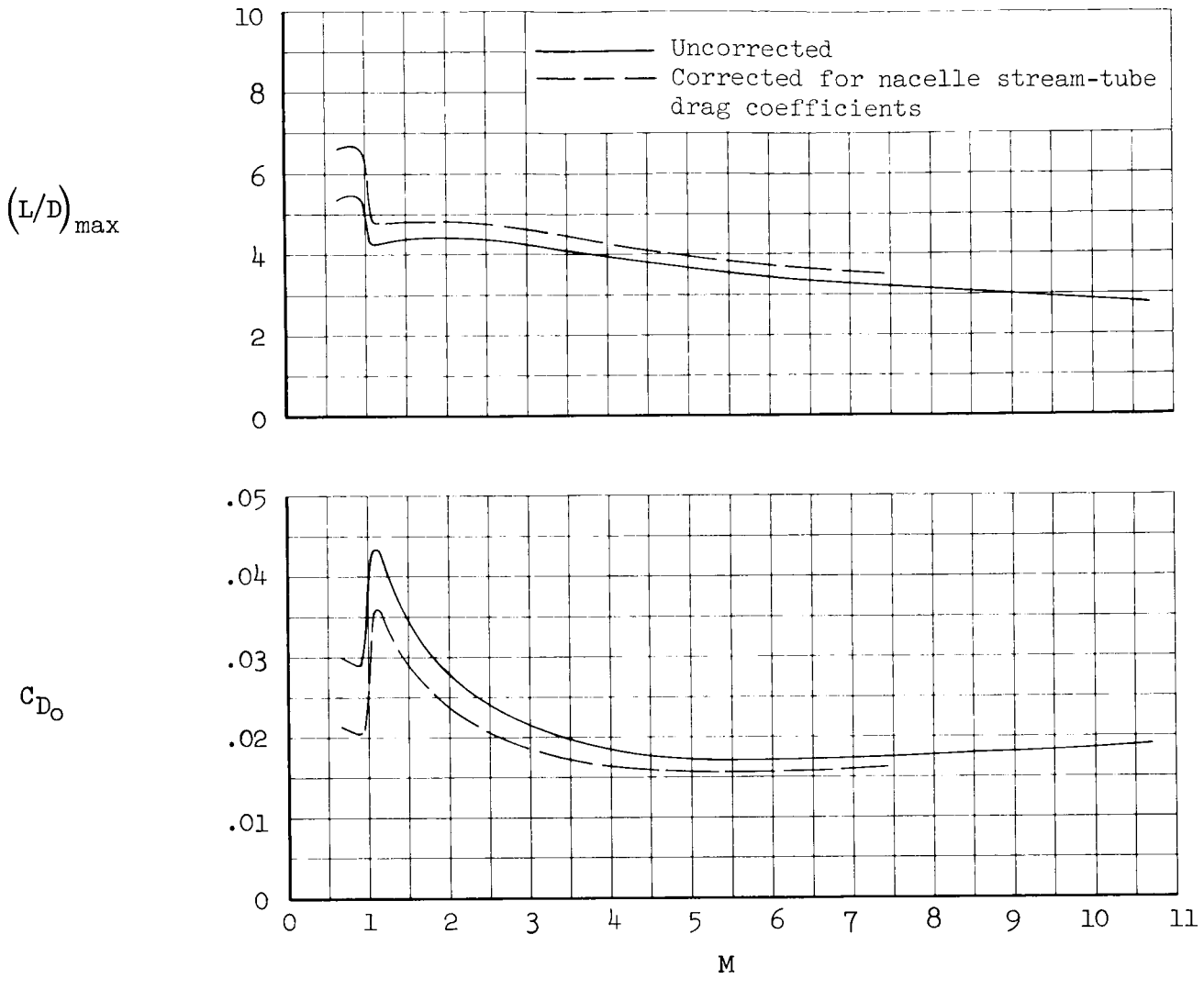


(d) Blended configuration ($W_1$BVRN)

Figure 18.- Concluded.



NASA-Langley, 1970 —— 1 A-3597